ปฏิกิริยาไฮโดรจิเนชันแบบเลือกเกิดของอะเซทิลีนบนตัวเร่งปฏิกิริยาแพลเลเดียมบนท่อนาโนไทเทเนตที่ปรับปรุงด้วยซิลิกา

นายจิตกร เจษฎาคม

วิทยานิพนธ์นี้เป็นส่วนหนึ่งของการศึกษาตามหลักสูตรปริญญาวิศวกรรมศาสตรมหาบัณฑิต
สาขาวิชาวิศวกรรมเคมี ภาควิชาวิศวกรรมเคมี
คณะวิศวกรรมศาสตร์ จุฬาลงกรณ์มหาวิทยาลัย
ปีการศึกษา 2556
ลิขสิทธิ์ของจุฬาลงกรณ์มหาวิทยาลัย

SELECTIVE HYDROGENATION OF ACETYLENE OVER SiO2-MODIFIED TITANATE NANOTUBES SUPPORTED PALLADIUM CATALYSTS

Mr. Jittrakorn Jeasadakom

A Thesis Submitted in Partial Fulfillment of the Requirements
for the Degree of Master of Engineering Program in Chemical Engineering
Department of Chemical Engineering
Faculty of Engineering
Chulalongkorn University
Academic Year 2013

Thesis Title	SELECTIVE HYDROGENATION OF ACETYLENE OVER SiO2-MODIFIED TITANATE NANOTUBES SUPPORTED PALLADIUM CATALYSTS
By	Mr. Jittrakorn Jeasadakom
Field of Study	Chemical Engineering
Thesis Advisor	Associate Professor Joongjai Panpranot, Ph.D.

Accepted by the Faculty of Engineering, Chulalongkorn University in Partial Fulfillment of the Requirements for the Master's Degree

.....Dean of the Faculty of Engineering

(Professor Bundhit Eua-arporn, Ph.D.)

THESIS COMMITTEE

.....Chairman

(Associate Professor Bunjerd Jongsomjit, Ph.D.)

.....Thesis Advisor

(Associate Professor Joongjai Panpranot, Ph.D.)

.....Examiner

(Assistant Professor Suphot Phatanasri, D.Eng.)

.....External Examiner

(Assistant Professor Okorn Mekasuwandamrong, D.Eng.)

จิตกร เจษฎาคม : ปฏิกิริยาไฮโดรจิเนชันแบบเลือกเกิดของอะเซทิลีนบนตัวเร่งปฏิกิริยาแพลเลเดียมบนท่อนาโนไทเทเนตที่ปรับปรุงด้วยซิลิกา. (SELECTIVE HYDROGENATION OF ACETYLENE OVER SiO2-MODIFIED TITANATE NANOTUBES SUPPORTED PALLADIUM CATALYSTS) อ.ที่ปรึกษาวิทยานิพนธ์หลัก: รศ. ดร.จูงใจ ปั้นประณต , 103 หน้า.

สังเคราะห์ท่อนาโนไทเทเนตที่ปรับปรุงด้วยซิลิกาที่อัตตราส่วนโดยโมลของ Ti/Si เท่ากับ 95:5, 90:10, 80:20 และ 50:50 ด้วยวิธีไฮโดรเทอร์มอลของไทเทเนียมไดออกไซด์ในสารละลายโซเดียมไฮดรอกไซด์และเตตระเอทิลออโทซิลิเกตที่อุณหภูมิ 150 องศาเซลเซียส จากนั้นนำไปใช้เป็นตัวรองรับตัวเร่งปฏิกิริยาแพลเลเดียมที่เตรียมโดยวิธีเคลือบฝัง และทดสอบในปฏิกิริยาไฮโดรจิเนชันแบบเลือกเกิดของอะเซทิลีน วิเคราะห์คุณลักษณะของตัวเร่งปฏิกิริยาด้วยวิธีเอ็กซเรย์ดิฟแฟรกชัน กล้องจุลทรรศน์อิเล็กตรอนแบบส่องกราด กล้องจุลทรรศน์อิเล็กตรอนแบบส่องผ่าน ฟูเรียร์ทรานฟอร์มอินฟราเรดสเปกโทรสโคปี เอ็กซเรย์โฟโตอิเลคตรอนสเปกโทรสโคปี การดูดซับทางกายภาพด้วยแก๊สไนโตรเจน การดูดซับทางเคมีด้วยแก๊สไฮโดรเจน และ การดูดซับทางเคมีด้วยแก๊สเอทิลีน การปรับปรุงท่อนาโนไทเทเนตด้วยซิลิกาส่งผลให้การกระจายตัวของแพลเลเดียมสูงขึ้น นอกจากนี้การเกิดพันธะ Ti-O-Si ช่วยยับยั้งการเปลี่ยนเฟสของไทเทเนตเป็นไทเทเนียอนาเทส เมื่อทำการรีดิวซ์ที่อุณหภูมิ 150 องศาเซลเซียส ตัวเร่งปฏิกิริยาแพลเลเดียมบนท่อนาโนไทเทเนตที่ปรับปรุงด้วยซิลิการ้อยละ 50 โดยโมล ให้ร้อยละผลได้ของเอทิลีนสูงที่สุด การปรับปรุงด้วยซิลิกาทำให้แรงในการดูดซับของเอทิลีนต่ำลงส่งผลให้การเลือกเกิดเป็นเอทิลีนสูงขึ้น สำหรับตัวเร่งปฏิกิริยาที่รีดิวซ์ที่อุณหภูมิ 500 องศาเซลเซียส พบว่าตัวเร่งปฏิกิริยาแพลเลเดียมบนท่อนาโนไทเทเนตที่ปรับปรุงด้วยซิลิการ้อยละ 5-20 โดยโมล มีประสิทธิภาพสูงขึ้นเมื่อเปรียบเทียบกับตัวเร่งปฏิกิริยาที่รีดิวซ์ที่อุณหภูมิ 150 องศาเซลเซียส ในขณะที่ตัวเร่งปฏิกิริยาที่มีร้อยละ 50 โดยโมลซิลิกา มีประสิทธิภาพต่ำลงเนื่องจากการเกิดสารประกอบเชิงซ้อนโซเดียมไททาโนซิลิเกต

ภาควิชา วิศวกรรมเคมี ลายมือชื่อนิสิต .....

สาขาวิชา วิศวกรรมเคมี ลายมือชื่อ อ.ที่ปรึกษาวิทยานิพนธ์หลัก .....

ปีการศึกษา 2556

5570141121 : MAJOR CHEMICAL ENGINEERING
KEYWORDS: TITANATE NANOTUBES / SILICA-MODIFIED / HYDROTHERMAL METHOD / SUPPORTED PALLADIUM CATALYSTS / ACETYLENE HYDROGENATION

JITTRAKORN JEASADAKOM: SELECTIVE HYDROGENATION OF ACETYLENE OVER SiO2-MODIFIED TITANATE NANOTUBES SUPPORTED PALLADIUM CATALYSTS. ADVISOR: ASSOC. PROF. JOONGJAI PANPRANOT, Ph.D., 103 pp.

Silica-modified titanate nanotubes with various Ti/Si molar ratios of 95:5, 90:10, 80:20 and 50:50 were prepared via the hydrothermal treatment of titanium dioxide powder in an aqueous NaOH solution containing different amounts of tetraethyl orthosilicate at 150 °C. The silica-modified titanate nanotubes were used for preparation of supported Pd catalysts by the incipient wetness impregnation method. The catalysts were tested in the gas-phase selective acetylene hydrogenation and characterized by XRD, SEM, TEM, FTIR, XPS, N_2 physisorption, H_2 chemisorption and Ethylene TPD. The presence of silica in the titanate nanotubes supports resulted in higher Pd dispersion. In addition, the formation of Ti-O-Si bond could suppress the titanate phase transformation to anatase TiO_2. When reduced at 150 °C, the highest ethylene yield was obtained over Pd/T50:S50 catalysts. The modification of silica on titanate nanotubes supports weakened ethylene adsorption on Pd catalyst surface so that the selectivity of ethylene was increased. For high reduction temperature of 500 °C, the 5-20 mol% silica-modified titanate nanotubes supported Pd catalysts exhibited better catalytic performance than the ones reduced at 150 °C. Due probably to the formation of $Na_2(TiO)(SiO_4)$ complex, sintering of Pd occurred on Pd/T50:S50 under high reduction temperature and poor catalytic performance was obtained instead.

Department: Chemical Engineering Student's Signature .....

Field of Study: Chemical Engineering Advisor's Signature .....

Academic Year: 2013

ACKNOWLEDGEMENTS

First of all, the author would like to express my sincere and deepest appreciation to my advisor, Associate Professor Joongjai Panpranot for their invaluable suggestions, support, encouragement, and help during the course of my graduate study. In additional, the author would also be grateful to Associate Professor Bunjerd Jongsomjit, as the chairman, Assistant Professor Suphot Phatanasri, and Assistant Professor Okorn Makasuwandamrong as the members of the thesis committee.

Most of all, the author would like to express his highest gratitude to his parents who always pay attention to him all the times for their suggestions and have provided support and encouragements. The most success of graduation is devoted to his parents.

Finally, the author wishes to thank the members of the Center of Excellence on Catalysis and Catalytic Reaction Engineering, Department of Chemical Engineering, Faculty of Engineering, Chulalongkorn University for friendship. To the many others, not specifically named, who have provided his with support and encouragement, please be assured that he thinks of you.

CONTENTS

Page

Page

Page

LIST OF TABLES

Page

LIST OF FIGURES

Page

CHAPTER I

INTRODUCTION

1.1 Rationale

Ethylene is one of important molecules as a starting material for many petrochemical products, particularly for polyethylene production that is the most widely produced in the world. Typically an ethylene is produced from naphtha cracker unit but unfortunately has to contain about 0.1 to 1% of acetylene as an impurity in ethylene rich feedstocks, which is required to be removed to less than 5 to 10 ppm because it poisons ethylene polymerization catalysts and eventually degrades the quality of the produced polyethylene. Usually acetylene impurities are removed by two methods, that is, adsorption with zeolite and conversion to ethylene by selective hydrogenation using catalysts, but the first method have a limitation for very difficultly and costly processes. While, the latter method more commonly being used and has received great attention in catalysis research [1].

The most studies in selective hydrogenation of acetylene have been extensively using of supported Pd catalysts due to their good catalytic activity and selectivity for this reaction [2-7]. The remarkable properties of Pd are their ability to dissociate and dissolve hydrogen, and also adsorb large quantities of hydrogen [8]. Particularly, many catalysis researchers have found that the sequence of catalytic performances of selective hydrogenation of acetylene is Pd > Pt >Ni [9-11]. However, the catalytic performances could be improved by using a novel supports or promoters in order to obtain high acetylene activity and high ethylene selectivity.

Several support materials have been employed for Pd catalysts in the selective hydrogenation of acetylene including SiO_2 [12, 13], Al_2O_3 [14, 15], and TiO_2 [16-18]. Typically SiO_2 and Al_2O_3 are used as supports for Pd catalysts. However, a recent study has been reported that Pd/TiO_2 exhibited higher activity and selectivity in hydrogenation of acetylene than Pd/Al_2O_3 [19], and also oligomer or green oil formation during reaction was inevitable over Pd/Al_2O_3 [20]. It is well known that TiO_2

exhibits the strong metal-support interaction (SMSI) phenomenon [21]. The charge transfers from Ti^{3+} species to Pd weakened the adsorption strength of ethylene on the Pd surface hence higher ethylene selectivity was obtained. Moreover, the amount of green oil formation was reduced due to suppression of the multiply coordinated Pd site resulting in an improved catalyst lifetime [20]. For a good support, a large surface area is the essential feature to disperse the active species. In addition, the microstructure and morphology of the support framework or the method by which the active species introduce affects not only the dispersion but also the structure and chemical environment of the active species [22].

Titanate nanotubes, produced by hydrothermal treatment in alkali solution [23, 24], is a novel and intensively studied material characterized by a mesopore-range internal diameter about 4 to 10 nm and unique combination physicochemical properties. It is expected that the layered structure would provide sites for the intercalation of metal ions, thus assisting in accommodation of the active species as well as preventing agglomeration [22]. This material shows promise of variety of application, including solar cells, hydrogen storage, gas sensors, photocatalysis and catalysis [25-29] because of their high surface area with open mesoporous morphology should facilitate transport of reagents during a catalytic reaction [30], the diameter is larger than the dynamic diameter of a free hydrogen molecule which could accommodate hydrogen [31] and high cation exchange capacity should enable high loading of an active species with even distribution and high dispersion [32]. Applications of titanate nanotubes as Pd catalyst support in selective hydrogenation have not been studied too much degree. Recently, the Pd supported on titanate nanotubes have been investigate in the selective hydrogenation of 1-heptyne obtained higher activity and selectivity than Pd supported on commercial anatase TiO_2 [33]. In addition, there are no reports of using titanate nanotubes as a support for Pd catalyst in selective hydrogenation of acetylene.

Moreover, the improvement in catalytic performances could be obtained by adding promoters to modify the physicochemical properties of titanate nanotubes. The TiO_2-SiO_2 mixed oxides have attracted considerable interest due to their potential applications as catalysts and supports in a wide variety of reactions. For

instance, many study reported that TiO_2-SiO_2 mixed oxides were appearing very attractive to improve the mechanical strength, thermal stability, and surface area of TiO_2 [34-39]. A recent study, found that Si^{4+} with higher electronegativity may replace the Ti^{3+} in TiO_2-SiO_2 composite system, leading to the formation of Si-O-Ti bonds. With Si-O-Ti bonds formed, more surface defects may appear. These defects can not only capture the photogenerated electrons or holes but also increase the reaction activity of hydroxyls, both of which increase the photocatalytic activity of TiO_2 [40, 41]. The TiO_2-SiO_2 mixed oxides also were used as effective catalysts of selective oxidation due to the synergistic effect between TiO_2 species and transition metal related to the generation of new catalytic site for selective oxidation [35, 37], and exhibited a large number of acidic site and acid strength more than pure TiO_2 [42]. Shin and co-worker [43, 44] reported that Si-modified Pd catalyst improved selectivity of selective acetylene hydrogenation due to surface Si species retard the formation of β-Pd hydride. Since, the β-Pd hydride is responsible for non-selective hydrogenation of acetylene. Moreover, the yield of green oil formation is retarded when Pd surface is geometrically blocked by inactive Si species [45]. However, the SiO_2-modified titanate nanotubes supported catalyst has not been reported in the selective hydrogenation of acetylene.

Thus, it is the aims of this study to investigate and compare the catalytic performances of titanate nanotubes and its SiO_2 modified supported Pd catalysts in the selective hydrogenation of acetylene in the presence of excess ethylene. The effect of SiO_2-modified titanate nanotubes on morphology and physicochemical properties were characterized by various analytical techniques.

1.2 Research Objectives

1. To investigate the effect of silica-modified titanate nanotubes with various Ti/Si ratios on the formation of titanate nanotubes during hydrothermal synthesis.

2. To investigate the characteristics and the catalytic properties of titanate nanotubes and its silica modified supports for Pd catalysts in the selective hydrogenation of acetylene.

1.3 Research Scopes

1. Synthesis of titanate nanotubes by hydrothermal method at 150 °C for 24 h in alkali solution.
2. Preparation of titanate nanotubes supported Pd catalysts by an incipient wetness impregnation method through using Palladium(II) acetate as the Pd precursor with Pd loading of ca. 1 wt%.
3. Characterization of the catalysts using several techniques, such as X-ray diffraction (XRD), N_2 physisorption, transmission electron microscopy (TEM), scanning electron microscopy (SEM), X-ray photoelectron spectroscopy (XPS), Fourier transform infrared spectroscopy (FTIR), H_2 chemisorption and Ethylene temperature programmed desorption.
4. The catalytic performance of the titanate nanotubes supported Pd catalysts was investigated in the selective hydrogenation of acetylene with various reaction temperature of 40-100 °C.
5. The effect of high reduction temperature at 500 °C on the performance of the titanate nanotube supported Pd catalysts was investigated in the selective hydrogenation of acetylene with various reaction temperature of 40-100 °C.

1.4 Research Methodology

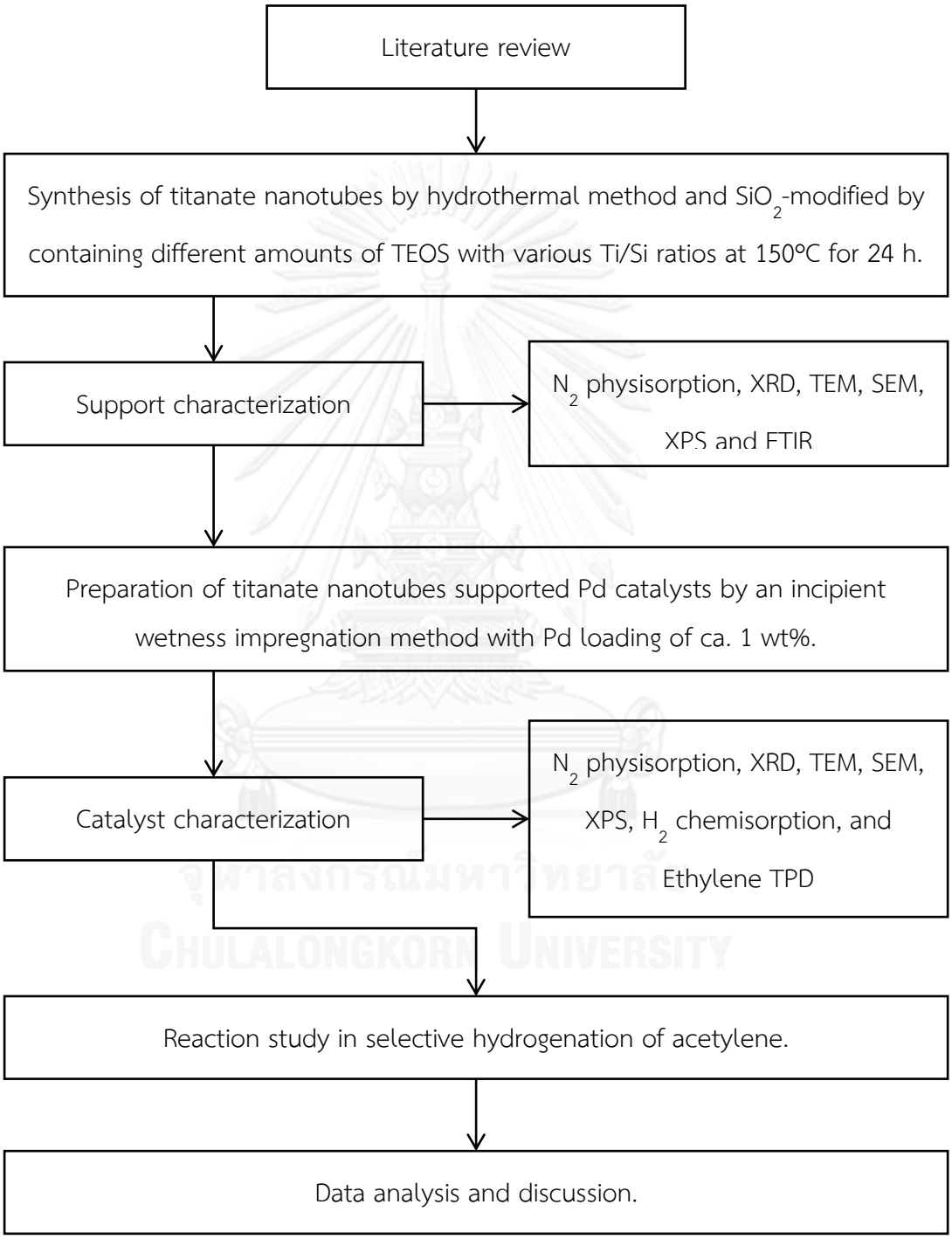

CHAPTER II

LITERATURE REVIEWS

Titanate nanotubes has been widely applied in variety of application, including solar cells, hydrogen storage, gas sensors, photocatalysis and catalysis etc. Although the developments of titanate nanotubes mostly has been reported in photocatalysis. However, recent researches have reported that used titanate nanotubes as a support catalyst, which investigated in the selective hydrogenation obtained higher activity and selectivity than commercial anatase TiO_2. In light of this, the literature review presented here covers topics that are concerned with the various factors influence to the synthesis titanate nanotubes.

Selective hydrogenation of acetylene to ethylene is a well-known catalytic reaction used to purity ethylene feedstocks for the production of polyethylene. Typically, supported Pd catalyst is employed for this process due to its high activity and selectivity. In this chapter is introduced briefly to the mechanism of acetylene hydrogenation and the palladium-hydrogen transformation because they are the basis understanding of the Pd catalysts performance.

This chapter summarizes the recent reports about (1) synthesis of titanate nanotubes by hydrothermal method, (2) selective hydrogenation of acetylene, (3) supported Pd catalyst in selective hydrogenation of acetylene, (4) titanate nanotubes supported Pd in selective hydrogenation reaction and comments on previous studies which are given in section 2.1-2.5 respectively.

2.1 Synthesis of titanate nanotubes by hydrothermal method

In 1998, Kasuga et al., [23] first reported a simple method for the preparation of TiO_2 nanotubes, without the use of sacrificial templates, by treatment of amorphous TiO_2 with a concentrated solution of NaOH (10 mol dm^{-3}) in a polytetrafluoroethylene-lined batch reactor at elevated temperatures. In a typical

process, several grams of TiO_2 raw material can be converted to nanotubes, with close to 100 % efficiency, at temperatures in the range 110-150 °C, followed by washing with water and 0.1 mol dm^{-3} HCl. It has since been demonstrated that all polymorphs of TiO_2 (anatase, rutile, brookite, or amorphous forms) can be transformed to the nanotubular or nanofibrous TiO_2 under alkaline hydrothermal conditions.

Following the discovery of titanate nanotubes by Kasuga et al., many investigations have been carried out on the formation, morphology, and structure of titanate nanotubes. It has been found that the hydrothermal temperature [46, 47], treatment duration, starting materials [48, 49], ratio of titania and NaOH [47], concentration of base solution [50] and difference pH values of post-treatment washing have strong effects on controlling the phase and morphology of the resulting materials [51]. Summaries of difference preparation conditions that have been many investigated are shown in **Table 2.1** as follow:

Table 2.1 Nanotubes of Different Structures Prepared from Different TiO2 Precursors, NaOH Treatment Conditions,a and Post-Treatment Washing Processes [51].

Precursor	NaOH treatment	Post-treatment	Refference
Nanotube Structure: Anatase TiO_2			
anatase	hydro/110 °C/20 h	HCl + water	Kasuga et al., (1998)
rutile	chem/110 °C/20 h	HCl + water	Kasuga et al., (1999)
anatase	chem/150 °C/12 h	water	Seo et al., (2001)
anatase	hydro/110 °C/20 h	HNO_3 + water	Zhang et al., (2002)
anatase	chem/110 °C/20 h	HCl + water	Wang et al., (2002)
anatase	hydro/150 °C/12 h	HNO_3 + water	Yao et al., (2003)
anatase/rutile	hydro/130 °C/24 h	HCl	Tsai and Teng., (2004)
anatase	chem/180 °C/30 h	HCl + water	Wang et al., (2004)
Nanotube Structure: Anatase TiO_2/$H_2Ti_3O_7$□$0.5H_2O$			
rutile	chemi/110 °C /4 h[b]	HNO_3 + water	Zhu et al., (2001)

Nanotube Structure: $A_2Ti_2O_5 \square H_2O$			
TiO_2 powder	chem/110 °C/20 h	HCl + water	Yang et al., (2003)
anatase	chem/110 °C/20 h	HCl + water	Zhang et al., (2004)
Nanotube Structure: $A_2Ti_3O_7$			
anatase	hydro/130 °C/72 h	HCl + water	Du et al., (2001)
anatase	hydro/130 °C/72 h	HCl + water	Chen et al., (2002)
anatase	hydro/130 °C/72 h	water	Chen et al., (2002)
anatase/rutile	hydro/150 °C/20 h	water	Tian et al., (2003)
any crystals	hydro/130 °C/72 h	water	Zhang et al., (2003)
anatase	hydro/180 °C/48 h	water	Sun and Li., (2003)
anatase	hydro/180 °C/24 h	HCl + water	Yuan and Su., (2004)
rutile	hydro/150 °C/72 h	HCl + water	Thorne et al., (2005)
anatase/rutile	hydro/130 °C/72 h	water	Zhang et al., (2005)
Nanotube Structure: $H_2Ti_4O_9 \square H_2O$			
anatase/rutile	hydro/110 °C/96 h	HCl + water	Nakahira et al., (2004)
Nanotube Structure: Lepidocrocite Titanates			
anatase	hydro/150 °C/48 h	water + HCl	Ma et al., (2003)
anatase	hydro/130 °C/24 h	water + HCl	Ma et al., (2005)

[a] Treatment conditions refer to chemical or hydrothermal processes, temperature (°C), and duration (h), respectively. [b] Sonication at 280 W before chemical treatment.

Yuan et al., [52] have been developed to synthesize low-dimensional titanate nanostructures with a simple one-step hydrothermal reaction among TiO_2 powders and alkaline solution. They found that the morphologies of the obtained nanomaterials depend on the process parameters: the structure of raw material, the nature and concentration of alkaline solution, reaction temperature and time, which suggests that the nanostructure synthesis could be controllable. Titanium oxide nanotubes can be formed in the range of reaction temperature of 100-180 °C when either crystalline anatase or rutile or commercial P-25 was used as the raw materials.

The yield of nanotubes increased with the hydrothermal temperature when the temperature was in the range of 100-150 ℃, resulting in the higher yield of nanotubes of 80-90%. Little nanotubes formed when the temperature was lower than 100 ℃ or higher than 180 ℃. The surface areas of the products are also influenced by the particle size of the raw materials. The commercial P-25 powder is known to be very fine with a particle size of 25–30 nm, while the anatase particles are relatively large (more than 50 nm). Correspondingly, the surface areas of the produced nanotubes from P-25 is higher than that from anatase, though the effect of the particle size of the raw materials to the yield of the produced nanotubes is quite small in comparison to the hydrothermal temperature that is shown variation graphical in **Figure 2.1.** Additionally, the concentration of NaOH solution is also a critical parameter during the formation of nanotubes. Little nanotubes were observed when the NaOH concertration is lower than 5 mol/L or as strong as 20 mol/L. High yield of nanotubes can be obtained when the NaOH concentration was 10-15 mol/L, and their surface areas can be as large as 350 m2/g. While nanofibers structure was formed when amorphous TiO_2 was treated with NaOH at 100-160 ℃. Pentatitanate nanoribbons were obtained either crystalline or amorphous TiO_2 in NaOH solution at the temperature above 180 ℃.

Chang et al., [53] report the effects of different concentration of NaOH on the morphologies of titanate nanostructures. They synthesized titanate nanostructures by hydrothermally treated at 140 ℃ for 48 h. with various NaOH aqueous solutions of 5 M, 8 M and 10 M. As shown in **Figure 2.2**, sample (a) and (b) both exhibited sheet-like structures that are titanate nanosheets could be prepared in the relatively low concentrations of NaOH aqueous solutions about 5-8 M, which a several folded edges in them implied a tendency of rolling-up. In sample (c) high alkalinity NaOH concentration is 10 M was consistent with the threshold concentration for titanate nanotubes.

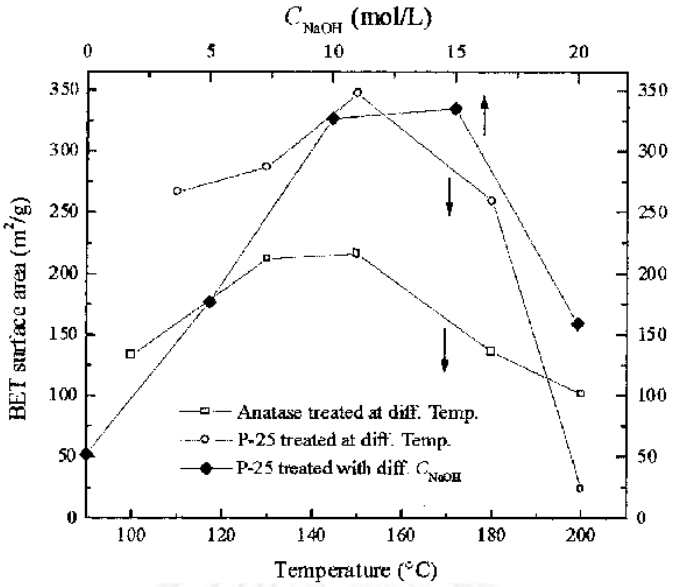

Figure 2.1 BET surface areas of the products obtained from anatase and P-25 with 10 mol/L NaOH at different temperatures for 24 h, and the products from P-25 with different content of NaOH at 110 °C for 20h [52].

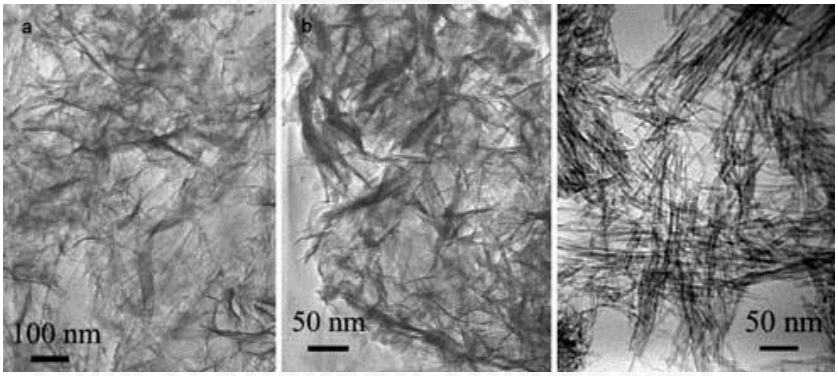

Figure 2.2 TEM micrographs of titanate nanostructures prepared in pure aqueous solutions with different NaOH concentration: (a) 5 M, (b) 8 M and (c) 10 M.

Tasi et al., [51, 54] synthesized titanate nanotubes with different post-treatment acidity and hydrothermal treatment temperature. In part of investigated the influence in different post-treatment washing. After the samples were washed with HCl, nanotubes became the dominant component of specimens with a washing pH of less than 8. In the pH-decreasing course with HCl washing, the diffraction peaks

obtained from XRD have been assigned to the diffraction of titanates such as $A_2Ti_2O_5 \square H_2O$, $A_2Ti_3O_7$ and lepidocrocite titanates. In the pH-descending course, the surface area increases to reach a maximum at pH = 1.6 is about 397 m^2/g, and it then decreases. Due to at pH = 1.6 the nanotube aggregates should be in a loose configuration, because the porosity was contributed to by the internal space as well as the interstice of the nanotubes. At pH = 12.2 sample not obtained nanotubes structure, which the sample contains granules composed of layered structure with an interlayer distance of ca. 0.8 nm. The layers would peel off with further acid washing, forming nanotubes. The nanotubes obtained at pH values of 6.3 and 1.6, respectively. Nanotubes with intact walls can be observed for the pH = 6.3 sample are shown in **Figure 2.3** whereas there are defects on the walls of the pH = 1.6 sample. The defects may be caused by the partial transformation of the titanate structure to anatase TiO_2 at this pH. With a further decrease in pH to 0.38, the structure transformed to coagulated particles. This shows that the anatase TiO_2 formed under such a highly acidic environment comprises turbostratic stacking of the (101) faces with a defective alignment.

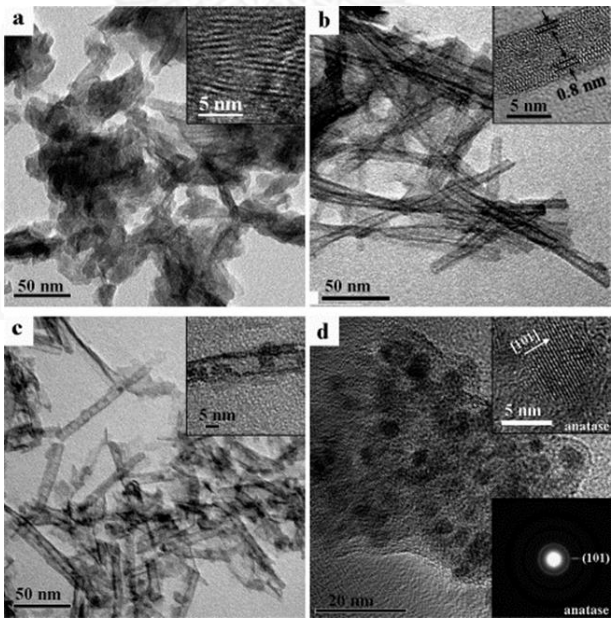

Figure 2.3 TEM images of specimens prepared from hydrothermal treatment on TiO_2 at 130 ℃ followed by washing with HCl to pH values of (a) 12.2, (b) 6.3, (c) 1.6, and (d) 0.38.

In the influence of hydrothermal treatment temperature, ranging within 110-150 °C. The surface area of the nanotube aggregates increases with the treatment temperature to reach a maximum of ca. 400 m^2/g at 130 °C, and then decreases with further increase of the temperature. The increase in surface area or pore volume with the hydrothermal treatment temperature in the low-temperature regime (<130 °C) can be attributed to the enhanced rupture of Ti-O-Ti bonds in the nanoparticles to form Ti-O-Na and Ti-OH. The rupture leads to the formation of lamellar TiO_2 sheets because of the electrostatic repulsion of the charge on sodium. The sheets would scroll to become nanotubes after HCl washing. Treatment at 110 °C may only result in a low extent of bond rupture, forming plates thicker than the lamellar sheets obtained at higher treatment temperatures. These plates cannot scroll to become nanotubes after HCl washing. For the hydrothermal treatment at temperatures higher than 130 °C, the surface area and pore volume of the products decrease with the temperature. The pore volume decrease with temperature mainly results from the loss of pores of smaller sizes. It is possible that the extensive treatment at high temperatures causes the destruction of the lamellar TiO_2.

Table 2.2 Pore structures of TiO_2 nanotube aggregates from hydrothermal treatment in NaOH at different temperatures [a] [54].

hydrothermal treatment temperature (°C)	S_{BET} (m^2/g)	V_{total} (cm^3/g)	peak pore size (nm)
110	207	0.24	3.8
120	245	1.41	20.9
130	399	1.47	18.1
140	348	1.18	18.5
150	209	0.84	31.1

[a] The treatment was followed by washing several times with 1 L of 0.1 N HCl until pH < 7 was reached.

2.2 Selective hydrogenation of acetylene

2.2.1 The mechanism of acetylene hydrogenation

In a constant volume system, high selectivity of ethylene could be maintained as long as any acetylene remained, even in the presence of excess hydrogen but, while it was possible in the region of room temperature, the use of higher temperatures encouraged the simultaneous formation of ethane. When this occurred, however, the two processes occurred in parallel; but the selectivity remained constant while any acetylene was left. When all of the acetylene had reacted, the ethylene was then hydrogenated more quickly, so that the rate of pressure fall increased [55-57]. This proved very clearly that under these conditions there were no sites available for ethylene hydrogenation that were not occupied by acetylene, that is, re-adsorption of gaseous ethylene was forbidden. The simultaneous formation of ethane must, therefore, have arisen by reaction of ethylene before it had desorbed. This led to the recognition of two factors in high selectivity shown by palladium: (i) a thermodynamic factor, which secures the preferential coverage of the surface by acetylene through its greater heat of adsorption; and (ii) a mechanistic factor, by which ethylene desorbs and is replaced by acetylene before it has a chance to react [58-61]. The network of the main reactions proceeding during acetylene hydrogenation in ethylene-rich streams is shown in **Figure 2.4**.

This scheme does not show the mechanism of the reactions but rather the reactions having a main influence on the mass balance of the process and on the process operation. The only desired reaction is acetylene half-hydrogenation to ethylene. During acetylene hydrogenation in ethylene-rich streams, at steady state conditions, the rates of reactions (3-6) are small as compared to the rates of reactions (1) and (2). However, reactions (4-6) play an important role in the process. Reaction (4) produces C_4 hydrocarbons, which were suggested to be the precursors of heavier C_{6+} hydro-oligomers containing even numbers of carbon atoms (5) and of carbonaceous residues (6). The liquid part of the hydrocarbons accumulates in the catalyst's pores and also appears downstream, where it can cause plugging of pipes. When carbon monoxide is co-fed the liquid hydrocarbons have a green color and are

called “green oil”. The irreversibly adsorbed heavy hydrocarbons on the catalyst surface (6, 7) modify the catalyst properties (increase or decrease of the catalyst’s activity and selectivity to ethylene) [62-65].

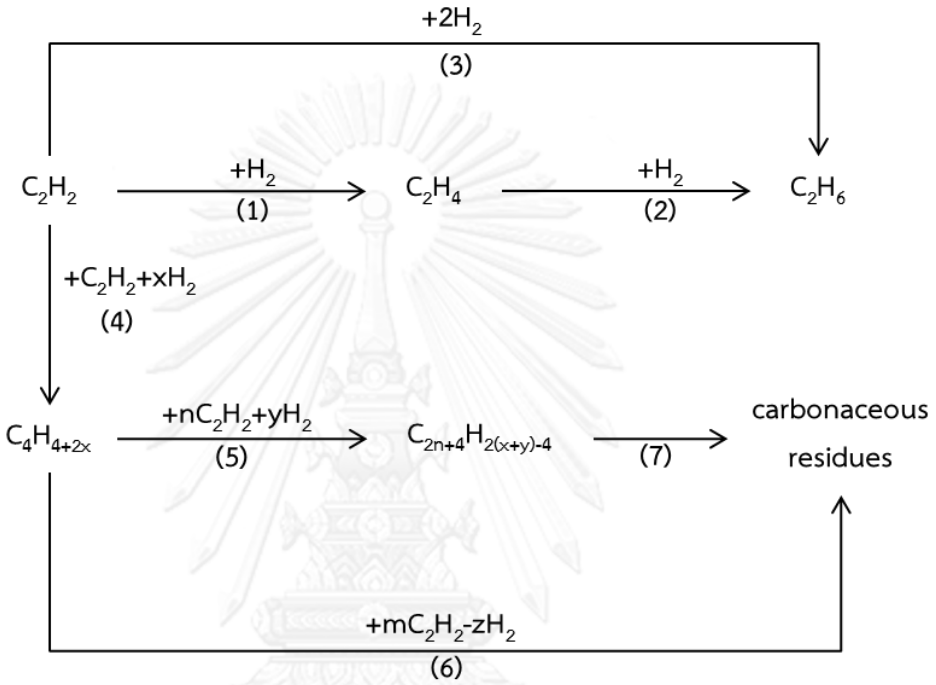

Figure 2.4 The network of the main reactions proceeding during acetylene hydrogenation in ethylene-rich streams. The reactions are denoted by numbers in the circles: 1) acetylene half-hydrogenation to ethylene, 2) ethylene hydrogenation to ethane, 3) acetylene hydrogenation to ethane, 4) hydro-oligomerization of acetylene to C_4 hydrocarbons (value x may be equal to: 0, 1, 2), 5) formation of C_{6+}hydro-oligomers of acetylene (value y may be equal to: 0, 1, 2, 3,. . . n), 6), and 7) formation of carbonaceous residues (value z may be equal to: 0, 1, 2, 3,. . . z).

In the partial catalytic hydrogenation of acetylenic compounds, the triple bond has to be converted into a double bond. In doing so, there arise the following problems of selectivity [66]:

a) The double bond which is formed can be further hydrogenated.

b) The double bond which is formed can be displaced (position isomerism).
c) The double bond which is formed can have cis or trans configuration (geometric isomerism).

Since acetylene only has two carbon atoms, the problems stated in (c) are not applicable. To achieve high selectivity, the catalyst must not further hydrogenate the partially hydrogenated product. This can be affected by two factors, the kinetics and the thermodynamic factors. Kinetic and thermodynamic effects are frequently combined, and they cannot readily be distinguished. Further, not only the catalyst but also the chemical structure can have an influence on the selectivity.

In case of the subsequent reactions (undesired reaction) proceeding much more slowly than the partial hydrogenation (desired reaction); the selectivity is then based on a mechanistic (kinetic) factor. Besides, the partially hydrogenated product can also be protected from subsequent reactions by being rapidly desorbed from the catalyst surface and then not being re-adsorbed again. This thermodynamically dependent selectivity is based on the triple bond being more strongly adsorbed than the corresponding double bond, because it is more electrophilic character. Even relatively small differences in the adsorption energy are sufficient for the acetylenic compound to immediately displace the primary resulting hydrogenation product from the catalyst surface and accordingly act as a "poison" for the subsequent reactions. The poisoning action is naturally only effective as long as the acetylenic compound is still present.

Acetylene itself is a good example of thermodynamically controlled selectivity. This can be proven from the effluence of a fixed bed palladium catalyst reactor, where the resulting ethylene only contains 1-5 % ethane although this catalyst have 10 to 100 times greater activity for the hydrogenation of ethylene than for the hydrogenation of acetylene [66].

2.2.2 The α-PdH to β-PdH transformation

Ethylene adsorption and the detailed mechanism of its hydrogenation on metal surfaces is still one of the most widely studied and debated problems in catalysis. The great complexities of hydrogenation of acetylene/ethylene mixtures

over palladium catalysts is the reason for slow progress in establishing a molecular mechanism for the process, and the nature and the types of active site. The role of carbonaceous species adsorbed on metal surfaces has been studied using various techniques. There are two main difficulties in these studies: (i) the existence of the pressure gap between studies on model catalysts and kinetic measurements on supported catalysts, (ii) the species active in hydrogenation reactions may be moderately adsorbed, so their surface coverage may be very low, whereas strongly adsorbed species, which are much easier to determine, may only play the role of spectator [67-69]. The catalytic process may proceed via several parallel and sequential steps on various specific types of active sites both on metal and support surfaces. An additional difficulty is connected with the various types of change that may occur in parallel to catalysts during use, such as phase transformations (Pd$\longrightarrow\beta$-PdHx and Pd$\longrightarrow$PdCx) and deposition of unreactive hydrogen-deficient polymeric species on the metal surface and in the catalyst's pores, which may affect the catalyst's properties [70]. Explanation of unusually high selectivity of palladium in hydrogenation of acetylene to ethylene is one of the most interesting questions addressed by this process.

When a palladium catalyst is stabilized during hydrogenation of acetylene or acetylene-ethylene mixtures, it undergoes fast and slow changes that modify its properties.

First, the palladium surface is immediately covered by associatively $[(C_2H_2)_{ad}]$ and dissociatively $[(C_2H)_{ad}]$ chemisorbed acetylene, and the half-hydrogenated state $(C_2H_3)_{ad}$ (ethylidyne) [71]. Secondly, the α-PdH$\longrightarrow\beta$-PdH phase transition may rapidly occur at room or higher temperatures and high hydrogen pressure [72]; and, thirdly, carbon is gradually incorporated into palladium lattice [73, 74] and acetylene-derived oligomers and polymers are covering the palladium [14, 75] as well as support surfaces [76, 77]. After about 4-24 hours a pseudo-steady state is achieved, but very slow deactivation of the catalyst proceeds as a result of deposition of coke (high polymer, perhaps graphitic, certainly with a low H/C ratio) in the catalyst pores [78, 79]. At the pseudo-steady state of the reaction carbonaceous deposits are present in the catalyst pores and the palladium surface is covered by a carbonaceous

overlayer, which consists of various species, such as: C_2H_x (x = 1, 2, and 3), and surface oligomers/polymers ($C_{2n}H_m$) [80].

Palladium has the specific ability to form a β-PdH phase at relatively low hydrogen pressures. The properties of palladium hydrides were widely investigated and described in several monographs and reviews [81]; the phase diagram of PdH system is shown in **Figure 2.5**. It represents the experimental relations between hydrogen pressure and concentration of hydrogen in PdH solution (H/M atomic ratio) derived from solid/gas equilibration studies at various temperatures.

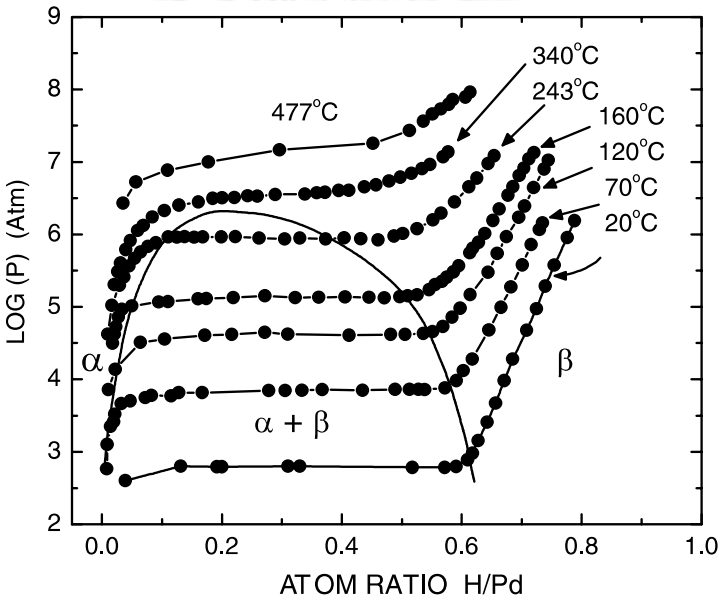

Figure 2.5 The phase diagram for PdH solutions. The numbers indicate the temperature in °C for given hydrogen sorption isotherms. The solid line enclosed the area of coexistence of α-PdH and β-PdH phases [82].

The presence of the β-PdH phase during the hydrogenation of alkynes or alkenes cannot be proved simply on the basis of thermodynamics of the palladium-hydrogen system. The reason is that the hydrogenations may consume hydrogen from the hydride, so the partial pressure of hydrogen must be increased to allow formation of the β-PdH phase. This decomposes (or forms) very fast, so it has to be

detected in situ, during the reaction. The amount of β-PdH phase present was assessed only by TPR measurements starting at room temperature after helium flushing, but of course the phase transformation may have occurred during the cooling and flushing. Interpretation of results obtained using catalysts having different palladium particle sizes is fraught with difficulty, as the pressure needed for hydride formation increases with decreasing size [83] and also the rate of decomposition of β-PdH phase for highly dispersed catalysts can be higher. Thus the β-PdH phase is more likely to have decomposed in the case of the more highly dispersed catalyst.

In summary, the studies of acetylene hydrogenation performed with in situ measurements of the extent of β-PdH phase formation are self-consistent and show that this phase is more active and less selective to ethylene than is the α-PdH phase.

2.3 Supported Pd catalyst in selective hydrogenation of acetylene

Sárkány, A. et al. [84] studied the hydrogenation of a mixture of 0.29 mol % C_2H_2, 0.44 mol % H_2 balanced by C_2H_4 as a reactant gas, they has been investigated on Pd-black and on various Pd/Al_2O_3 catalysts. Hydrogenation of C_2H_4 increased with time on stream for all the Al_2O_3-supported catalysts; the opposite behavior was noted with palladium black. Polymer formation was noted for all catalysts studied and also increased with time. It was recognized that a small number of C_2H_4 hydrogenation sites were located on the metal but the majority were on the polymer-covered support. The authors proposed that C_2H_4 adsorbed on the support and was hydrogenated there. Spillover hydrogen was tentatively identified as the source of hydrogen. Because of the parallelism between polymer formation and ethylene hydrogenation, it was proposed that the surface polymer served as a hydrogen pool or facilitated diffusion of hydrogen from Pd to the support.

Shin, E.W. et al. [43] synthesized supported Pd catalysts modified with Si deposited on the support by silane decomposition when used in acetylene hydrogenation; the Si-modified catalysts show higher selectivity for ethylene and produce less amount of green oil than unmodified Pd catalysts. They suggested that

Si covers the Pd surface as Si or SiO_2 patches. The Pd surface is diluted with the deposited Si. However, the electronic property of the Pd surface seems to be unaffected by the Si species. They conclude that improved performance of the Si modified catalysts comes mostly from geometric modification of the Pd surface by Si. Due to the adsorption strength of ethylene on Pd surface becomes weak and the amount of adsorbed hydrogen decreases [44]. The Si modification also reduces the amounts of surface hydrocarbons or carbonaceous species that are deposited on the catalyst either during the temperature programmed desorption (TPD) of ethylene or by surface reactions between co-adsorbed acetylene and hydrogen. The hydrocarbon deposited on the Si modified catalyst has a shorter chain length than those produced on the Pd-only catalyst. All these results are consistent with the improvement in ethylene selectivity on the Si-modified Pd catalyst, which has been explained based on the reaction mechanism of acetylene hydrogenation.

Kang, J.H. et al. [85] studied the effect of transition-metal oxides as promoter of the Pd catalyst foe acetylene hydrogenation. Transition-metal oxides added to Pd/SiO_2 improve significantly the activity and the ethylene selectivity of the catalyst in acetylene hydrogenation, which is caused by the interaction between the oxides and the Pd surface similar to case of the oxide-supported catalysts. They confirmed that metal oxide spread on and modify both geometrically and electrically the Pd surface after the catalyst is reduced at 500 °C. Such a behavior of metal oxides in the catalyst is correlated well with their promotional effect on the catalyst performance. They found that the oxide on the Pd surface retard the sintering of the dispersed Pd particles, suppresses the adsorption of ethylene in the multiply-bound mode and facilitates the desorption of ethylene produced by acetylene hydrogenation. Among the three metal oxides examined in this study, titanium oxide is found to have the most promotional effect.

Zhang, Q. et al. [3] studied an alloy of palladium and silver dispersed on Al_2O_3 for the selective hydrogenation of acetylene. They reported that the activity of Pd-Ag catalyst is lower than that of pure metal Pd catalyst. But the selectivity of Pd-Ag catalyst is higher and less impaired by temperature increase than that of Pd catalyst. They also found the metal Pd and Ag can form an alloy on the surface of

Al_2O_3. There synergetic effect in the hydrogenation of acetylene over Pd-Ag catalyst. Addition of Ag to Pd catalyst decreases the quantity of absorption hydrogen, and reduces absorption hydrogen spillover from the bulk of the metals to react with acetylene, which increases the selectivity of acetylene hydrogenation to ethylene.

Sárkány, A. et al. [12] investigated acetylene hydrogenation and formation of surface deposition on two series of Pd and Pd-Au/SiO_2 catalysts differing in the metal partical size (D = 0.47 and 0.08). Au was deposited via ionization of pre-adsorbed hydrogen over pre-reduced Pd/SiO_2 in order to ensure selective poisoning of the Pd surface. The non-steady-state regime of operation and the accumulation of hydro carbonaceous over layer were tested in pulse-floe experiments. They determined concentration of surface hydro carbonaceous deposits accumulated during different treatments by temperature programmed oxidation (TPO) They also observed hydrocarbon over layer to form immediately and its presence appeared to be a necessary requisite to get steady-state conversion and selectivity data. They suggested that a large excess of hydrogen suppressed the formation of carbonaceous lay down and increased the over-hydrogenation of acetylene. Presences of Au decreased the carbon coverage and improve the ethylene selectivity. Decoration of Pd by Au and the morphology of particles explain the ethylene selectivity improvement.

Zhang, Y. et al. [86] reported that Ag- and Au-Pd/SiO_2 bimetallic catalysts showed increased selectivity of acetylene conversion to form ethylene, rather than ethane, at high coverages. The catalyst performance results suggest that at high coverages of Ag or Au on Pd, that result in small ensembles of Pd sites, acetylene is adsorbed as a **π**-bonded species that favors hydrogenation to ethylene. At low coverages, where ensemble sizes of contiguous Pd surface sites are much larger, acetylene is strongly adsorbed as a multi-**σ**-bonded species, which preferentially forms ethane, lowering the selectivity to ethylene. Both kinetic analyses and the calculated turnover frequencies of acetylene conversion and ethane formation were consistent with the above explanation. The similar performance trends for Ag- and Au-Pd/SiO_2 suggest that the bimetallic effect for these catalysts is geometric and not electronic in nature

Kang, J.H. et al. [21] investigated the performance of TiO_2-modified Pd catalysts, containing TiO_2 either as an additive or as a support, in the selective hydrogenation of acetylene were investigated using a steady state reaction test. They reported that TiO_2 add Pd catalyst reduced at 500 °C (Pd-Ti/SiO_2/500 °C) shown a higher selectivity for ethylene production than ether the Pd/TiO_2 or Pd/SiO_2 catalyst. The amounts of chemisorbed H_2 and CO were significantly reduced and, in particular, the adsorption of multiply coordinated CO species was suppressed on Pd-Ti/SiO_2/500 °C, which is characteristic of the well-known strong-metal-support interaction (SMSI) phenomenon that has been observed with the TiO_2-support Pd catalyst reduced at 500 °C, Pd/TiO_2/500 °C. Moreover, XPS analyses of Pd-Ti/SiO_2/500 °C suggested an electronic modification of Pd by TiO_2, and the TPD of ethylene from the catalyst shown the weakening in the ethylene adsorption on the Pd surface. The 1,3-butadiene was produced in smaller amounts when using Pd-Ti/SiO_2/500 °C than when using Pd/SiO_2/500 °C, indicating that the polymerization of C_2 species leading to catalyst deactivation proceeds at slower rates on the former catalyst than on the latter. They also suggested that the enhanced ethylene selectivity on Pd-Ti/SiO_2/500 °C might be explained by correlating the catalyst surface properties with the mechanism of acetylene hydrogenation.

Kim, W.J. et al. [45] studied the deactivation behavior of Si-modified Pd catalysts in acetylene hydrogenation. TGA and IR analyses of green oil produced on the catalyst indicate that it is produced in smaller amounts and its average chain length is shorter on a Si-modified catalyst than on an unmodified one. The above findings are due to deposition of Si species on the Pd surface; such deposits effectively block multiply-coordinated adsorption sites on the catalyst and suppress the formation of green oil on the catalyst surface, specifically on or in the vicinity of Pd. The Si species also retard the sintering of Pd crystallites during the regeneration step and allow for the slow deactivation of the catalyst during acetylene hydrogenation, after regeneration. The improvement in the deactivation behavior of the Si-modified catalyst is believed to arise from the geometric modification of the Pd surface with small clusters of the Si species.

Panpranot, J. et al. [17] investigated catalytic performance for selective acetylene hydrogenation of nanocrystalline titania supports for Pd and Pd–Ag catalysts. Nanocrystalline titania prepared by thermal decomposition of titanium (IV) n-butoxide in two different solvents (toluene and 1,4-butanediol) at 320 °C. The titania products obtained from both solvents were pure anatase phase with relatively the same crystallite sizes and BET surface areas. However, due to different crystallization pathways, the number of Ti^{3+} defective sites as shown by ESR results of the titania prepared in toluene was much higher than the ones prepared in 1,4-butanediol. It was found that the use of anatase titania with higher defective sites as a support for Pd catalysts resulted in lower activity and selectivity in selective acetylene hydrogenation. However, this effect was suppressed by Ag promotion.

Kontapakdee, K. et al. [16] studied the effect of difference between anatase and rutile TiO_2 phase were used for supported Pd and Pd–Ag catalysts for selective hydrogenation of acetylene. It was found that Pd/TiO_2-anatase exhibited higher acetylene conversion and ethylene selectivity than rutile TiO_2 supported ones. However, addition of Ag to Pd/TiO_2-anatase catalyst resulted in lower ethylene selectivity while that of Pd/TiO_2-rutile increased. It is suggested that Ag addition suppressed the beneficial effect of the Ti^{3+} sites presented on the anatase TiO_2 during selective acetylene hydrogenation whereas without Ti^{3+}, Ag promoted ethylene selectivity by blocking sites for over-hydrogenation of ethylene to ethane.

2.4 Titanate nanotubes supported Pd in selective hydrogenation reaction

The properties of elongated morphology, high surface area render nanostructure titanate promising for many applications such as photocatalysis, hydrogen production and storage, solar cells, and catalyst support. Titanate nanotubes are used in heterogeneous catalytic process as supports. The high surface area of the support facilitates a high dispersity of the catalyst, while an open mesoporous structure provides an efficient transport of reagents and products.

The selective hydrogenation of o-chloronitrobenzene (o-CNB) over Pd supported titanate nanotubes catalyst was investigated by Sikhwivhilu, L. M. et at.

[87]. Titanate nanotube was synthesized by treating P-25 Degussa TiO_2 with a concentrated (18 M) KOH solution. The vapour-phase hydrogenation of o-CNB was performed in ethanol at 523 K and atmospheric pressure over a Pd/TiO_2 derived nanotube catalyst (Pd/TiO_2-M). The result showed that Pd/TiO_2-M gave complete conversion (100 %) of o-CNB with the selectivity to ortho-chloroaniline (o-CAN) of 86 % which higher than P-25 TiO_2 commercial supported Pd. The stability of the Pd/TiO_2-M catalyst was tested over 5 h during which time the conversion slowly dropped to 80 % (selectivity 93 %) due to catalyst poisoning. The TPR analysis revealed the existence of a strong palladium-support interaction and this was found to be crucial to the overall activity of the catalyst. In addition, Sikhwivhilu, L. M. et at. [88] synthesized nanotubular titanates by using a commercial TiO_2 (Degussa P25 containing anatase and rutile phases) and a base (KOH) solution at 120 °C for 20 h. Prior to the removal of KOH, the samples of TiO_2 were aged for three different time intervals (0, 2, and 61 days). Pd was loaded to the titanate support by wet impregnation with 1 wt% Pd content. The catalytic performance was tested in the gas-phase phenol hydrogenation reaction within the temperature range of 165-300 °C under atmospheric pressure. It was found that aging for 2 days showed the best activity (conversion 97 %) and total selectivity to cyclohexanone (99 %). The Pd (II) and Pd (0) catalysts supported on to titanate nanotubes ($H_2Ti_3O_7$) prepared by an ion-exchange technique was studied by Murciano, L. T. et al. [89]. The titanate nanotubes prepared by hydrothermal at 140 °C. The catalysts were characterised by narrow size distribution of metal nanoparticles on the external surface of the nanotubes. Pd (II) catalysts show high selectivity toward double-bond migration reaction versus hydrogenation in linear olefins. The Pd (II) was shown to be rapid reduced to Pd (0) by appropriate choice of solvent. Prereduced Pd (0) catalysts were found to be less active toward double-bond migration and more selective toward hydrogenation.

Recently, Putdee, S. et al. [33] investigated the catalytic performance of Pd nanoparticles supported on titania, titanate nanotubes, and nanowires in the liquid-phase selective hydrogenation of 1-heptyne. The titanate nanostructure synthesized with various hydrothermal treatment temperature in 10 M NaOH. They found that

the Pd catalysts supported on titanate nanotubes exhibited better performance in the liquid phase selective hydrogenation of 1-heptyne to 1-heptene than the ones supported on titanate nanowire and the commercial titania that consistent with amount of Pd active sites and highly dispersion from CO chemisorption result. They reported that the high surface area and porosity of nanotubular catalysts promise to be advantageous for catalytic activity.

2.5 Comments on previous studies

From the previous studies, hydrothermal method is suitable route for synthesis of titanate nanotubes. Reaction temperature, reaction time, concentration of NaOH, and size of raw TiO_2 powder were considered as the predominant factors in the formation of nanotubes. In the selective hydrogenation of acetylene, supported Pd catalyst is employed for this reaction due to its high activity and selectivity and the common supports used for Pd catalysts include SiO_2, Al_2O_3, and TiO_2. However, many researches have found that Pd/TiO_2 exhibited higher activity and selectivity in hydrogenation of acetylene and also suppress the formation of green oil on the catalyst surface. In addition, their Si-modified catalysts show higher selectivity for ethylene and produce less amount of green oil than unmodified Pd catalysts. Recently, the titanate nanotube supported Pd has been reported that exhibited better performance in the liquid phase selective hydrogenation of 1-heptyne to 1-heptene. Nevertheless, it has not been reported in gas phase selective hydrogenation of acetylene. Moreover, the SiO_2-modified titanate nanotubes supported catalyst also has not been reported as well. Thus, the purpose of this study is to investigate the formation and characterization of titanate nanotubes and its silica-modified. The catalytic performance of titanate nanotubes supported Pd catalyst for selective hydrogenation of acetylene to ethylene is also obtained.

CHAPTER III

THEORY

3.1 Titanium dioxide

3.1.1 Physical and chemical properties

Titanium (IV) oxide occurs naturally in three crystalline forms:

1. Anatase, which tends to be more stable at low temperatures. Anatase TiO_2 generally exhibits a higher activity in hydrogenation and photocatalytic than other types of titanium dioxide. The three forms of titanium (IV) oxide have been prepared in laboratories but only rutile, the thermally stable form, has been obtained in the form of transparent large single crytal. The transformation from anatase to rutile is accompanied by the evolution of ca. 12.6 kJ/mol (3.01 kcal/mol), but the rate of transformation is greatly affected by temperature and the presence of other substances, which may either catalyze or inhibit the reaction. The lowest temperature at which transformation from anatase to rutile takes place at a measurable rate is around 700 ℃, but this is not a transition temperature. The change is not reversible since ΔG for the change from anatase to rutile is always negative.

2. Brookite, which is usually found only in minerals and has a structure belonging to orthorhombic crystal system. Brookite has been produced by heating amorphous titanium (IV) oxide, which is prepared from an alkyl titanate or sodium titanate, with sodium or potassium hydroxide in an autoclave at 200 to 600 ℃ for several days.

3. Rutile, which tends to be more stable at high temperature and thus is sometimes found in igneous rocks. The titanium dioxide use in industrial products, such as paint, is almost a rutile type. These crystals are substantially pure titanium dioxide but usually amount of impurities, e.g., boron, Magnesium or calcium, which darken them. The important commercial forms of titanium (IV) oxide are anatase and

rutile, and they can readily be distinguished by X-ray diffractometry. A summary of crystallographic properties and crystal structures of the three varieties is given in **Table 3.1** and **Figure 3.1.**

Table 3.1 Crystallographic properties of anatase, brookite, and rutile.

Properties	Anatase	Bookite	Rutile
Crystal structure	Tetragonal	Orthorhombic	Tetragonal
Optical	Uniaxial, negative	Biaxial, positive	Uniaxial, negative
Density (g/cm3)	3.9	4.0	4.23
Harness (Mohs scale)	5½ - 6	5½ - 6	7 - 7½
Unit cell	D_4a^{19} . $4TiO_2$	D_2h^{15} . $8TiO_2$	D_4h^{12} . $3TiO_2$
Dimension (nm)			
a	0.3758	0.9166	0.4584
b		0.5436	
c	0.9514	0.5135	2.953

The three allotropic forms of titanium dioxide have been prepared artificially but only rutile, the thermally stable form, has been obtained in the form of transparent large single crystal. The transformation from anatase to rutile is accompanied by the evolution of ca. 12.6 kJ/mol (3.01 kcal/mol), but the rate of transformation is greatly affected by temperature and by the presence of other substance which may either catalyze of inhibit the reaction. The lowest temperature at which conversion of anatase to rutile takes place at a measurable rate is ca. 700 °C, but this is not a transition temperature. The change is not reversible; ΔG for the change from anatase to rutile is always negative.

Although anatase and rutile are both tetragonal, they are not isomorphous. The two tetragonal crystal types are more common because they are easy to make. Anatase occurs usually in lnear-regular octahedral, and rutile forms slender prismatic crystal, which are frequently twinned. Rutile is the thermally stable form and is one of the two most important ores of titanium.

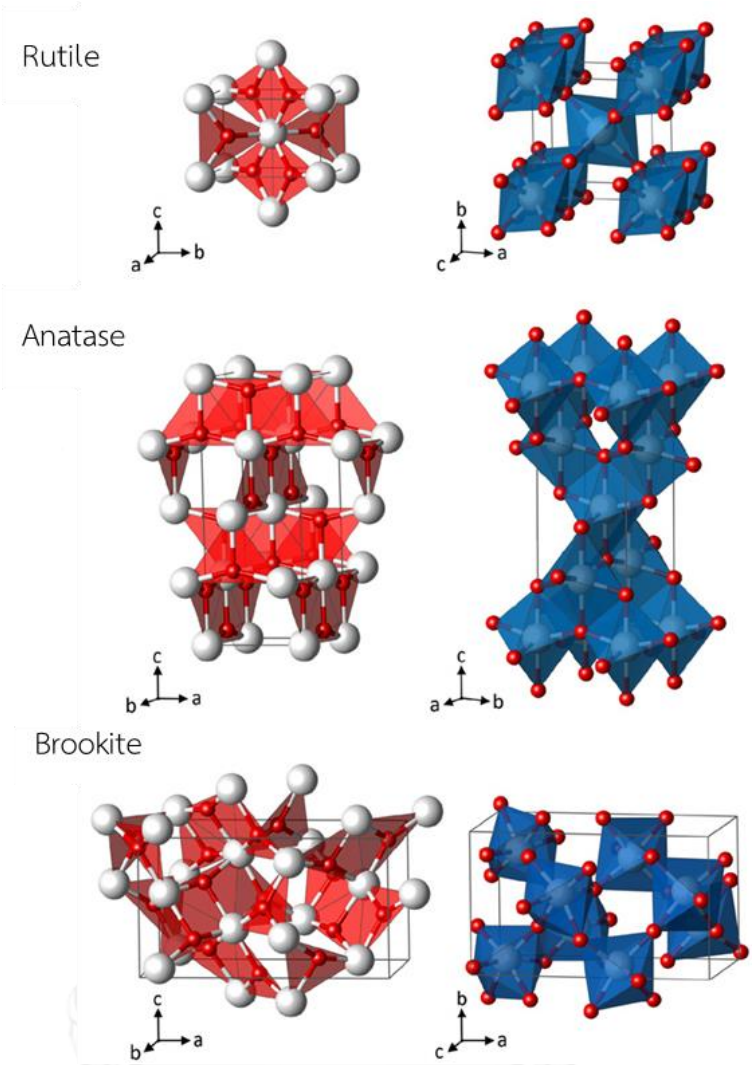

Figure 3.1 Crystal structures of titanium dioxide in rutile, anatase and brookite [90].

Since both anatase and rutile are tetragonal, they are both anisotropic, and their physical properties, e.g. refractive index, vary according to the direction relative to the crystal axes. In most applications of these substances, the distinction between crystallographic directions is lost because of the random orientation of large numbers of small particles, and it is mean value of the property that is significant.

Measurement of physical properties, in which the crystallographic directions are taken into account, may be made of both natural and synthetic rutile, natural anatase crystal, and natural brookite crystals. Measurement of the refractive index of titanium dioxide must be made by using a crystal that is suitably orientated with

respect to the crystallographic axis an as a prism in a spectrometer. Crystals of suitable size of all three modifications occur naturally and have been studied. However, rutile is the only form that can be obtained in large artificial crystals form melts. The refractive index of rutile is 2.75. The dielectric constant of rutile varies with direction in the crystal and with any variation from the stoichiometric formula, TiO_2; an average value for rutile in powder form is 114. The dielectric constant of anatase powder is 48.

Titanium dioxide is thermally stable (mp 1855 °C) and very resistant to chemical attack. When it is heated strongly under vacuum, there is a slight loss of oxygen corresponding to a change in composition to $TiO_{1.97}$. The product is dark blue but reverts to the original white color when it is heated in air.

Hydrogen and carbon monoxide reduce it only partially at high temperatures, yielding lower oxides or mixtures of carbide and lower oxides. At ca. 2000 °C and under vacuum, carbon reduces it to titanium carbide. Reduction by metal, e.g., Na, K, Ca, and Mg, is not complete. Chlorination is only possible if a reducing agent is present; the position of equilibrium in the system is the reactivity of titanium dioxide towards acid is very dependent on the temperature to which it has been heated. For example, titanium dioxide that has been prepared by precipitation from a titanium (IV) solution and gently heated to remove water is soluble in concentrated hydrochloric acid. If the titanium dioxide is heated to ca. 900 °C, then its solubility in acids is considerably reduced. It is slowly dissolve in hot concentrate sulfuric acid, the rate of salvation being increased by the addition of ammonium sulfate, which raises the boiling point of the acid. The only other acid in which it is soluble is hydrofluoric acid, which is used extensively in the analysis of titanium dioxide for trace elements. Aqueous alkaline have virtually no effect, but molten sodium and potassium hydroxides, carbonates, and borates dissolve titanium dioxide readily. An equimolar molten mixture of sodium carbonate and sodium borate is particularly effective as is molten potassium pyrosulfate.

$$TiO_2 + 2Cl_2 \longleftrightarrow TiCl_2 + O_2$$

3.2 Titanate nanotubes

Titanium dioxide (TiO_2) is an exceptional material that has many promising applications as a catalyst, catalyst support, photocatalysis, solar cells, and sensors [25-29]. A main limitation to the use of TiO_2 obtained by conventional methods is its low surface area. There are some ways to be studied for obtaining TiO_2 with larger surface area. Recently, titanate nanotubes, nanobelts, nanowires and nanorods have received much attention because of the wide applications and relatively simple preparation procedures needed to fulfill the requirements of various applications. One-dimensional single-crystalline Ti-O based nanomaterials have properties that compare with nanoparticles titania but possess a high surface-to-volume ratio as well [91]. Various morphologies types of titanate nanostructure are show in **Figure 3.2**.

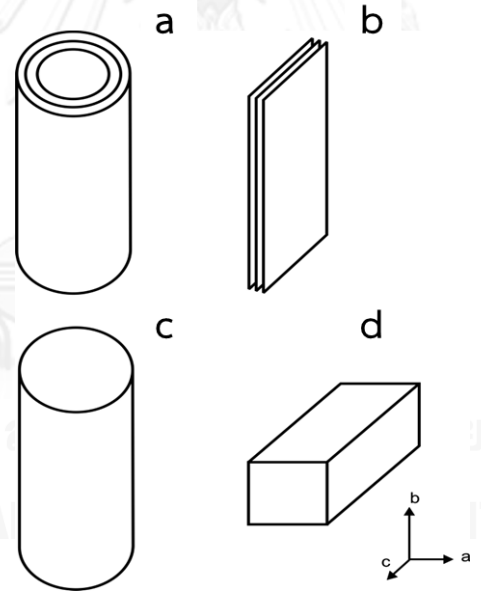

Figure 3.2 Four different morphologies observed during alkaline hydrothermal reaction of TiO_2. Nanotubes (a), nanosheets (b), nanorods or nanowires (c), and nanofibers, nanoribbons, or nanobelts (d) [92].

3.2.1 Synthesis method

Over the past few years, many methods have been developed for the successful fabrication of one-dimensional TiO_2 nanomaterials as show a timeline describing the development in **Figure 3.3**, including the hydrothermal method, the sol-gel method, template-based synthetic approaches and electrochemical synthesis. Hoyer first reported TiO_2-based nanotubes via the template-assisted method. Thereafter, electrochemical anodic oxidation and hydrothermal treatment succeeded in fabricating titanate nanotubes. Each fabrication method can have unique advantage sand functional features and comparisons among these three approaches have been compiled in **Table 3.2**. Regarding the template-assisted method, anodic aluminum oxide (AAO) nanoporous membrane, which consists of an array of parallel straight nanopores with uniform diameter and length, is usually used as template. The scale of TNTs can be moderately controlled by applied templates. However, the template-assisted method often encounters difficulties of prefabrication and post-removal of the templates and usually results in impurities [93]. Concerning electrochemical anodic oxidation, the self-assembled TiO_2 nanotubes (π -TiO_2) with highly ordered arrays was discovered by Grimes' group, and the method is based on the anodization of Ti foil to obtain nanoporous titanium oxide film. They also demonstrated the crystallization and structure stability of π-TiO_2. The comprehensive reviews associated with the fabrication factors, characterizations, formation mechanism, and the corresponding applications of TiO_2-based nanotubes arrays have been also conducted by Grimes' group. These methods, other than the hydrothermal process, are either not suitable for large scale production or not able to yield very low dimensional, well separated, crystallized nanotubes. The demonstrated architecture of TiO_2-based nanotubes constructed via the hydrothermal treatment is capable of good crystalline formation and establishment of a pure-phase structure in one step in a tightly closed vessel.

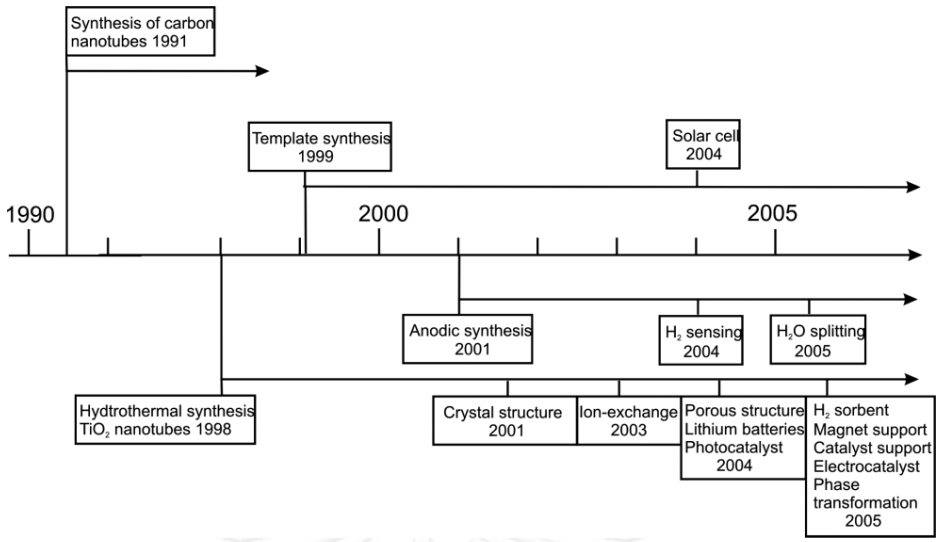

Figure 3.3 Simplified timeline describing the development of TiO_2 nanotubular structures [92].

Among the aforementioned fabrication approaches, both electrochemical anodic oxidation and hydrothermal treatment received wide investigation, owing to their cost-effective, easy route to obtain nanotubes, and the feasibility/availability of wide spread application.

For hydrohermal method, Kasuga et al. first discovered this route for the synthesis titanium oxide nanostructures having a tubular shape in 1998 [23]. The search for nanotubular materials was inspired by the discovery of carbon nanotubes by Iijima et al. in 1991. The TiO_2 nanotubes have a large specific surface area of ~ 400 m^2/g.

3.2.2 Structure

Ti-O based nanotubes are thought to be caused by scrolling of an exfoliated TiO_2-derived nanosheet into a hollow multiwall nanotube with spiral cross section. Unlike carbon nanotubes produced by the catalytic pyrolysis of hydrocarbons, titania nanotubes produced via the alkaline hydrothermal method have never been observed in single layer form. All reports of TiO_2 nanotubes describe the samples as multilayer-walled nanotubular structures. The number of layers varies from two to ten. They are open-ended with several wall layers on both sides [91].

Table 3.2 Comparisons of current methods in titanate nanotubes fabrication [93].

Fabrication method	Advantages	Disadvantage
Template-assisted method	- The scale of nanotube can be moderately controlled by applied template	- Complicated fabrication process - Tube morphology maybe destroyed during fabrication process
Electrochemical anodic oxidation method	- More desirable for practical applications - Feasible for extensive application - Ordered alignment with high aspect ratio	- Mass production is limited - Highly expense of fabrication apparatus
Hydrothermal method	- Easy route to obtain nanotube morphology - Feasible for extensive applications	- Long reaction duration is needed - Highly concentrated NaOH must be added

Up to now, several possible crystal structures of nanotubular products from the alkaline hydrothermal treatment of TiO_2 have been proposed, including hydrogen titanate $H_2Ti_3O_7$, orthorhombic titanates $Na_2Ti_2O_4(OH)_2$, tetratitanates $H_2Ti_4O_9$, and monoclinic TiO_2-B [91, 94, 95]. The exact determination of crystal structures of nanotubes is still incomplete because of several intrinsic difficulties posed by the nanostructures, including their small crystallite size and the wrapping of the structures along a certain crystallographic axis, both resulting in broadening of the diffraction signals. The low weight of hydrogen atoms also results in difficulties in locating their precise positions and population inside the crystals. From literature surveys, the chemical composition of $Na_xH_{2-x}Ti_3O_7$ and $Na_xH_{2-x}Ti_2O_4(OH)$ groups were more acceptable than other structures. The lattice parameters for each chemical structure of titanate nanotubes are shown in **Table 3.3**.

Table 3.3 Proposed chemical structures of titanate nanotubes and their corresponding lattice parameters [93].

Chemical structure	Lattice parameters
Anatase TiO_2	Tetragonal; a = 3.79 nm, b = 3.79, c = 2.38
$N_2Ti_3O_7$, $Na_xH_{2-x}Ti_3O_7$	Monoclinic; a = 1.926 nm, b = 0.378, c = 0.300, β = 101.45°
$H_2Ti_2O_4(OH)_2$, $Na_2Ti_2O_4(OH)_2$	Orthorhombic; a = 1.808 nm, b = 0.379, c = 0.299
$H_xTi_{2-x/4}\square_{x/4}O_4$ (H_2O)	Orthorhombic; a = 0.378 nm, b = 1.874, c = 0.298
$H_2Ti_4O_9$ (H_2O)	Monoclinic; a = 1.877 nm, b = 0.375, c = 1.162, β = 104.6°

$\square$ indicates a vacancy.

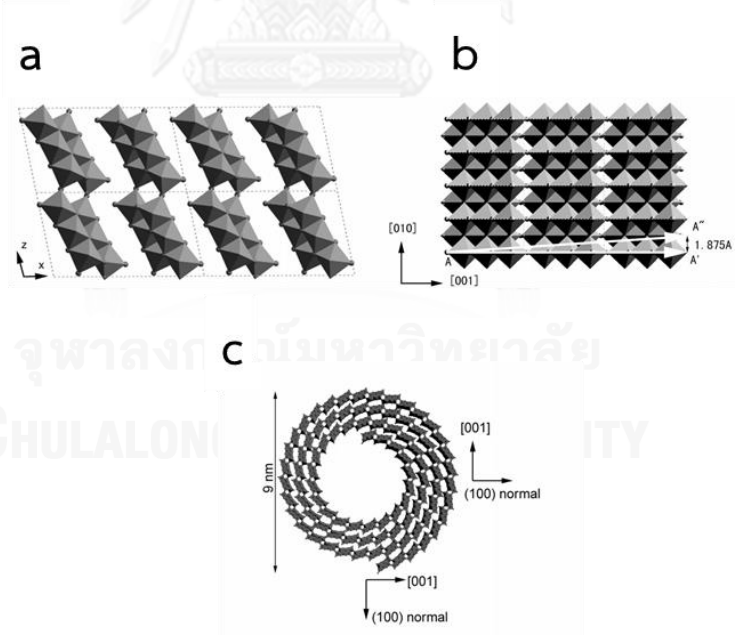

Figure 3.4 Structure models of $H_2Ti_3O_7$ (a) unit cells on the [010] axis, (b) layer of $H_2Ti_3O_7$ on the (100) plane and (c) the structure of trititanate nanotubes.

Peng and co-workers [96, 97] A schematic showing the crystal structure of monoclinic trititanic acid in a TiO_6 edge-sharing octahedron representation are shown in **Figure 3.4**, the three different projections corresponding to crystallographic axes. A nanotubular morphology of layered trititanic acid can be obtained by rolling several (100) planes around axis [010] or [001]. It has been proposed that rolling of the plane occurs around the [010] axis such that the axis of the nanotube is parallel to the y-axis of monoclinic $H_2Ti_3O_7$. [30] Recently, Wu, D. et al. [98] have proposed that rolling of the (100) plane could occur around axis [001]. In both cases, the walls of the nanotubes consist of several layers, typically separated by 0.72 nm. The structure of each layer corresponds to the structure of the (100) plane of monoclinic titanates, which is a set of closely packed TiO_6, edge-sharing octahedral.

3.2.3 Mechanism of titanate nanotube formation by hydrothermal method

Several researchers have studied the mechanism of titanate nanotubes formation by using both theoretical and experimental. There is a general agreement that the reaction proceeds through several stages are shown in **Figure 3.5** [91, 94, 99]:

1. Slow dissolution of raw TiO_2 accompanied by epitaxial growth of layered nanosheets of sodium titanates.
2. Exfoliation of the nanosheets
3. Folding of the nanosheets into tubular structures (seeds).
4. Growth of the nanotubes along the axis.
5. Exchange of sodium ions by protons during washing and separation of nanotubes.

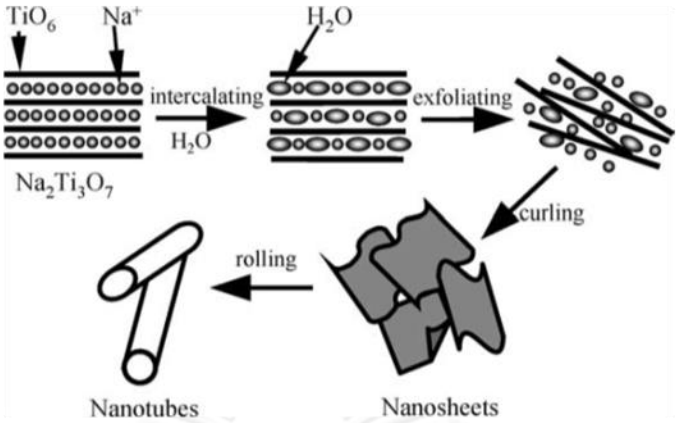

Figure 3.5 Schematic exfoliating-rolling model of nanotubes formation from the layered $Na_2Ti_3O_7$ [100].

3.3 Palladium metal

Palladium as a group VIII noble metal has unique catalytic properties in homogeneous and in heterogeneous reactions, that has the physical properties as in **Table 3.4**. In heterogeneous catalysis palladium is used for oxidation and hydrogenation reactions. One of the most remarkable properties of palladium is the ability to dissociate and dissolve hydrogen. Atomic hydrogen occupies the octahedral interstices between the Pd atoms of the cubic-closed packed metal. Palladium can absorb up to 935 times of its own volume of hydrogen.

Palladium can be used for hydrogenation of unsaturated hydrocarbons. Palladium shows the highest selectivity of group VIII metals in heterogeneously catalyzed semi-hydrogenation of alkynes and dienes to the corresponding alkenes. Activity of palladium for hydrocarbon hydrogenation is based on the ability for the dissociative adsorption of hydrogen and chemisorption of unsaturated hydrocarbons. Palladium shows a strong deactivation behavior because of hydrocarbon and carbon deposits. For heterogeneous system in particular catalyst performance is strongly influence by, firstly the ability to get reactant to the active sites, then to establish the optimum hydrogen-to-hydrocarbon surface coverage, and, finally, the rapid removal of the hydrogenated products.

Table 3.4 Some physical properties of palladium.

Atomic number	46
Atomic weight	106.42
Atomic diameter	275.2 pm
Melting point	1827 K
Crystal structure	Cubic closed packed
Electron configuration	$[Kr]4d^{10}$

3.4 Selective hydrogenation of acetylene

Generally, there are two primary reactions proceeding during acetylene hydrogenation:

$$C_2H_2 + H_2 \xrightarrow{k_1} C_2H_4 \qquad \Delta H = -42{,}000 \text{ kcal/kmol} \qquad (3.1)$$

$$C_2H_4 + H_2 \xrightarrow{k_2} C_2H_6 \qquad \Delta H = -32{,}900 \text{ kcal/kmol} \qquad (3.2)$$

The first reaction (3.1) is the desired reaction whereas the second reaction (3.2) is an undesired side reaction due to the consumption of ethylene product. There is also a third reaction occurring during normal operation, which adversely affects the catalyst performance, i.e., the polymerization reaction of C_2H_2 with itself to form a longer chain molecule, commonly called “green oil”.

$$C_2H_2 + (n)C_2H_2 \xrightarrow{k_3} C_xH_x \qquad \text{(polymer or green oil)} \qquad (3.3)$$

According to the above reactions involving acetylene hydrogenation, two influencing parameters on the desired reaction can be assigned. The first parameter is reaction temperature, which has a direct relationship with the kinetics of the system. However, it affects not only the reaction rate of the desired reaction (k_1), but

also the rate of ethylene hydrogenation (k_2). The rate of polymerization (k_3) also increases with temperature and the resulting green oil can affect catalyst activity by occupying active sites. When the catalyst is new or has just been regenerated, it has high activity. With time on stream, activity declines as the catalyst become fouled with green oil and other contaminants. By the end-of-run (EOR), the inlet temperature must be increased (25-40 °C) over start-of-run (SOR) inlet temperature in order to maintain enough activity for complete acetylene removal. In order to selectivity hydrogenate acetylene, it is critical to maintain the differential between the activation energy of reaction (eq. 3.1) and (eq. 3.2). However, it is desirable that the ethylene remains intact during hydrogenation. Once energy is supplied to the system over a given catalyst by increasing the temperature, the differential between the activation energies disappears and complete removal of acetylene, which generally has the lower partial pressure, becomes virtually impossible. In other words, higher temperature reduces selectivity; more hydrogen is used to convert ethylene to ethane, thereby increasing ethylene loss. The inlet temperature should therefore be kept as low as possible while still removing acetylene to specification requirements. Low temperatures minimize two undesirable side reactions and help optimize the converter operation.

Another crucial parameter affecting the selectivity of the system is the ratio between hydrogen and acetylene (H_2 : C_2H_2). Theoretically, the H_2 : C_2H_2 ratio would be 1:1, which would mean that no hydrogen would remain for the side reaction (eq. 3.2) after acetylene hydrogenation (eq. 3.1). However, in practice, the catalyst is not 100% selectivity and the H_2 : C_2H_2 ratio is usually higher than 1:1 to get complete conversion of the acetylene. As hydrogen is one of the reactants, the overall acetylene conversion will increase with increasing hydrogen conversion. Increasing the H_2 : C_2H_2 ratio can have a cost in selectivity which leads to ethylene loss. Typically, the H_2 : C_2H_2 ratio is between 1.1 and 2.5 [101, 102].

The mechanism of acetylene hydrogenation involves four major paths as shown in **Figure. 3.6.** Part I is the partial hydrogenation of acetylene to ethylene, which is either desorbed as a gaseous product or further hydrogenated to ethane via Part II. It previously was proposed that Part I proceeds mostly on Pd sites, which are

covered to a great extent with acetylene under typical industrial reaction conditions, and Part II occurs on support sites, particularly those covered with polymer species.

Consequently, selectivity may be improved by reducing both the strength of ethylene adsorption on Pd and the amount of polymer, which accumulates on the catalyst. One of the methods for improving selectivity is to maintain a low H_2 : C_2H_2 ratio in the feed stream such as the low hydrogen concentration on Pd retards the full hydrogenation of the ethylene spicies on the Pd surface. However, this method has the drawback of accelerating the polymer formation and therefore the H_2 : C_2H_2 ratio must be managed deliberating or sometimes controlled in two step. Part III, which allows for the direct full hydrogenation of acetylene, becomes negligible at high acetylene coverage and low hydrogen partial pressures. Ethylidyne was suggested as an intermediate in Part III but was later verified to be a simple spectator of surface reactions. Path IV, which allow for the dimerization of the C_2 species, eventually leads to the production of green oil and the subsequent deactivation of the catalyst. Polymer formation lowers ethylene selectivity because it consumes acetylene without producing ethylene and, in addition, the polymer species, which is usually located on the support, acts as a hydrogen pool, thus promoting ethane formation [21].

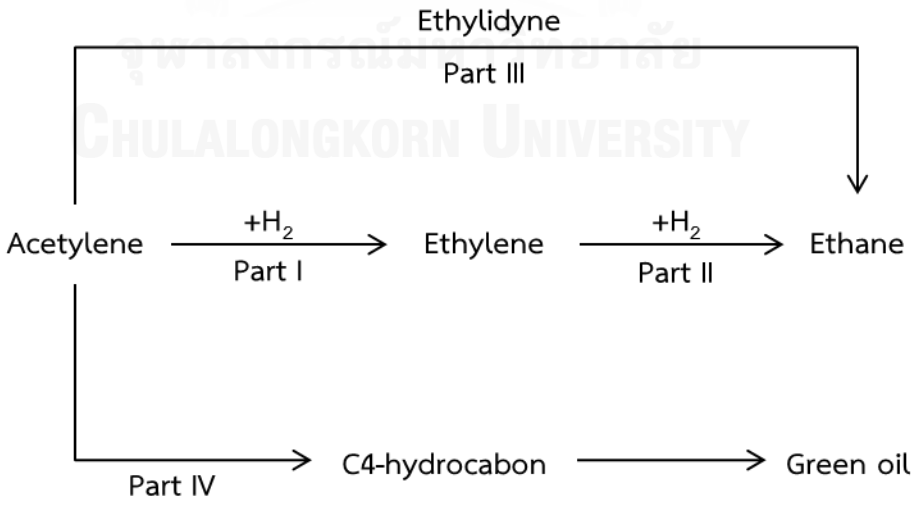

Figure 3.6 Major reaction path of acetylene hydrogenation.

Considering the mechanism of acetylene hydrogenation described above, it was found that ethylene selectivity is improved when the C_2 species produced by Path I is readily desorbed from the catalyst surface and the other path are simultaneously retards.

CHAPTER IV

EXPERIMENTAL

This chapter describes the experimental procedure used in this research, which can be divided into three sections. The first part explains support and catalyst preparation. The reaction study in selective hydrogenation of acetylene is explained in second part. Finally, the properties of the catalyst characterized by various techniques are discussed in section three.

4.1 Catalyst preparation

This research focuses on the silica modified titanate nanotubes from the hydrothermal method for supported Pd; therefore, the details of preparation procedure is important because of minimize the formation of surface oligomers and undesirable products of acetylene hydrogenation.

4.1.1 Chemicals

The support and metal precursors used for the catalyst preparation are listed in **Table 4.1**.

Table 4.1 Details of chemical reagents used for the catalyst preparation.

Chemical	Formula	Manufacturer
1. Titanium(IV) oxide, anatase ≥ 99%	TiO_2	Sigma-Aldrich
2. Sodium hydroxide, ≥ 99%	NaOH	Merck
3. Hydrocalic acid, 37%	HCl	QReC
4. Tetraethyl orthosilicate, 98%	$SiC_8H_{20}O_4$	Sigma-Aldrich
5. Palladium(II) acetate, 98%	$Pd(CH_3CO_2)_2$	Sigma-Aldrich
6. Acetonitrile, ≥ 99%	C_2H_3N	Fisher Chemical

4.1.2 Preparation of titanate and silica modified supports

Preparation of titanate nanotubes was carried out by hydrothermal method using anatase TiO_2 as a starting material. Firstly, 1.5 g of TiO_2 powder was mixed with 40 ml of 10 M NaOH and modified by containing different amounts of tetraethyl orthosilicate with various Ti/Si ratios including 95:5, 90:10, 80:20 and 50:50 mol% then the mixture was sonicated for 10 min. Thereafter the mixture was transferred to a Teflon-lined stanless steel autoclave, and heated at 150 ℃ for 24 h. in oven. After hydrothermal reaction, the autoclave was cooled to room temperature by natural cooled down. Then the sample was washed with 0.1 M HCl for several times and followed by de-ionized water until pH value approached deionized water. Finally, the sample was dried at 110 ℃ for 24 h. The dried powder was calcined in air at 450 ℃ with a heating rate of 10 ℃/min for 2 h.

4.1.3 Preparation of titanate supported Pd catalysts

The titanate supported Pd catalysts were prepared by an incipient wetness impregnation method through using Palladium(II) acetate as the Pd precursor and acetonitrile as a solvent with Pd loading of ca. 1 wt%. A gram of titanate support was placed in a ceramic cup then the palladium solution was gradually dropped into the support. Blending the support continuously during impregnation was required to ensure the homogenous distribution of Pd metal on the support. Then the impregnated catalyst was stood at room temperature for 6 h, dried at 110 ℃ in an oven overnight, the catalyst was calcined air at 450 ℃ with a heating rate of 10 ℃/min for 3 h.

4.2 Catalyst evaluation

The catalytic performance for the selective hydrogenation of acetylene was investigated using a volumetric flow rate of 10 cm^3/min. A temperature programmed reaction was conducted from 40 to 100 ℃. Materials, apparatus and operating procedures are detailed as follow:

4.2.1 Chemicals

The reaction study was carried out using a gas feed compositions of 1.5 mol% acetylene and 1.68 mol% hydrogen in balanced with ethylene. For reduction process was used ultra high purity hydrogen as a reduce gas and high purity argon as a cooling gas. All of the gases were supplied by the Linde (Thailand) Public Company Limited.

4.2.2 Apparatus

The catalytic test was performed in a flow system as shown diagrammatically in **Figure 4.1**. The apparatus consisted of a glass tubular reactor, electrical furnace and an automation temperature controller. The instruments used in this system are listed and explained as follow:

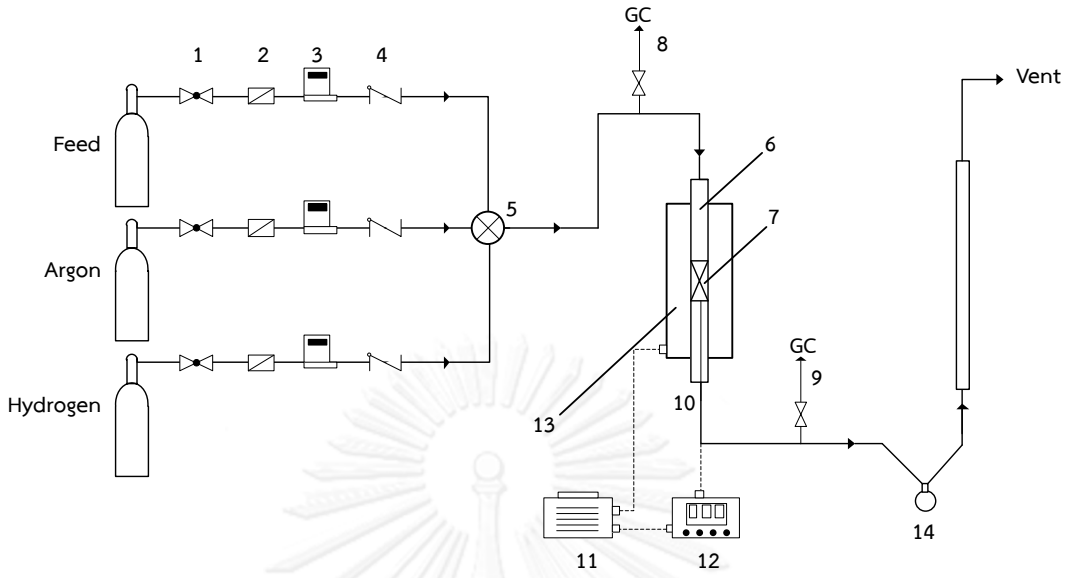

1. On-off valve
2. Filter
3. Mass flow controller
4. Check valve
5. 4-ways fitting
6. Reactor
7. Catalyst bed
8. Sampling point (feed)
9. Sampling point (product)
10. Thermocouple
11. Variable voltage transformer
12. Temperature controller
13. Electric furnace
14. Bubble flow meter

Figure 4.1 Flow diagram of the selective hydrogenation of acetylene.

4.2.2.1 Reactor

The reaction was performed in a conventional glass tubular reactor (inside diameter of 0.9 cm) at atmospheric pressure.

4.2.2.2 Automation temperature controller

This unit consisted of a magnetic switch connected to a variable transformer and a thermal overload relay (HITACHI, TR1 2B-1E, AC 600 V) linked to a temperature controller (Shinks, ECS, 220-R/E) in which connected to a thermocouple attached to the catalyst bed in a reactor. A dial setting established a set point at any

temperature within the range between 0 and 999 °C. The accuracy was of ± 2 °C.

4.2.2.3 Electrical furnace

The furnace supplied the required temperature to the reactor which could be operated from room temperature up to 500 °C at maximum voltage of 220 volts.

4.2.2.4 Gas controlling system

Reactant, hydrogen and argon for the system were each equipped with a pressure regulator and on-off valve and the gas flow rates were adjusted by using mass flow controller (AALBORG, GFC).

4.2.2.5 Gas chromatograph

The products and feeds were analyzed by a gas chromatograph equipped with a FID detector (SHIMADZU FID GC 8APF, carbosieve column S-II) for separating CH_4, C_2H_2, C_2H_4 and C_2H_6. H_2 was analyzed by a gas chromatograph equipped with a TCD detector (SHIMADZU TCD GC 8APT, molecular sieve 5A). The operating conditions for each instrument are summarized in **Table 4.2.**

Table 4.2 Operating condition of gas chromatograph.

Gas chromatograph	SHIMADZU FID GC 8A	SHIMADZU TCD GC 8A
Carrier gas	Ultra high purity Ar	Ultra high purity N_2
Carrier gas flow rate (ml/min)	40-60	40-60
Injector temperature (°C)	180	80
Initial column temperature (°C)	100	50
Programmed rate (°C/min)	10	-
Final column temperature (°C)	160	50
Current (mA)	-	70

4.2.3 Procedures

The catalyst was packed in a glass tubular down flow reactor by setting up catalyst bed length was about 9 mm. The reactor was placed into the furnace and argon was introduced into the reactor in order to remove remaining air. Prior to the start of each experimental run, the catalyst was reduced in situ with 100 ml/min hydrogen by heating from room temperature to 150 °C at a heating rate of 10 °C/min and held at that temperature for 2 h. Then the reactor was purged with argon and cooled down to the initial reaction temperature of 40 °C.

The reaction was carried out using a feed composition of 1.5 mol% acetylene, 1.68 mol% hydrogen, and balanced ethylene with a various reaction temperature from 40 to 100 °C and 1 atm. At each condition, sampling was undertaken when the steady state of the system was reached, which was approximately within 1 h. Effluent gases were analyzed by a gas chromatographs equipped with a FID detector (SHIMADZU FID GC 8A, carbosieve column S-II) and TCD detector (SHIMADZU TCD GC 8A, molecular sieve-5A).

4.3 Catalyst Characterization

Various characterization techniques were used in this study in order to clarify the catalyst structure, the morphology and the surface composition. The various silica content modified titanate nanotubes supported Pd catalysts were characterized by various techniques are discussed below.

4.3.1 N_2 Physisorption

The BET surface areas of the titanate supports were measured by N_2 physisorption, with nitrogen as the adsorbate using a Micrometritics model ASAP 2000 automated system degassing at 200 °C for 1 h prior to N_2 physisorption. Calculations were performed on the basis of the BET (Stephen Brunauer-Paul Hugh Emmett-Edward Teller) isotherm for specific surface area and pore size distribution was calculated by BJH (Barrett-Joyner-Halenda) desorption branch analysis. Specific pore volume was determined from the single point adsorption total pore volume of pores

at relative pressure (P/P_0) <0.99 and the average pore diameter was calculated from BJH desorption branch.

4.3.2 X-ray Diffraction (XRD)

The crystallinity, structure and composition of the titanate supports and Pd catalysts showed by X-ray diffraction (XRD) pattern were carried out using ex situ employing an X-ray diffractometer, BRUKER D8 ADVANCE, with Cu Kα radiation with a Ni filter in the 2θ range of 10° to 90° and resolution of 0.02°.

4.3.3 Transmission Electron Microscopy (TEM)

The distribution of palladium on titanate supports were observed using JEOL Model JEM-2010 transmission electron microscope operated at 200 keV at the National Metal and Materials Technology Center (MTEC). The sample powder was dispersed in absolute ethanol and sonicated for about 15 minutes before dropping on a copper grid.

4.3.4 Scanning Electron Microscope (SEM)

The catalyst granule morphology and elemental distribution were obtained using a Hitachi s-3400N scanning electron microscope. The SEM was operated using the back scattering electron (BSE) mode at 20 kV. The catalysts were prepared with platinum coating prior to analysis.

4.3.5 X-ray Photoelectron Spectroscopy (XPS)

The XPS analysis was performed using an AMICUS photoelectron spectrometer equipped with an Mg Kα X-ray as primary excitation and KRATOS VISION2 software. XPS elemental spectra were acquired with 0.1 eV energy step at a pass energy of 75 kV. The C 1s line was taken as an internal standard at 285.0 eV.

4.3.6 Fourier Transform Infrared Spectroscopy (FTIR)

The functional groups on the catalyst surface are identified on the Thermo Nicolet model Impact 400 by FT-IR technique. The sample is mixed with KBr with ratio of sample: KBr equal to 1:100 and then pressed into a thin wafer. The spectrum is recorded in the range of wavenumber between 400 and 4000 cm^{-1} with resolution

of 0.02 cm^{-1}.

4.3.7 H_2 Pulse Chemisorption

The amounts of H_2 chemisorbed on the titanate supported Pd catalysts were measured at room temperature by using a Micromeritic Chemisorb 2750 automated system attached with ChemiSoft TPx software.

Approximately 0.1 g of catalyst was placed in a sample cell. Prior the measurement, 30 ml/min of He gas was introduced into the sample cell in order to remove the remaining air. The system was switched to 50 ml/min of H_2 and heated to 150 °C with a heating rate of 10 °C/min. The temperature was kept constant for 2 h and then cooled down to the room temperature. Carbon monoxide was pulsed over the reduced catalyst until the TCD signal became constant. Palladium dispersion was estimated from the amount of CO chemisorbed assuming a stoichiometry of H_2/Pd =1.

4.3.8 Temperature Programmed Desorption of Ethylene

Temperature Programmed Desorption of Ethylene was carried out in a Micromeritic Chemisorb 2750 automated system attached with ChemiSoft TPx software at room temperature. Approximately 0.1 g of catalyst was per-reduced at 150 °C in H_2 for 2 h with flow rate of 50 cm^3/min and following cooled down to room temperature. Then ethylene adsorption was performed at 35 °C by continuous pulse injection until disappear of ethylene adsorption. The temperature-programmed desorption was applied with a constant rate of 10 °C/min from 35 to 500 °C. The amount of desorbed ethylene was measured by analyzing the effluent gas with a thermal conductivity detector.

CHAPTER V

RESULTS AND DISCUSSION

This chapter describes the results with a discussion about the silica modified titanate nanotubes supported Pd catalysts in the selective hydrogenation of acetylene. The results and discussion are divided into two sections as followed: section 5.1 describes the characterization of silica modified titanate nanotubes supported Pd catalysts and their catalytic performances in the selective hydrogenation of acetylene and section 5.2 describes the effect of reduction temperature on the catalytic performances of silica-modified titanate nanotubes supported Pd catalysts in the selective acetylene hydrogenation.

5.1 SiO_2-modofied titanate nanotubes

The SiO_2-modofied titanate nanotubes supports used for preparation of supported Pd catalysts in this study were obtained by varying the Ti/Si molar ratios of 100:0, 95:5, 90:10, 80:20 and 50:50 mol% and were designated herein as T100:S0, T95:S5, T90:S10, T80:S20, and T50:S50, respectively.

5.1.1 Characterization of titanate nanotubes supports

The titanate nanotubes supports were characterized to clarify the structure, the morphology and the surface composition by various techniques and are discussed below.

5.1.1.1 X-ray Diffraction (XRD)

The XRD patterns of the starting titania powder that was used to synthesize titanate nanotubes are shown in **Figure 5.1**(a). It was demonstrated that only anatase phase TiO_2 was detected whereas the rutile or brookite phase was not observed. The XRD pattern of the as-synthesized titanate nanotubes product, obtained from titania anatase powder by hydrothermal method at 150 °C for 24 h are shown in **Figure 5.1**(b). The diffraction peaks of titanate were observed at the main characteristic

peaks positioned at 2θ = 24.4°, 28°, and 48.4°, that corresponding to the layered $Na_xH_{2-x}Ti_3O_7{\cdot}nH_2O$ with a monoclinic crystal structure [92].

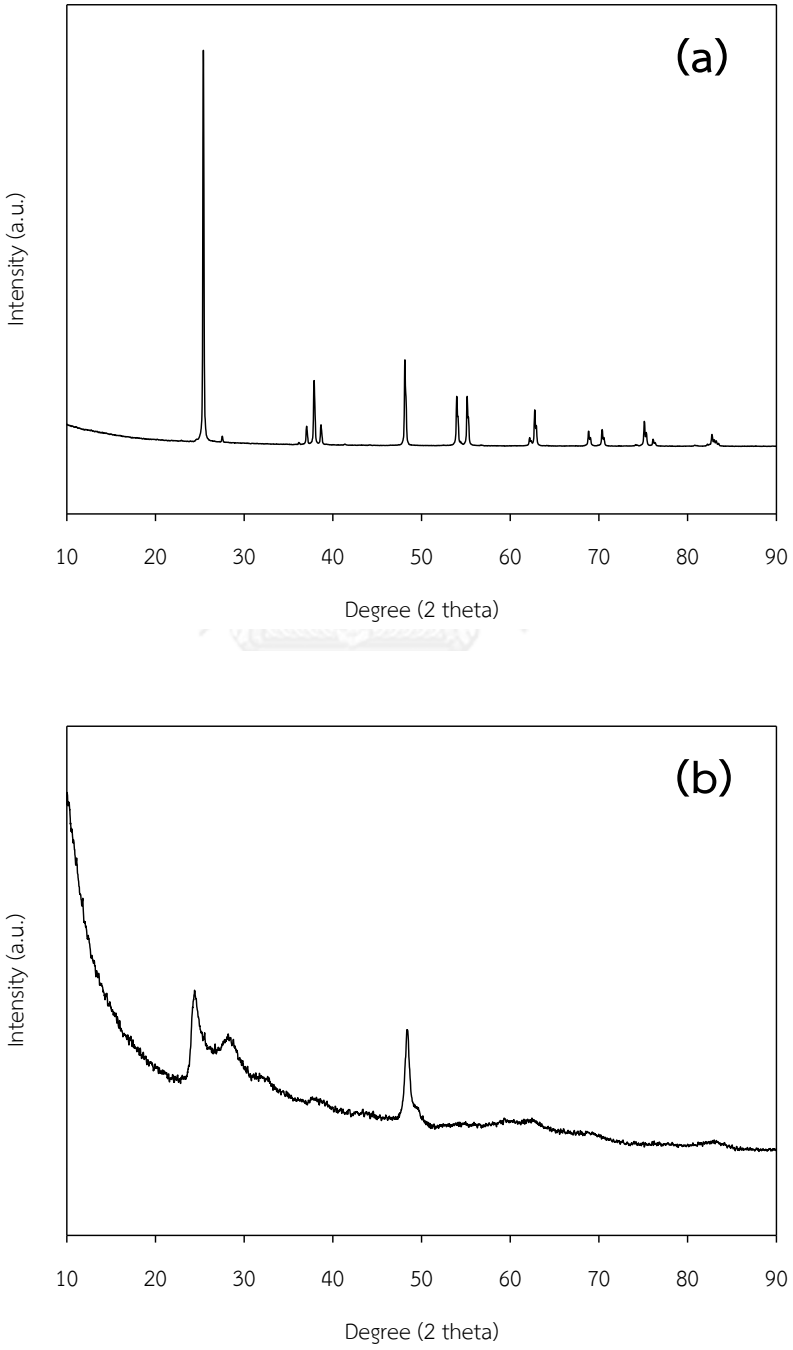

Figure 5.1 The XRD patterns of (a) starting anatase titania and (b) as-synthesized titanate nanotubes.

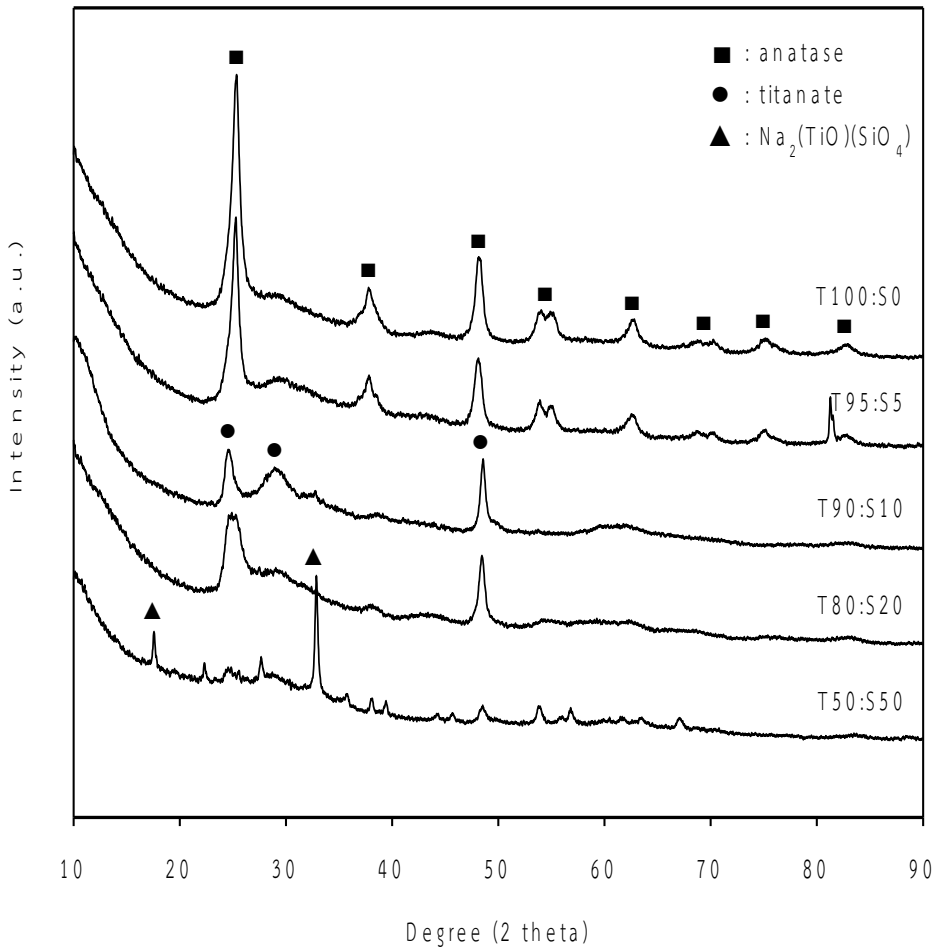

Figure 5.2 The XRD patterns of titanate nanotubes supports containing of various Ti/Si ratios.

The SiO_2-modified titanate nanotubes supports used for preparation of the Pd/nanotubes catalysts in this study were prepared with various amounts of tetraethyl orthosilicate in order to obtain Ti/Si ratios at 100:0, 95:5, 90:10, 80:20 and 50:50 mol%. All the supports were calcined at 450 ℃ for 2 h to remove any impurity that may be contaminated from the precursor. The XRD patterns of the supports are shown in **Figure 5.2**. Due to the high calcination temperature used, the titanate phase was transformed to anatase phase TiO_2 for all the samples. In particularly, for the 0-5 mol% SiO_2 containing samples, the peak intensities correspond to the anatase phase were clearly observed with higher peak intensities. It is suggeted that

the titanate phases in 0-5 mol% SiO_2 containing samples were completely transformed to anatase phase with higher crystallinity of the TiO_2. In addition, for the 10-20 mol% SiO_2 containing samples, the majority of the peaks corresponded to the titanate phase. It is suggeted that high thermal stability of SiO_2-mixed samples could suppress the titanate phase transformation to anatase TiO_2 [34]. However, the presence of larger amount of SiO_2, 50 mol% SiO_2, the pattern peaks correspond to the sample formed to $Na_2(TiO)(SiO_4)$ complex material [103].

5.1.1.2 Scanning Electron Microscopy (SEM)

The SEM micrograph of the as-synthesized titanate nanotubes obtained from hydrothermal synthesis is shown in **Figure 5.3**. The image shows the agglomerate of non-uniform spherical-like particle. however in an enlargement image show that the groups of agglomerate particle were grew from weaving of small uniform tubular-like structure. There the temperature was sufficiently to curl-up the nanosheet into tubular-like structure due to high surface energy. However, the SEM micrograph did not explain in any detailed of the structure whether it is hollow or non-hollow tubular structure.

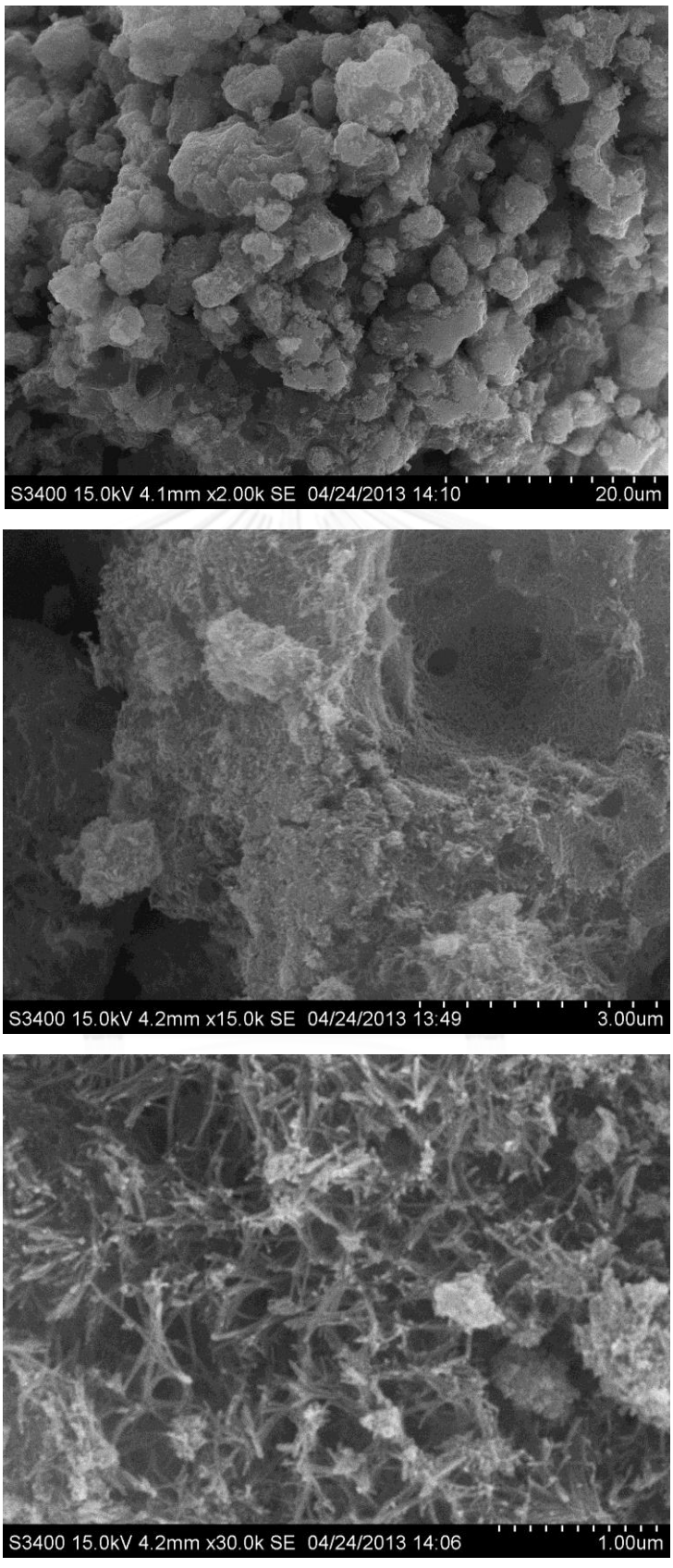

Figure 5.3 SEM micrograph of as-synthesized titanate nanotubes.

5.1.1.3 Transmission Electron Microscopy (TEM)

In order to verify the structure and morphology, TEM micrographs of the as-synthesized supports were acquired and the results are shown in **Figure 5.4**. For pure titanate sample (**Figure 5.4**(a)), the tubular structures with narrow size distribution were observed. The diameter of the tubular materials were uniform around 8-10 nm and the length from tens to several hundreds of nanometer. The tubes were hollow and open ended with an inner diameter of about 3-5 nm. The structure of 10 and 50 mol% of SiO_2 containing sample were similar to the pure titanate as seen in **Figure 5.4**(b) and (c) respectively. It indicates that the hydrothermal conditions used for synthesis at 150 ℃ were successful to fabricate the titanate nanotubes.

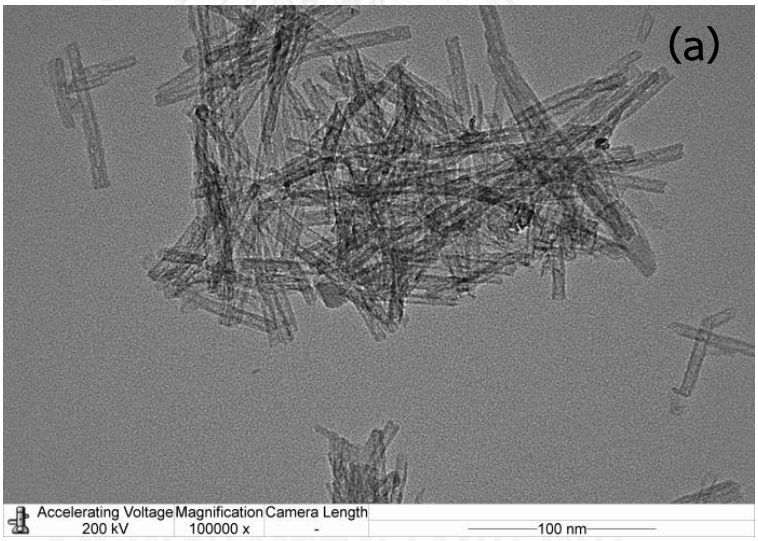

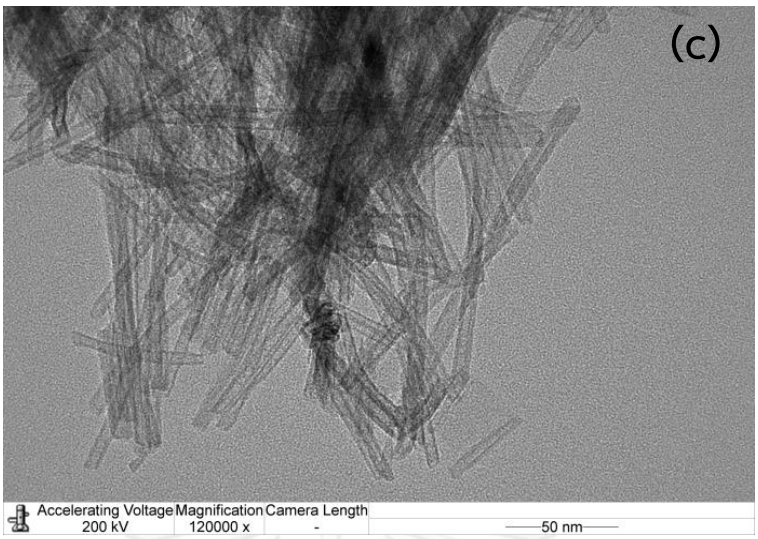

Figure 5.4 TEM micrographs of as-synthesized (a) T100:S0, (b) T90:S10 and (c) T50:S50 supports.

5.1.1.4 Nitrogen Physisorption

The BET surface area and total pore volume of the titanate nanotubes and SiO_2-modified supports are shown in **Table 5.1**. The specific surface area of the titanate nanotubes largely increased from the starting anatase TiO_2 powder (BET SA= 10 m^2/g). Compared to the bare titanate nanotube (BET SA 224 m^2/g), the addition of SiO_2 5-20 mol% resulted in a further increased surface area (231-281 m^2/g) with the 5 mol% SiO_2 showed the highest surface area. However, further increase of SiO_2 to 50 mol%, the specific surface area decreased to 157 m^2/g. The increase in surface area was accompanied by an increase in pore volume, in which the addition of SiO_2 5 mol% resulted in the highest pore volume whereas the 50 mol% SiO_2 had the lowest pore volume, consistent with the surface area results. The presence of SiO_2 may limit the agglomeration of titanate nanotubes so that the surface area increased [104].

The nitrogen adsorption isotherms of the as-synthesized nanotubes supports with various Ti/Si ratios are shown in **Figure 5.5**. All the supports presented a type IV isotherm with a hysteresis loop at relative pressure range of 0.6 to 0.98. It indicates that the supports are mainly mesoporous material. The shape of hysteresis loop was

intermediate between two types, which consisted of H1 hysteresis loop at relative pressures between 0.5 and 0.8, suggesting the existence of the cylindrical pore or the pore with high degree of pore size uniformity inside aggregates of particles, and H3 hysteresis loop at relative pressures between 0.8 and 1.0, suggesting the narrow slit-like shape pores being formed [105].

Table 5.1 The physical properties of as-synthesized nanotubes supports.

Samples	S_{BET} (m^2/g)	V_p (cm^3/g)	D_p (nm)
T100:S0	224	0.73	9.2
T95:S5	281	0.93	10.0
T90:S10	263	0.79	9.2
T80:S20	231	0.72	9.5
T50:S50	157	0.47	9.5

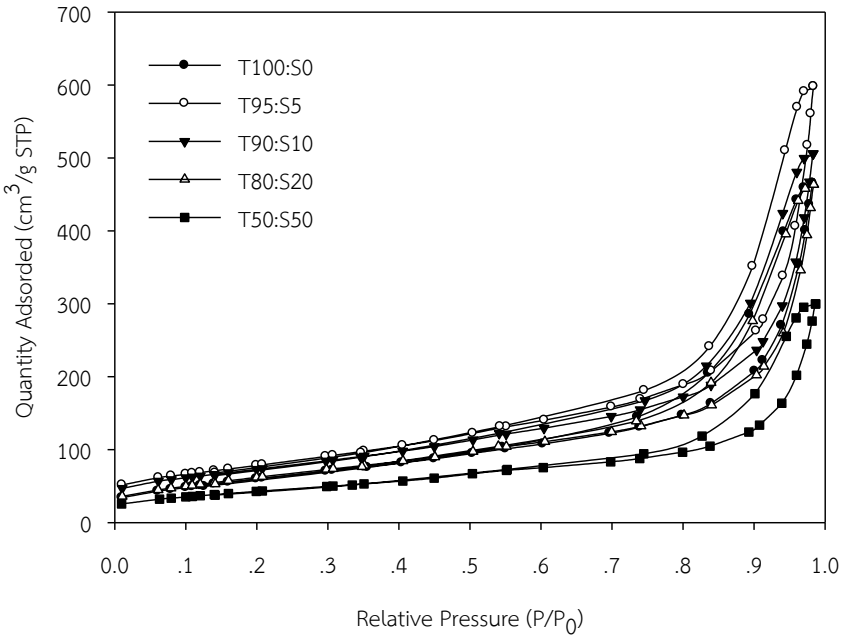

Figure 5.5 Nitrogen adsorption isotherm patterns of as-synthesized nanotubes supports.

The pore size distribution curves determined from BJH method of the as-synthesized nanotubes supports are shown in **Figure 5.6**. All supports showed mesoporous pore size and gave two sizes of pore structures; (i) a narrow pore size distribution at about 3 nm, of the hollow structure of an open ended nanotubes, consistent with the TEM observations and (ii) a board large pore size distribution in range of 10-30 nm, which may be attributed to the space of interpartical of the aggregates. The average pore size of the nanotubes support were remained the same at around 9.5-10 nm as shown in **Table 5.1**.

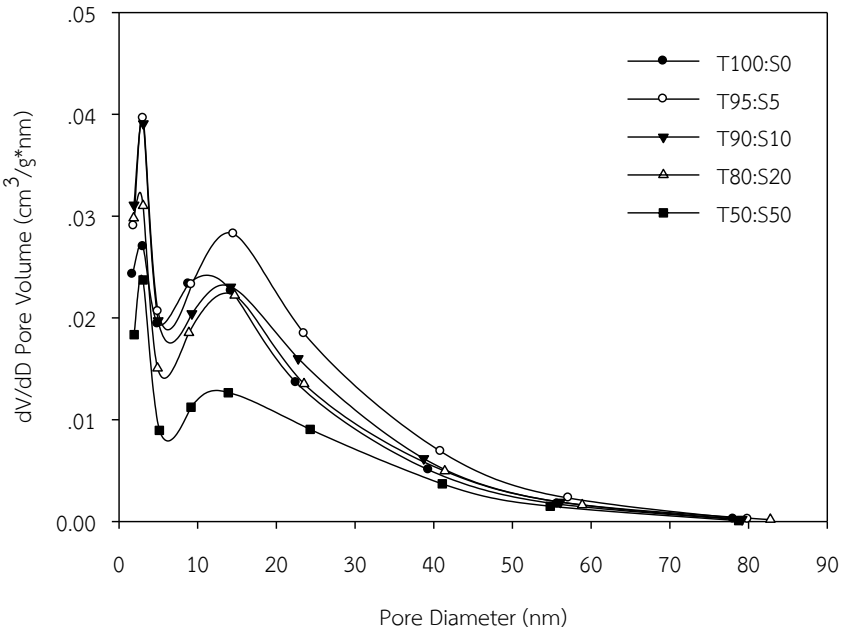

Figure 5.6 The BJH pore size distribution curves of as-synthesized nanotubes supports.

5.1.1.5 Fourier Transform Infrared Spectroscopy (FTIR)

The FTIR spectra of SiO_2-modified titanate nanotube are shown in Figure 5.7. The broad IR absorbance bands centered at about 700-650 cm^{-1} may be assigned to the bulk Ti-O-Ti. The weak band at 960 cm^{-1} was assigned to presence stretching vibration of Ti-O-Si bonds, indicating the substitution of tetrahedral coordinaton Ti^{4+}

ions by Si^{4+} ions in the bulk matrix of TiO_2-SiO_2 nanotubes [106]. The forming of Si-O-Ti chemical bonds modified thermal stability to supports, the titanate matrix may be inserted by Si atom during hydrothermal synthesis that could suppress the titanate phase transformation to anatase phase as consistent with XRD results. The bands at 1630 and 3420 cm^{-1} were attributed to the bending and stretching vibration of O-H bond, indicating the chemisorbed water and free water occluded in the supports respectively. However, the T50:S50 sample showed different IR absorbance spectra. It presented the band at 656, 719, and 890 cm^{-1}, which were the pattern absorption bands of Na titanosilicate compounds $Na_2(TiO)(SiO_4)$ [103].

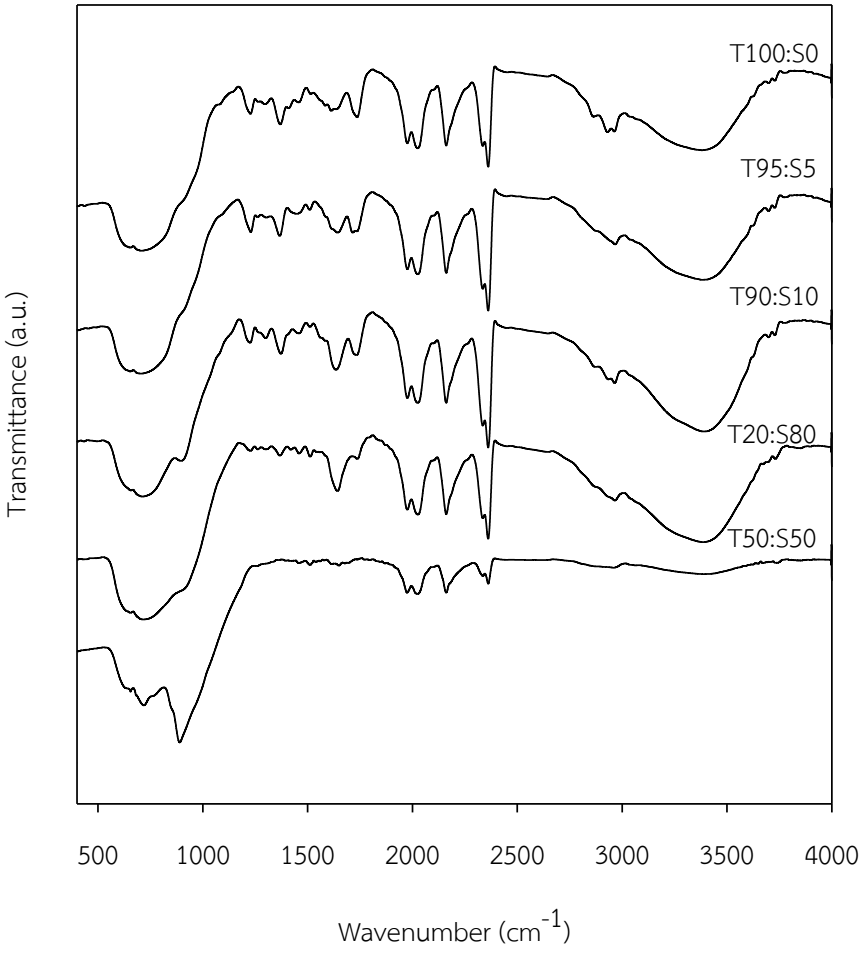

Figure 5.7 FTIR spectra of titanate nanotubes supports containing of various Ti/Si ratios.

5.1.1.6 X-ray Photoelectron Spectroscopy (XPS)

The XPS analysis was used to investigate the surface states of various titanate nanotube supports, the binding energy of Si 1s, Ti 2p and O 1s are observed in **Table 5.2**. For pure titanate nanotubes supports the binding energy of Ti $2p_{3/2}$ and O 1s were obtained at 458.9 and 530.3 eV respectively, which corresponds to the Ti^{4+} valence states in the TiO_2 lattice. The SiO_2-modified titanate nanotubes supports shows the binding energy of Si 2p was negative shifted from 103.3 eV of SiO_2 by 0.7, 0.9, 1.1 and 1.2 eV for 5-50 mol% SiO_2 containing supports respectively. It is suggested that the formation of Ti silicate was increased with increasing amount of SiO_2 added [107, 108]. However the binding energy of O 1s and Ti 2p of SiO2-modified supports were similar to the pure titanate nanotubes. The percentages of atomic concentration from XPS results are also reported, the Si/Ti ratios were increased and the Ti/O ratios were decreased with increasing amount of SiO_2 added, indicating that SiO_2 was dispersed on the catalyst surface. From these XPS results, for silica-modified titanate nanotubes support, it is indicated that Si was combined onto the surface of titanate nanotubes support, the formation of Si-O-Ti chemical bonds were obtained as consistent with the FTIR results.

Table 5.2 Physicochemical properties of titanate nanotubes supports containing of various Ti/Si ratios.

Samples	Binding Energy (eV)			Atomic concentration (%)	
	Si 1s	Ti 2p	O 1s	Si/Ti	Ti/O
T100:S0	-	458.9	530.3	-	0.241
T95:S5	102.6	458.6	530.0	0.018	0.238
T90:S10	102.4	458.7	530.3	0.023	0.227
T80:S20	102.2	458.9	530.3	0.071	0.237
T50:S50	102.1	459.0	530.6	0.285	0.202

5.1.2 Characterization of Pd/SiO_2-modified titanate nanotubes catalysts

5.1.2.1 X-ray Diffraction (XRD)

The Pd supported catalysts prepared by incipient wetness impregnation method using palladium acetate as the Pd precursor. The XRD patterns of the Pd/titanate nanotubes and the SiO_2-modified catalysts are shown in **Figure 5.8**. The XRD patterns showed the same peak pattern as the supports, indicating that the crystalline phase of nanotubes supports did not change after impregnation of Pd and calained at high temperature for all the catalyst samples. Both the Pd/titanate nanotubes and 5 mol% SiO_2 containing catalysts showed major peak at 2θ = 25°, 37.8, and 48.1 of titania antase phase. The 10-20 mol% SiO_2 containing catalysts showed majority of the patterns peaks corresponding to the titanate phase. Moreover, for 50 mol% SiO_2 containing catalyst the pattern peak of sodium titanosilicate phase, $Na_2(TiO)(SiO_4)$ were also observed. However, for the 5-50 mol% SiO_2 containing catalysts, small diffraction peak of PdO at 2θ = 34.1° was detected [107]. Without SiO_2 the Pd/T100:S0 catalyst exhibited only the main diffraction peaks of titania anatase.

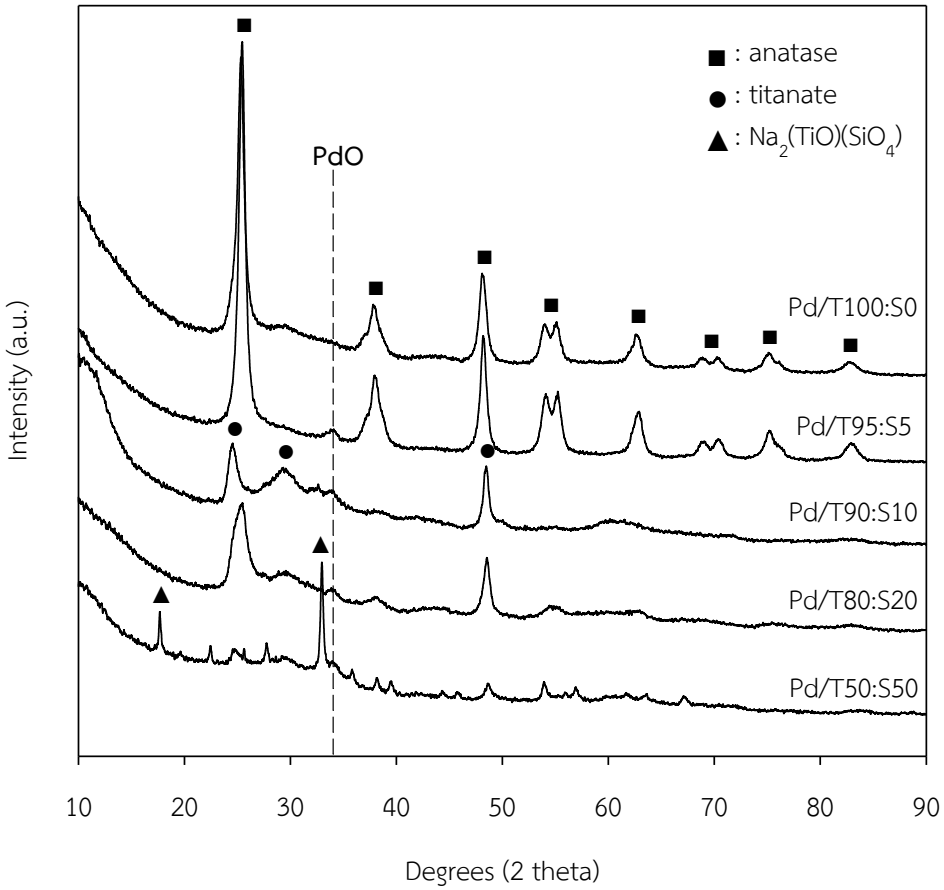

Figure 5.8 The XRD patterns of Pd/titanate nanotubes and the SiO_2-modified catalysts.

5.1.2.2 Nitrogen Physisorption

The BET surface areas, total pore volume and average pore size of the Pd/titanate nanotubes and the SiO_2-modified catalysts are given in **Table 5.3**. The decreases in BET surface areas and pore volumes of the Pd/titanate nanotube catalysts compared to the titanate nanotube supports suggested that palladium was deposited in some of the pores of supports, and also suggested that high calcination temperature prior to the impregnation step. The BET surface area of Pd/titanate nanotubes and 5 mol% SiO_2 containing catalysts were significantly decreased due to the phase transformation in calcination step. The titanate transformed to large crystallite size titania anatase phase, as confirmed by XRD results. In addition, the

high deposition of Pd was obtained in 5 mol% SiO_2 containing catalysts that caused the BET surface area and pore volume of Pd/T95:S5 catalysts more decreased than Pd/T100:S0 catalysts. It is suggested that Pd were more deposited in the pores. As in 10 mol% SiO_2 containing catalysts, the BET surface area and pore volumes were largely decreased eventhough high thermal stability and little phase transformation were obtained, due probably to high Pd deposition on Pd/T90:S10 catalysts. For 20 mol% Si containing catalysts the BET surface area and pore volume were not significantly decreased, suggesting low phase transformation and low Pd deposition. However, the BET surface area and pore volume of 50 mol% SiO_2-modified titanate supported Pd catalysts was largely decreased by 73% and 71%, respectively due to Pd was deposited on the surface and sodium titanosilicate phase, $Na_2(TiO)(SiO_4)$ being formed [103].

Table 5.3 The physical properties of Pd supported on titanate nanotubes catalysts.

Samples	S_{BET} (m^2/g)	V_p (cm^3/g)	D_p (nm)
Pd/T100:S0	154	0.65	13.1
Pd/T95:S5	145	0.71	15.5
Pd/T90:S10	164	0.63	11.9
Pd/T80:S20	210	0.73	10.7
Pd/T50:S50	42	0.14	10.2

The nitrogen adsorption isotherms of the Pd/titanate nanotubes and the SiO_2-modified catalysts with various Ti/Si ratios are shown in **Figure 5.9**. All the catalysts presented a type IV isotherm as same as the supports. The isotherms showed the behavior within high relative pressure range, which indicated that the supports were mainly mesoporous material. The shape of hysteresis loop also showed intermediate between H1 (at P/P_0 between 0.6 and 0.8) and H3 (at P/P_0 between 0.8 and 1.0) hysteresis loop, suggesting the existence of the uniform cylindrical pore and narrow slit-like shape pores being formed respectively [105]. However, the quantity of

nitrogen adsorbed decreased due to palladium deposited on the surface and pore blockages, especially for the Pd/T50:S50.

The pore size distribution curves determined from BJH method of the Pd/titanate nanotubes and the SiO_2-modified catalysts are shown in **Figure 5.10**. All the catalyst showed mesoporous pore size and gave two sizes of pore structures; (i) a narrow pore size distribution at about 3 nm, which imply that the hollow structure of an open ended nanotubes and (ii) a board large pore size distribution in range of 10-30 nm, which could be attributed to the space of interpartical of the aggregates as similar in the as-synthesized supports. Nevertheless, the pore volume of the pore size distribution at about 3 nm was much decreased. It should be noted that Pd was higher deposited in hollow pores of the nanotube supports than on the outer surface of the tube, excepting in 50 mol% SiO_2 containing catalysts that Pd was highly deposited in both the inner and outer of the tubes.

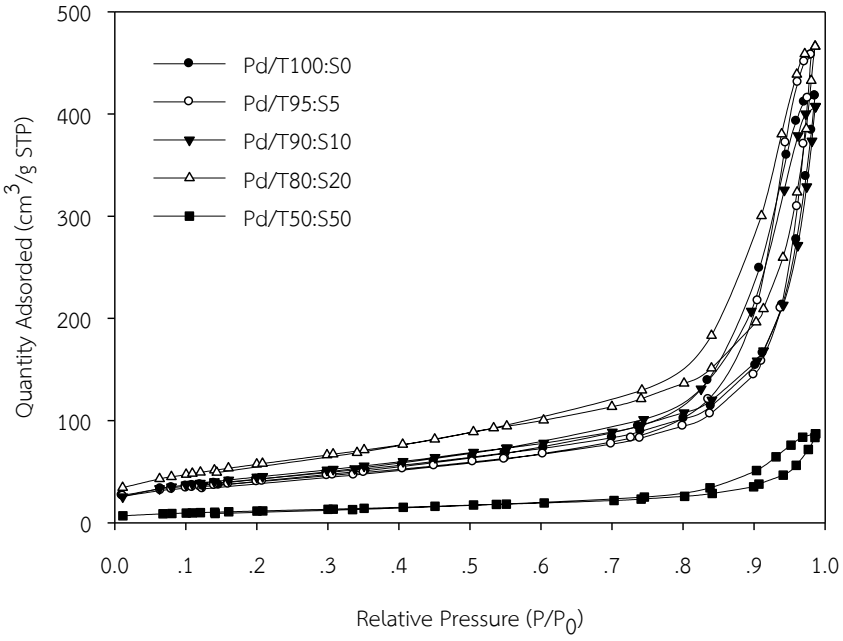

Figure 5.9 Nitrogen adsorption isotherm patterns of Pd supported on titanate nanotubes catalysts.

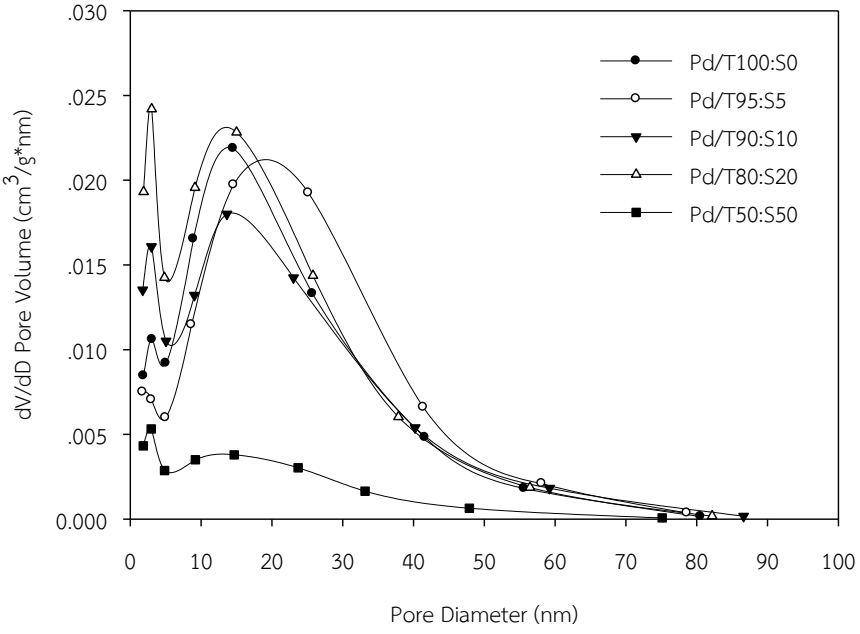

Figure 5.10 The BJH pore size distribution curves of Pd supported on titanate nanotubes catalysts.

5.1.2.3 Hydrogen Chemisorption

The H_2 chemisorption results such as the number of active Pd atoms, %Pd dispersion, and average Pd metal particle size are summarized in **Table 5.4**. The results were calculated from the assumption that the amount of H_2 molecule chemisorbed on Pd site of H/Pd =1 [109]. The number of Pd active sites and %Pd dispersion were increased with increasing amount of SiO_2 modified. It is suggested that the SiO_2-modified titanate catalysts with higher surface area can result in higher %Pd dispersion. Among these catalysts, 10 mol% SiO_2-modified titanate supported Pd catalysts exhibited the highest Pd active sites.

Table 5.4 Hydrogen chemisorption results of Pd supported on titanate nanotubes catalysts.

Samples	Pd Active Stites ($\times 10^{-18}$ H_2 molecule/g cat)	%Pd Dispersion	d_p Pd^0 (nm)
Pd/T100:S0	10.6	18.7	6.0
Pd/T95:S5	26.0	45.9	2.4
Pd/T90:S10	36.3	64.0	1.7
Pd/T80:S20	16.8	29.7	3.8
Pd/T50:S50	12.3	21.8	5.1

5.1.2.4 X-ray Photoelectron Spectroscopy (XPS)

The XPS analysis was also performed to determine the Pd electronic state and Pd/Ti atomic concentration on the catalyst surface are summarized in **Table 5.5**. For all the catalysts, the binding energy of Pd $3d_{5/2}$ was observed at around 336.3-336.8 eV, which was attributed to PdO species. The ratios of Pd/Ti atomic concentration were decreased with increasing amount of SiO_2 added, excepting that in 50 mol% SiO_2 containing catalyst. It should be noted that higher Pd surface concentrations or larger Pd particle size of 50 mol% SiO_2 containing catalyst may be due to the lower surface area of the supports and low interaction between Pd and

$Na_2(TiO)(SiO_4)$ as evidenced in low %Pd dispersion from H_2 chemisorption results. For 20 mol% SiO_2 containing catalyst that showed the lowest Pd/Ti atomic concentration ratios, which was suggested that low Pd deposition was obtained in consistent with the N_2 physisorption results.

Table 5.5 XPS results of Pd supported on titanate nanotubes catalysts.

Samples	Pd $3d_{5/2}$		Atomic Concentration Pd/Ti
	B.E. (eV)	FWHM	
Pd/T100:S0	336.6	0.864	0.004
Pd/T95:S5	336.3	0.685	0.002
Pd/T90:S10	336.3	0.800	0.002
Pd/T80:S20	336.5	0.453	0.001
Pd/T50:S50	336.8	1.720	0.032

5.1.2.5 Scanning Electron Microscopy (SEM)

The SEM micrographs of the pure titanate nanotubes and SiO_2-modified supported Pd catalysts are shown in **Figure 5.11**. The Pd/titanate nanotube and 5 mol% SiO_2 containing catalysts consisted of irregular shape of very fine particles agglomerated as obtained in **Figure 5.11**(a), (b), (c), and (d). The morphology of 50 mol% SiO_2 containing catalysts which are shown in **Figure 5.11**(e) and (f), consisted of larger uniform particles agglomerated.

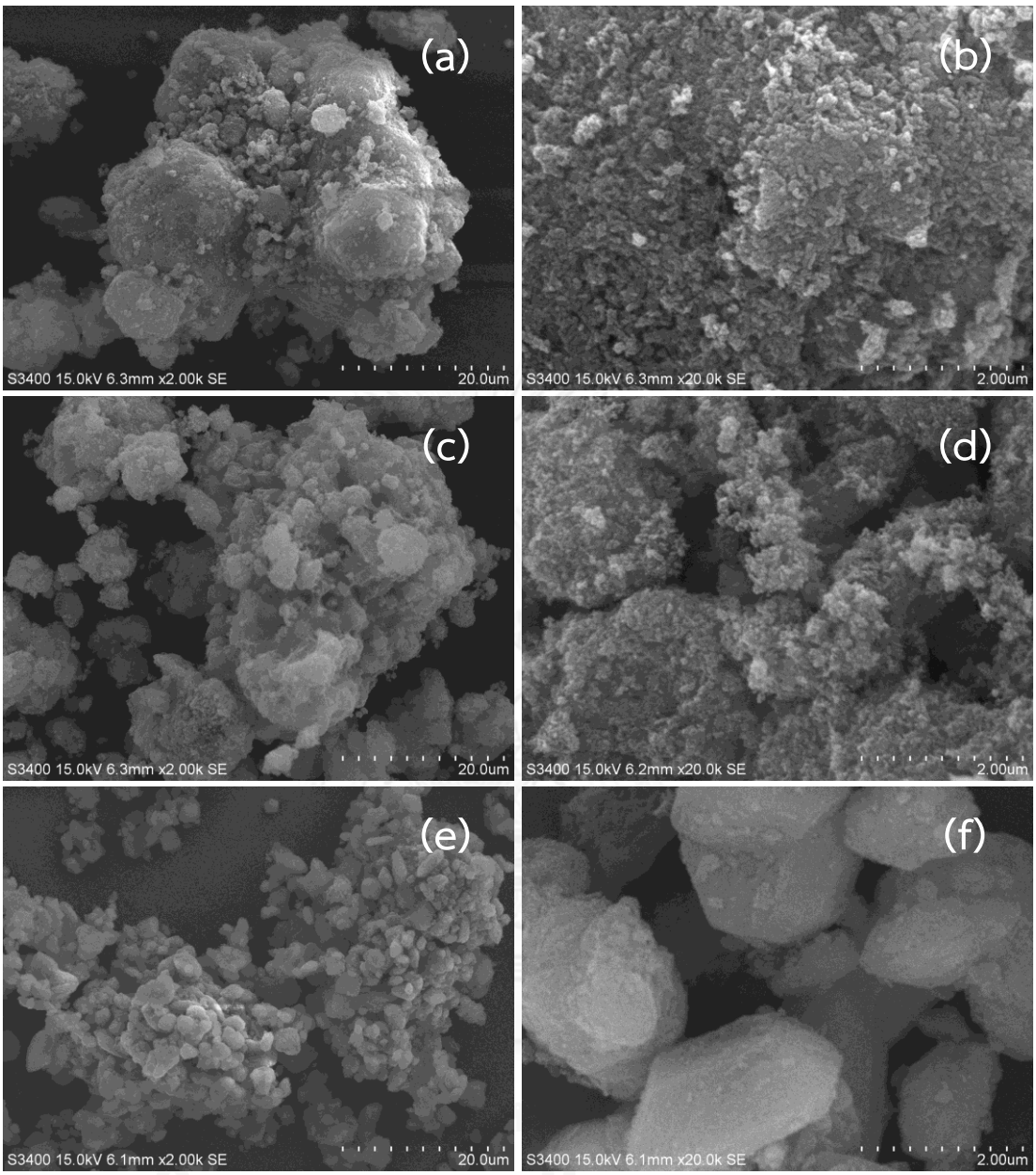

Figure 5.11 SEM micrograph of Pd supported on titanate nanotubes catalysts (a, b) Pd/T100:S0, (c, d) Pd/T95:S5 and (e, f) Pd/T50:S50 catalysts.

5.1.2.6 Transmission Electron Microscopy (TEM)

The TEM micrographs of Pd supported SiO_2-modified titanate nanotubes catalysts after reduced at 150 °C in hydrogen were also taken in order to physically measure the size of the palladium particles and/or palladium clusters on the various SiO_2 containing and the results are shown in **Figure 5.12** and **Figure 5.13** for Pd/T95:S5 and Pd/T50:S50 respectively. For 5 mol% SiO_2-modified titanate nanotube catalysts, the tubular structures with the tube walls were also observed. However, the tubes length was shorter than the supports and some of the titanate nanotubes were transformed into anatase TiO_2 nanorods and nanoparticles due to the high calcination temperature prior to the impregnation step. This was associated with the dehydration of the nanotubular structure and the collapse of the interlayer spacing between the walls of the nanotube, resulting of anatase phase as confirmed by the XRD results. The small dark spots in catalyst represented the palladium particles. The palladium particles were deposited both in the tubes hollow and on the surface of the tubes. The palladium particles that attached to the surface were mostly 6 nm in size. The 50 mol% SiO_2-modified titanate nanotube catalysts, all of the tubes was remained tubular structure with clearly the tube walls as similar to the supports. It is suggested high thermal stability as consistent with the XRD results. The palladium particles were mostly deposited on the surface of the titanate nanotubes and the spherical shape of palladium particles were observed. The average particles sizes of palladium were about 16 nm. Also the large palladium particle sizes are consistent with the XPS results.

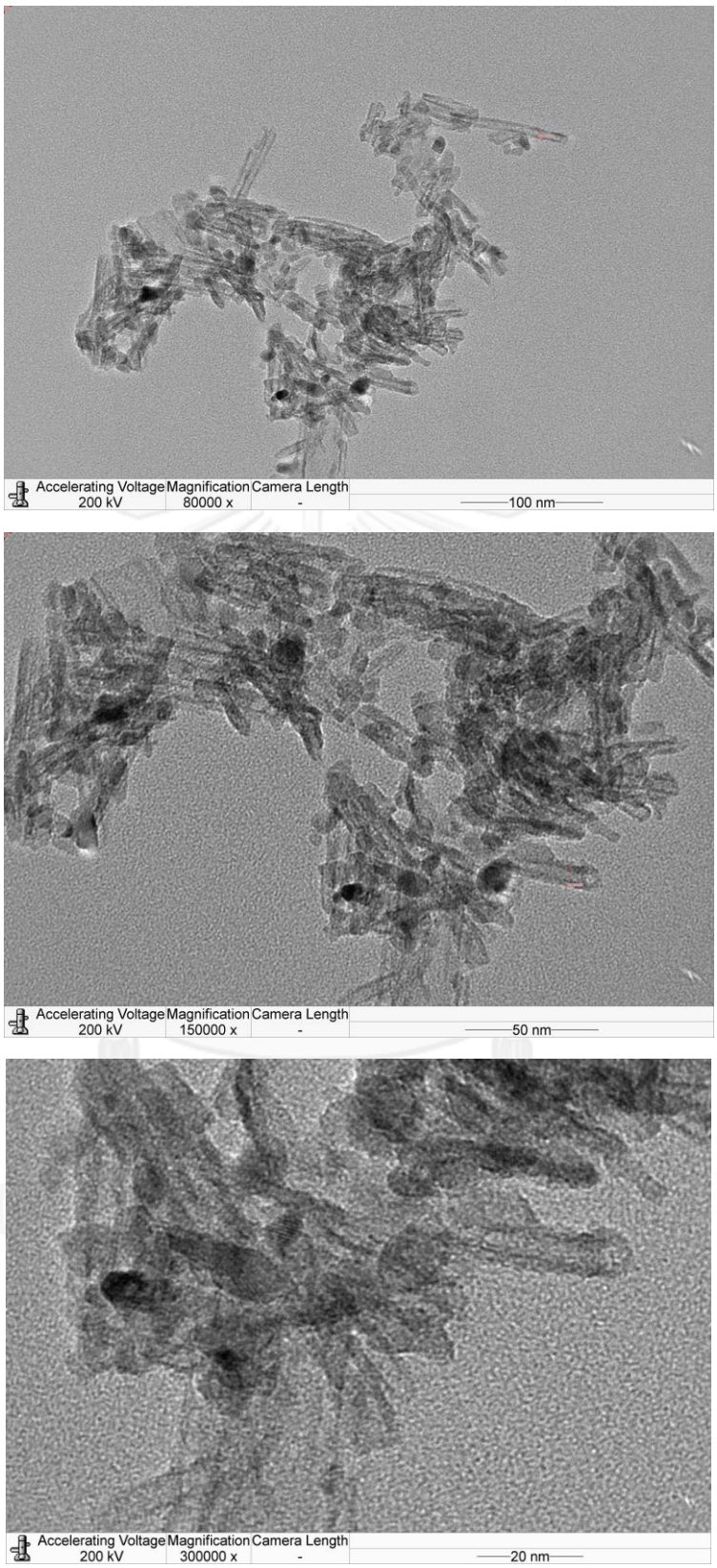

Figure 5.12 TEM micrographs of Pd/T95:S5 catalysts after reduced at 150 °C.

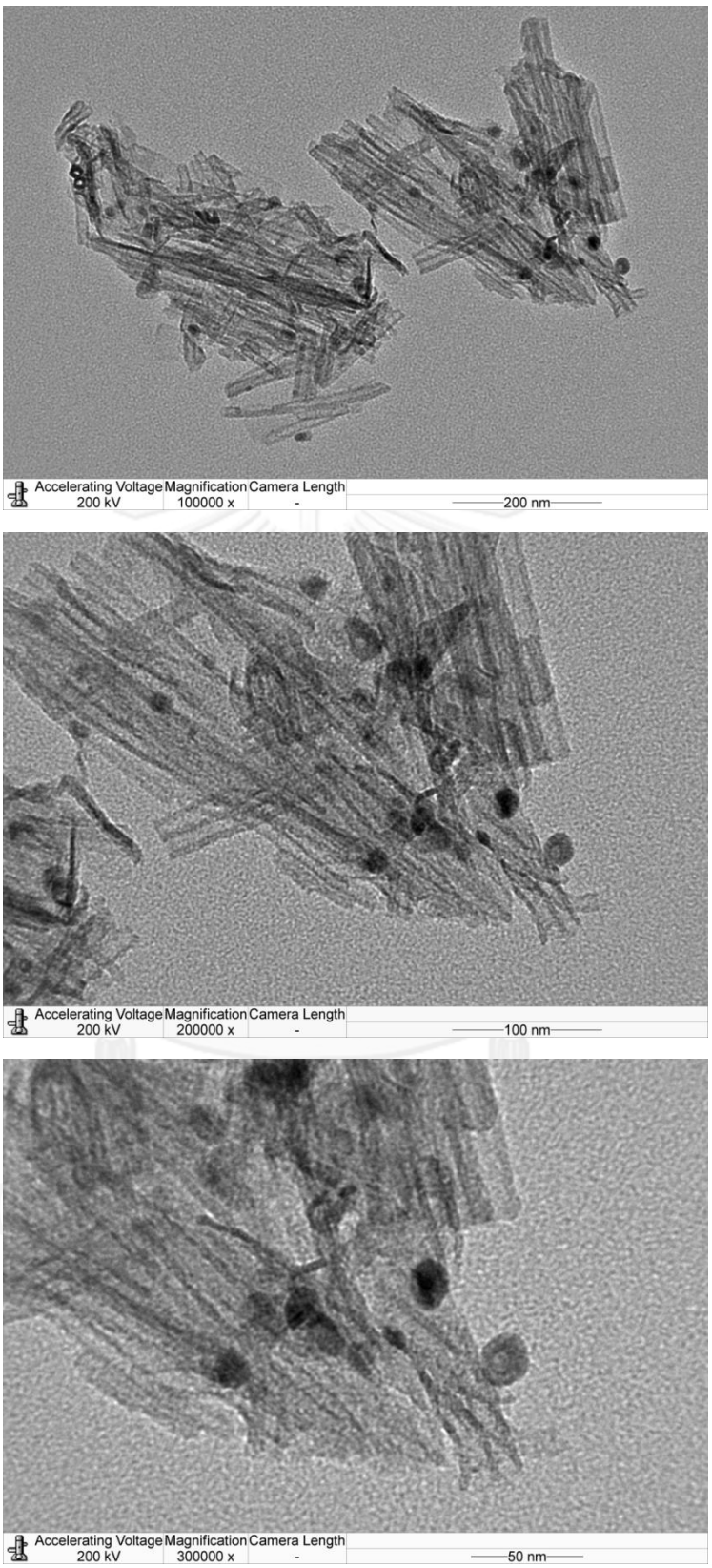

Figure 5 13 TEM micrographs of Pd/T50:S50 catalysts after reduced at 150 °C.

5.1.2.7 Temperature Programmed Desorption of Ethylene (TPD)

The ethylene TPD results of the Pd/titanate nanotubes and the SiO_2-modified catalysts are given in **Figure 5.14**. The peaks of ethylene TPD from the Pd surface appeared at different temperature ranges depending on the characteristic mode of the ethylene adsorption on the surface. Two main desorption peaks at ca. 93-140 °C and 235-310 °C were observed for all the catalyst samples. The lower temperature desorption peak was assigned to **π**-bonded ethylene species, which is weakly adsorbed ethylene and consequently desorbed without decomposition. Since higher temperature was assigned to di-**σ**-bonded ethylene, which undergoes decomposition followed by the recombination of the surface hydrocarbon species with hydrogen to produce ethylene as well as ethane [21]. For the 5 and 50 mol% SiO_2 containing, the lower and higher temperature peak were significantly reduced and shifted to lower temperature, indicating that decomposition of ethylene was suppressed.

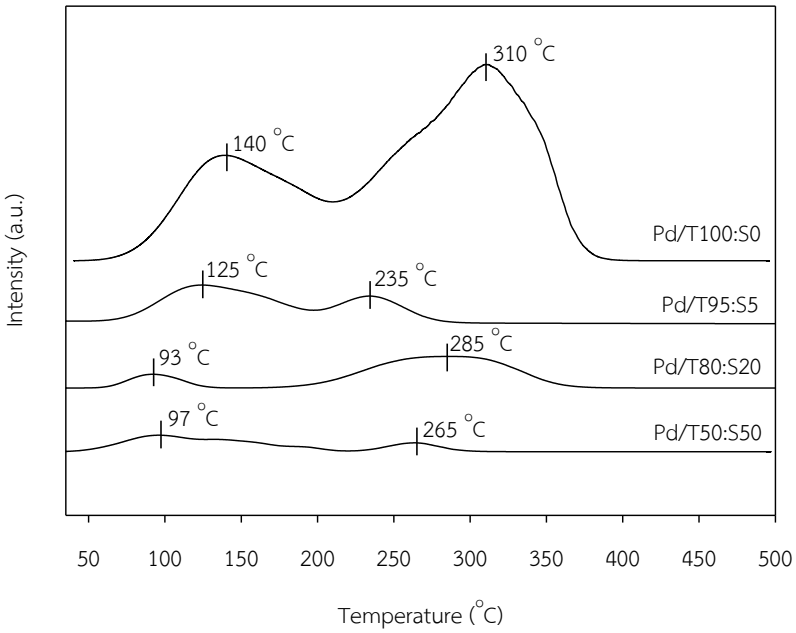

Figure 5.14 Temperature programed desorption of ethylene for Pd supported on titanate nanotubes catalysts.

5.1.3 Reaction study in selective acetylene hydrogenation

The catalytic performances of Pd supported titanate nanotubes catalysts were investigated in the selective hydrogenation of acetylene to ethylene. The reaction was performed in a 9 mm glass tube reactor using feed flow rate of 10 cm^3/min under various reaction temperatures from 40-100 °C. The performances of catalysts were determined in terms of acetylene conversion and ethylene selectivity. Acetylene conversion is defined as moles of acetylene converted with respect to acetylene in feed. Ethylene gain is defined as the percentage of acetylene hydrogenated to ethylene over totally hydrogenated acetylene. The ethylene being hydrogenated to ethane (ethylene loss) is the difference between all the hydrogen consumed and all the acetylene, which has been totally hydrogenated. This calculated value is the percentage of the theoretically possible ethylene gain that has been achieved in the operation. However, it should be noted that these calculations could not provide a measure of acetylene polymerization pathway that form carbonaceous species or green oil.

The conversion of acetylene and ethylene selectivity of the various Pd/nanotubes catalysts as a function of reaction temperature are shown in **Figure 5.15** and **Figure 5.16**, respectively. Typically, acetylene conversion increased with increasing reaction temperature. The 5 and 50 mol% SiO_2-modified titanate nanotube catalysts exhibited the highest acetylene conversion that reached 100% at ca. 60 °C for 5 mol% SiO_2 and 80 °C for 50 mol% SiO_2 while the other catalysts required higher temperature. According to higher number of Pd active sites and higher Pd dispersion as determined from H_2 chemisorption of 5 mol% SiO_2 containing, acetylene hydrogenation was promoted. The 50 mol% SiO_2 containing also exhibited high Pd surface concentrations which is caused by the large size of Pd particles as confirmed by XPS analysis and TEM micrographs. It is indicated that the larger Pd particles size with high catalytic activity for acetylene conversion was may be due to the influence of the support material and a weak metal–support interaction between Pd and $Na_2(TiO)(SiO_4)$ [110, 111]. However, the 80 mol% SiO_2-modified titanate nanotube catalysts presented the lowest acetylene conversion as it possessed the lowest number of Pd active sites. In addition the 10 mol% SiO_2 containing catalysts

presented the low acetylene conversion in spite of the highest Pd active sites as determined from H_2 chemisorption. It is suggested the formation of Pd hydride due to the measurement limitation of unappreciated hydrogen pressure was used to measured [2]. With appropriate amount of SiO_2, the SiO_2 modified titanate nanotube supports increased the BET surface area, total pore volume, Pd active site and the dispersion of Pd on nanotube supports, which promoted acetylene conversion. For ethylene selectivity, all the SiO_2-modified titanate nanotube catalysts exhibited higher selectivity of ethylene than pure titanate nanotube catalysts, excepting that of the 20 mol% SiO_2 containing. The pure titanate nanotube supported catalysts had low Pd deposition and low Pd surface concentrations as shown by the XPS results. In term of catalyst performance or ethylene yield, shown similar tendency as ethylene selectivity results was seen in the order: Pd/T50:S50 > Pd/T95:S5 > Pd/T90:S10 > Pd/titanate nanotubes > Pd/T80:S20 as shown in **Figure 5.17** and **Figure 5.18**. The improved catalytic performance in the selective hydrogenation of acetylene may be attributed to the weaker ethylene adsorption as shown in the TPD profiles, which the peak of di-**σ**-bonded ethylene were reduced [21]. In addition, the TPD profiles suggest that the SiO_2 modified catalyst showed lower amount of ethylene adsorbed on the catalyst surface and also the position of the peaks were shifted to lower temperature, indicating to ethylene species desorbed more easily from the Pd surface [112]. Moreover, the shift of Pd 3d peak in the XPS results of the 50 mol% SiO_2 containing toward higher binding energy was probably due to stronger interaction between Pd and supports, so that higher ethylene selectivity was obtained.

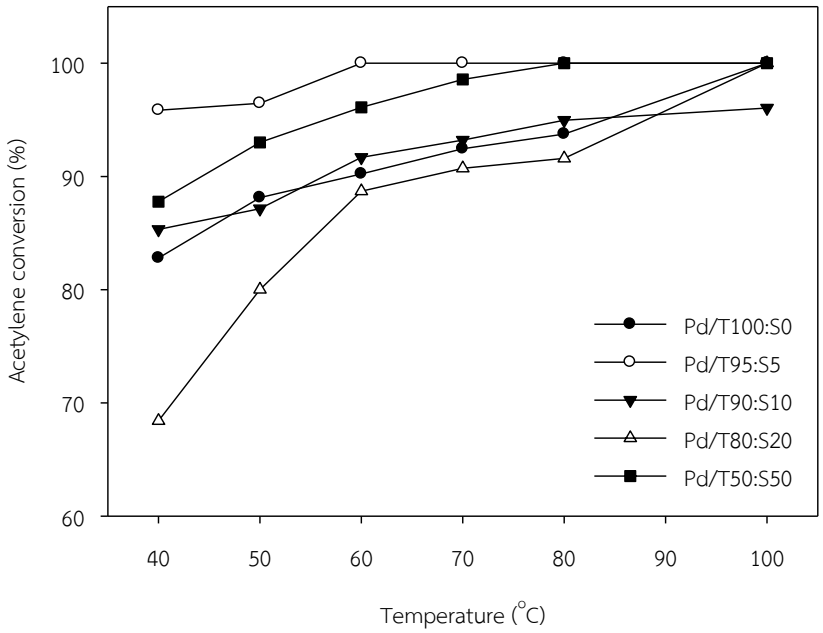

Figure 5.15 Acetylene conversion as a function of temperature for various nanotubes supported catalysts.

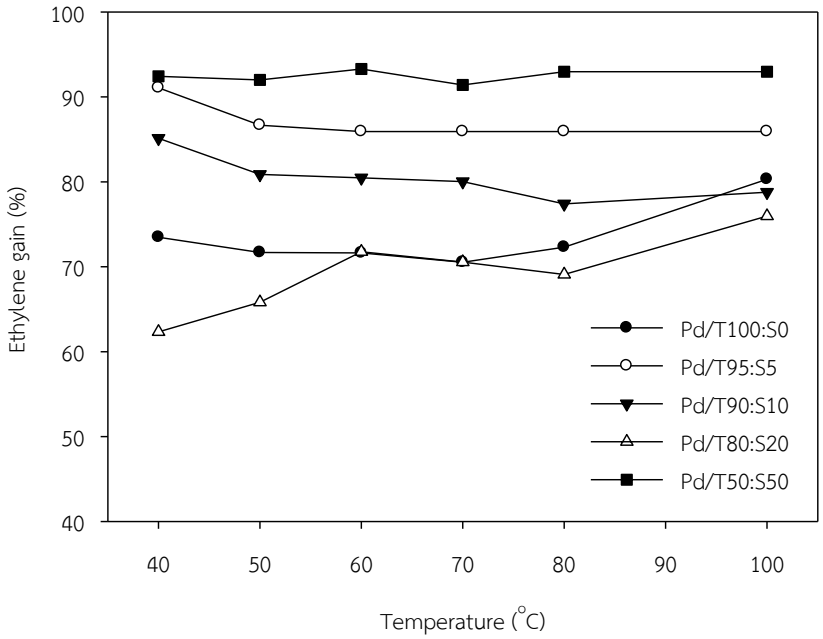

Figure 5.16 Ethylene selectivity as a function of temperature for various nanotubes supported catalysts.

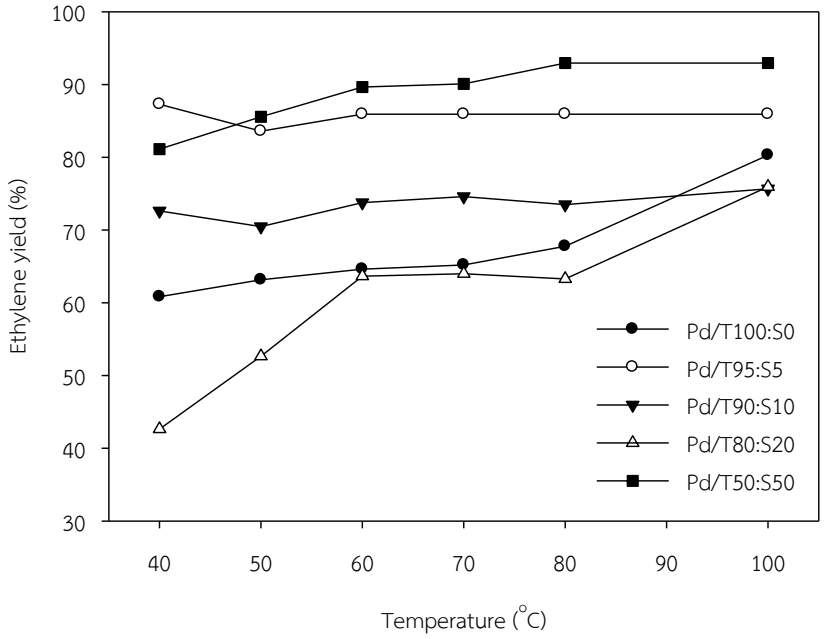

Figure 5.17 Ethylene yield as a function of temperature for various nanotubes supported catalysts.

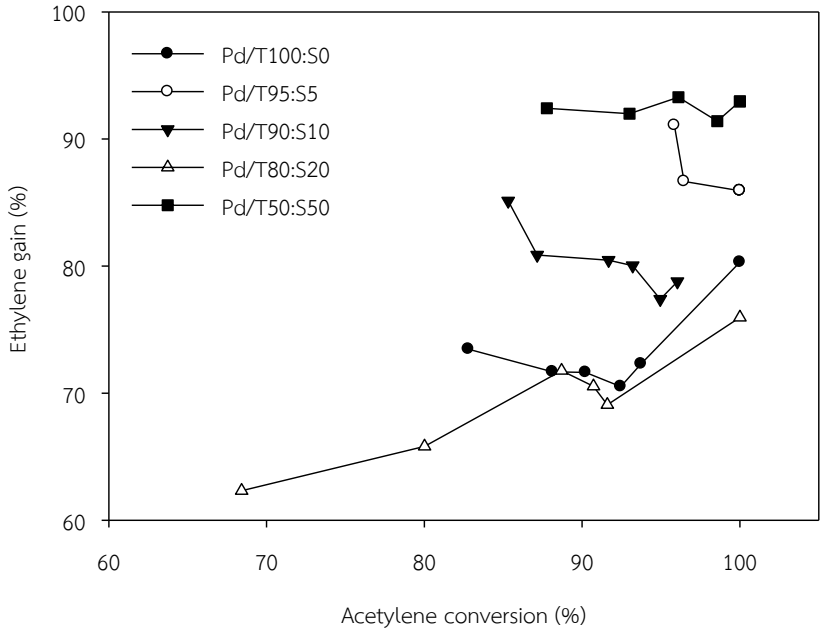

Figure 5.18 Catalytic performance of selective acetylene hydrogenation.

5.2 The effect of high reduction temperature at 500 °C on the performance of SiO_2-modified titanate nanotube supported Pd catalysts

5.2.1 Transmission Electron Microscopy (TEM)

The TEM micrographs of SiO_2-modified titanate nanotube supported Pd catalysts after reduced at 500 °C in hydrogen are shown in **Figure 5.19** and **Figure 5.20** for Pd/T95:S5 and Pd/T50:S50 respectively. All of 5 mol% SiO_2 containing catalysts (**Figure 5.19**) showed the transformation into anatase TiO_2 nanorods and nanoparticles due to the high reduction temperature at 500 °C. The collapse of nanotubes to the shot rods and non-hollow structures were observed. The palladium particles were dispersed highly on the supports and the sizes of palladium particles were also remain the same as compared to the reduced ones at 150°C. These are indicated that the outstanding stability of palladium on the supports when modified with SiO_2 was due probably to high metal-support interaction between palladium and anatase titania supports. The average palladium particles size that attached to the surface was about 8 nm. The 50 mol% SiO_2-modified titanate nanotube catalysts after reduced at 500 °C (**Figure 5.20**), all of the tubes was remained tubular structure with clearly the tube walls. The collapse of the interlayer spacing between the walls of the nanotubes was not observed, indicating to high thermal stability as consistent with the XRD results. However, the tubes length was shorter than the reduction temperature at 150 °C and more agglomerated. The spherical shape of palladium particles dispersed on the surface of the nanotube supports in the 14 nm average size was also observed. In addition, in the dark region shows larger palladium particle sizes than on both nanotube supports and when reduced at 150 °C. It is suggested to palladium sintering occurred on $Na_2(TiO)(SiO_4)$ separate phase due probably to low metal-support interaction.

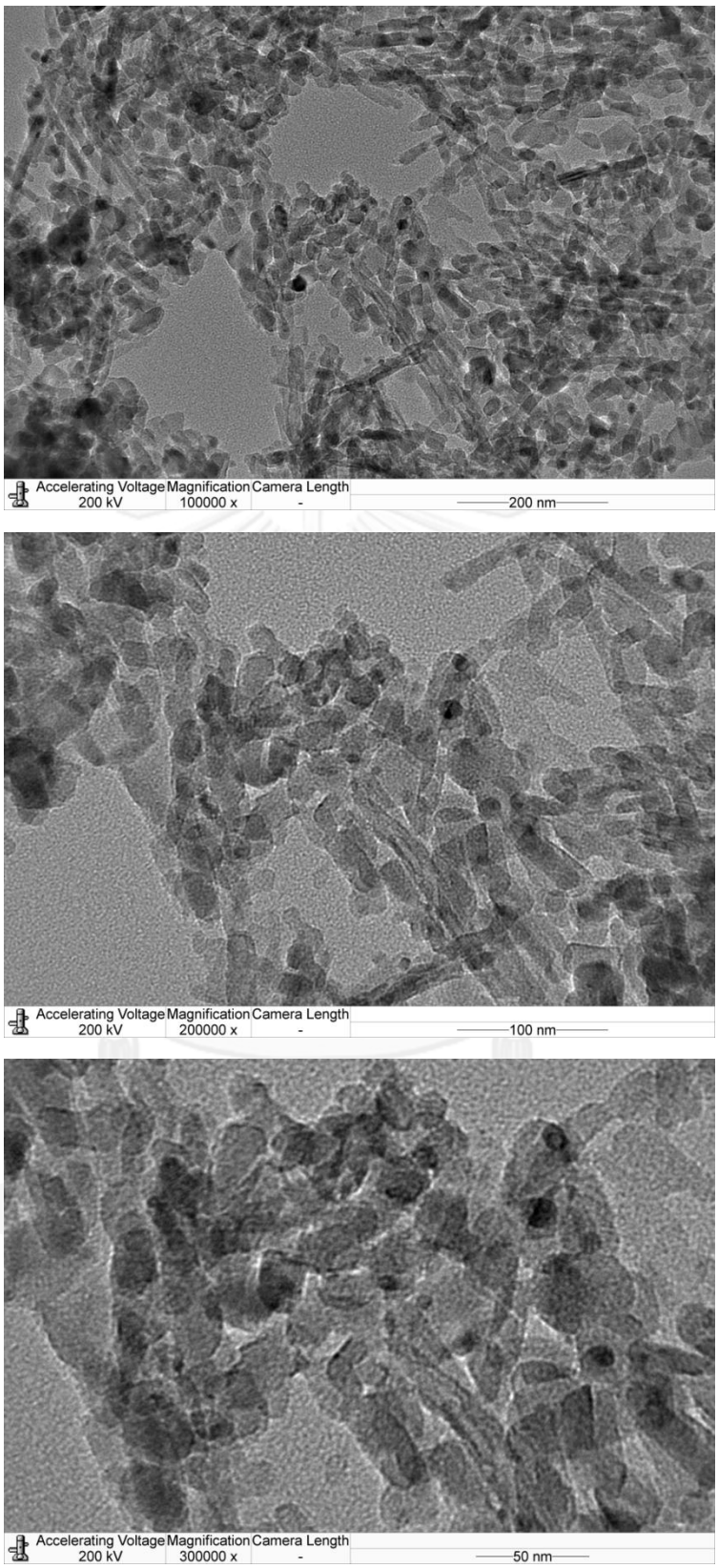

Figure 5.19 TEM micrographs of Pd/T95:S5 catalysts after reduced at 500 °C.

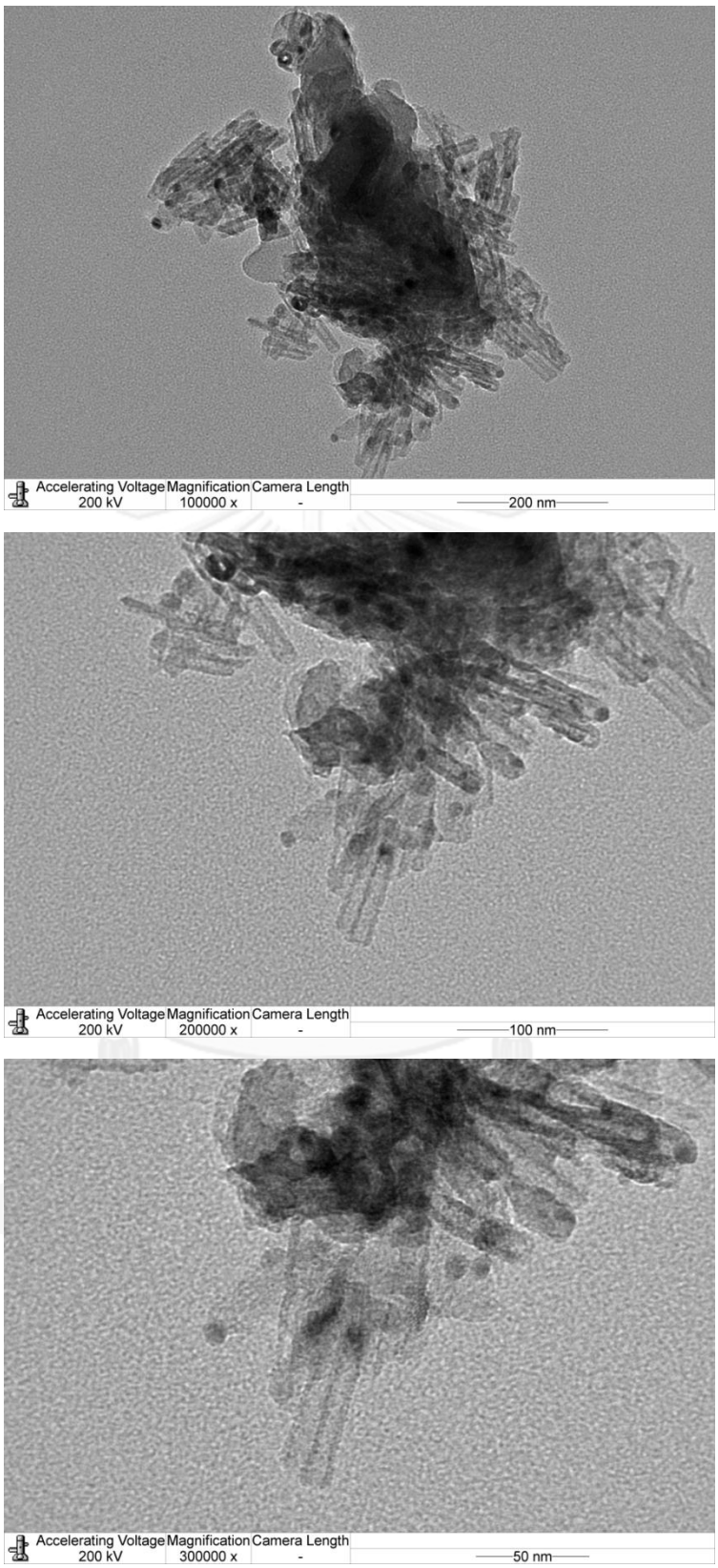

Figure 5.20 TEM micrographs of Pd/T50:S50 catalysts after reduced at 500 °C.

5.2.2 Hydrogen Chemisorption

The H_2 chemisorption results of Pd/titanate nanotubes and the SiO_2-modified catalysts when reduced at high reduction temperature of 500 °C are summarized in **Table 5.6**. It can be seen that the number of Pd active sites and %Pd dispersion were much decreased when reduced at 500 °C. The amounts of H_2 chemisorption were in the range 2.2×10^{-18} to 5.22×10^{-18} H_2 molecule/g cat, while 10 mol% SiO_2 containing Pd catalysts showed the lowest of Pd active sites and %Pd dispersion, due probably to the SMSI effect. It is generally know that SMSI occurs after reduction at high temperature due to the decoration of the metal surface by partially reducible meatal oxides and by an electron transfer between the support and the metals resulting in H_2 chemisorption suppression [113].

Table 5.6 Hydrogen chemisorption results of Pd supported on titanate nanotubes catalysts when reduced at high temperature of 500 °C.

Samples	Pd Active Stites ($\times 10^{-18}$ H_2 molecule/g cat)	%Pd Dispersion	d_p Pd^0 (nm)
Pd/T100:S0	5.1	9.0	12.5
Pd/T95:S5	5.2	9.3	12.1
Pd/T90:S10	2.4	4.3	26.2
Pd/T80:S20	3.9	6.8	16.4
Pd/T50:S50	2.2	3.9	28.8

5.2.3 Reaction study in selective acetylene hydrogenation

The conversion of acetylene and ethylene selectivity of the various Pd/nanotubes catalysts as a function of reaction temperature when the catalysts were reduced at 500 °C are shown in **Figure 5.21** and **Figure 5.22**, respectively. As can be observed, acetylene conversion increased with increasing reaction temperature. The acetylene conversion of all various catalysts was significantly decreased due to the decrease of Pd active sites. When the catalysts exhibited the

SMSI effect, the TiO_2 species were partially reduced and eventually migrated onto the Pd surface [113]. The selectivity of ethylene, for all the catalysts were improved when high reduction temperature at 500 °C was used. The presence of SMSI effect between Pd metal and titanate nanotubes support can result in lower adsorption strength of ethylene on the catalysts surface and promotes ethylene selectivity [20]. The direct ethane formation via H_2 spillover on Pd sites may be blocked by TiO_2 species [112]. The catalyst performance in term of ethylene yield are shown in **Figure 5.23**. The performance of Pd/nanotubes catalysts was improved in the order: Pd/T95:S5 > Pd/T90:S10 > Pd/T100:S0 ≈ Pd/T80:S20 > Pd/T50:S50. However, the 50 mol% containing SiO_2 showed the lowest performance when reduced at high temperature of 500 °C. It is likely that Pd sintering occurred.

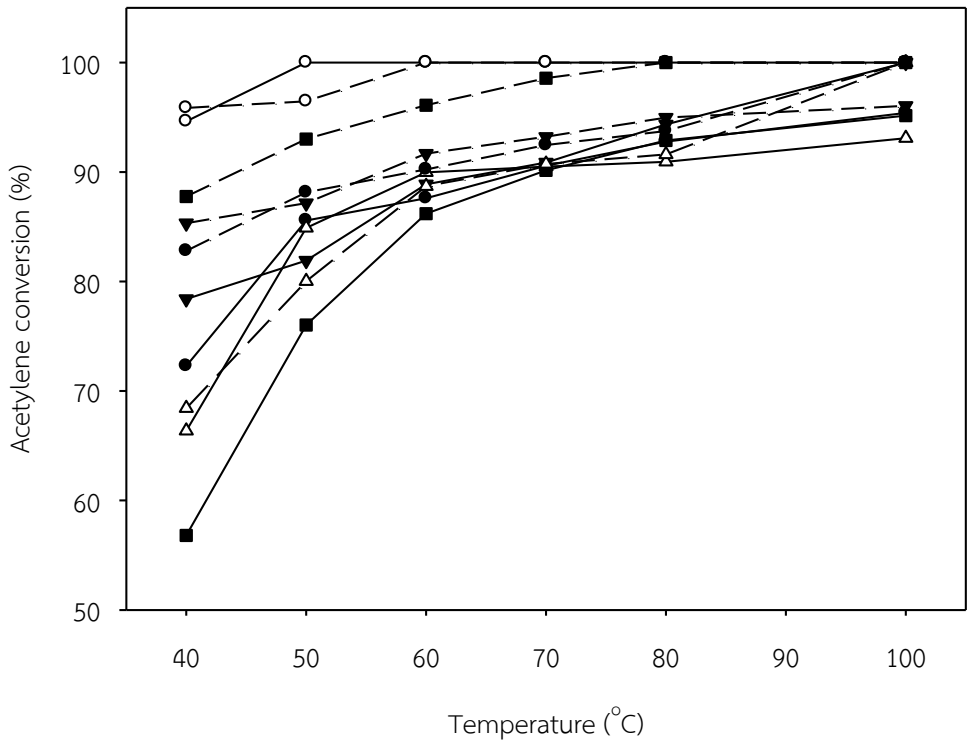

Figure 5.21 Acetylene conversion as a function of temperature for various nanotubes supported catalysts: ● = Pd/T100:S0, ○ = Pd/T95:S5, ▼ = Pd/T90:S10, Δ = Pd/T80:S20, ■ = Pd/T50:S50, solid line = reduced at 500 °C and dash line = reduced at 150 °C.

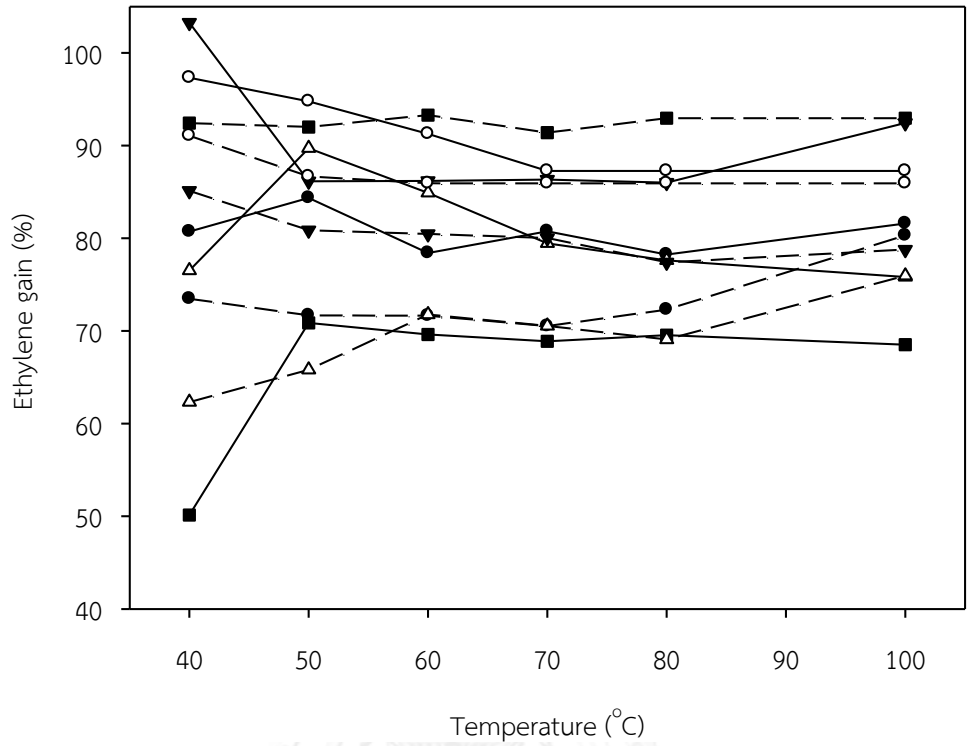

Figure 5.22 Ethylene selectivity as a function of temperature for various nanotubes supported catalysts: ● = Pd/T100:S0, ○ = Pd/T95:S5, ▼ = Pd/T90:S10, Δ = Pd/T80:S20, ■ = Pd/T50:S50, solid line = reduced at 500 ℃ and dash line = reduced at 150 ℃.

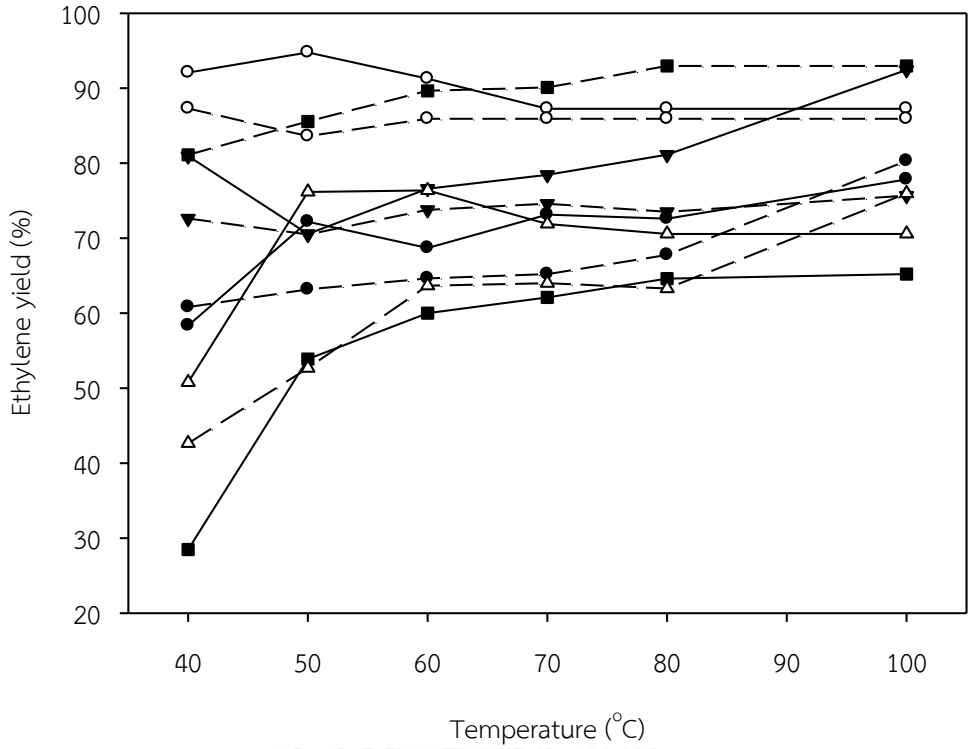

Figure 5.23 Ethylene yield as a function of temperature for various nanotubes supported catalysts: ● = Pd/T100:S0, ○ = Pd/T95:S5, ▼ = Pd/T90:S10, Δ = Pd/T80:S20, ■ = Pd/T50:S50, solid line = reduced at 500 ℃ and dash line = reduced at 150 ℃.

CHAPTER VI

CONCLUSIONS AND RECOMMENDATIONS

This chapter is divided into 2 sections as followed: section 6.1 provides the conclusions that obtained from the experimental results of the silica-modified titanate nanotubes supported palladium catalysts. Additionally, the recommendations for further study are given in section 6.2.

6.1 Conclusions

The SiO_2-modified titanate nanotubes were prerared by the hydrothermal method of TiO_2 powder in an aqueous NaOH solution using tetraethyl orthosilicate as the SiO_2 source at the temperature of 150 °C. Under the synthesis conditions, the temperature is high enough to curl-up the nanosheet into a uniform hollow nanotubular structure. The silica-modified titanate nanotubes supports at 5-20 mol% brought about higher BET surface area and the formation of Ti-O-Si bonds whereas increasing SiO_2 content to 50 mol%, $Na_2(TiO)(SiO_4)$ was formed instead. Although 5 mol% SiO_2-modified titanate nanotube catalysts exhibited the highest acetylene conversion according to its highest number of Pd active sites and highest %Pd dispersion, the 50 mol% SiO_2 containing exhibited the best performance in terms of ethylene yield. High selectivity of ethylene was attributed to the weakened ethylene adsorption strength on Pd catalyst surface as revealed by the temperature programmed desorption of ethylene. When reduced at high temperature of 500 °C, the catalytic performances were improved for all the SiO_2 containing catalysts compared to the non-modified ones except the 50 mol% SiO_2 in which Pd sintering occurred.

6.2 Recommendations

1. CO chemisorption should be used to verify the H_2 chemisorption results.

Because palladium hydride can be formed in the presence of hydrogen so that one hydrogen molecule may not adsorb on one palladium site.

2. The characterization of defective sites of silica-modified titanate nanotube supports should be investigated.

3. The infrared spectra of CO should be investigated for clearly understanding about coordinate adsorption site of Pd.

REFERENCES

[1] Kim, W.-J. and Moon, S.H. Modified Pd catalysts for the selective hydrogenation of acetylene. Catalysis Today 185(1) (2012): 2-16.

[2] Kim, S.K., Kim, C., Lee, J.H., Kim, J., Lee, H., and Moon, S.H. Performance of shape-controlled Pd nanoparticles in the selective hydrogenation of acetylene. Journal of Catalysis 306 (2013): 146-154.

[3] Zhang, Q., Li, J., Liu, X., and Zhu, Q. Synergetic effect of Pd and Ag dispersed on Al_2O_3 in the selective hydrogenation of acetylene. Applied Catalysis A: General 197(2) (2000): 221-228.

[4] Sárkány, A., Weiss, A., and Guczi, L. Structure sensitivity of acetylene-ethylene hydrogenation over Pd catalysts. Journal of Catalysis 98(2) (1986): 550-553.

[5] Kim, W.J., Kang, J.H., Ahn, I.Y., and Moon, S.H. Effect of potassium addition on the properties of a TiO_2-modified Pd catalyst for the selective hydrogenation of acetylene. Applied Catalysis A: General 268(1) (2004): 77-82.

[6] Han, Y., Peng, D., Xu, Z., Wan, H., Zheng, S., and Zhu, D. TiO2 supported Pd@ Ag as highly selective catalysts for hydrogenation of acetylene in excess ethylene. Chemical Communications 49(75) (2013): 8350-8352.

[7] He, Y., Liang, L., Liu, Y., Feng, J., Ma, C., and Li, D. Partial hydrogenation of acetylene using highly stable dispersed bimetallic Pd–Ga/MgO–Al_2O_3 catalyst. Journal of Catalysis 309(0) (2014): 166-173.

[8] Yamamoto, Y., et al. Synthesis of vanadium-doped palladium nanoparticles for hydrogen storage materials. Journal of Nanoparticle Research 13(12) (2011): 6333-6338.

[9] Gentle, T. and Muetterties, E. Acetylene, ethylene, and arene chemistry of palladium surfaces. The Journal of Physical Chemistry 87(14) (1983): 2469-2472.

[10] Berndt, G.F., Thomson, S.J., and Webb, G. Hydrogenation of acetylene over supported metal catalysts. Part 4.—[^{14}C] tracer studies of the reaction catalysed by nickel–silica. Journal of the Chemical Society, Faraday Transactions 1: Physical Chemistry in Condensed Phases 79(1) (1983): 195-207.

[11] Medlin, J.W. and Allendorf, M.D. Theoretical study of the adsorption of acetylene on the (111) surfaces of Pd, Pt, Ni, and Rh. The Journal of Physical Chemistry B 107(1) (2003): 217-223.

[12] Sarkany, A., Horvath, A., and Beck, A. Hydrogenation of acetylene over low loaded Pd and Pd-Au/SiO_2 catalysts. Applied Catalysis A: General 229(1) (2002): 117-125.

[13] Ahn, I.Y., Lee, J.H., Kim, S.K., and Moon, S.H. Three-stage deactivation of Pd/SiO_2 and Pd-Ag/SiO_2 catalysts during the selective hydrogenation of acetylene. Applied Catalysis A: General 360(1) (2009): 38-42.

[14] Leviness, S., Nair, V., Weiss, A.H., Schay, Z., and Guczi, L. Acetylene hydrogenation selectivity control on PdCu/Al_2O_3 catalysts. Journal of molecular catalysis 25(1) (1984): 131-140.

[15] Ngamsom, B., Bogdanchikova, N., Avalos Borja, M., and Praserthdam, P. Characterisations of Pd–Ag/Al_2O_3 catalysts for selective acetylene hydrogenation: effect of pretreatment with NO and N_2O. Catalysis Communications 5(5) (2004): 243-248.

[16] Kontapakdee, K., Panpranot, J., and Praserthdam, P. Effect of Ag addition on the properties of Pd–Ag/TiO_2 catalysts containing different TiO_2 crystalline phases. Catalysis Communications 8(12) (2007): 2166-2170.

[17] Panpranot, J., Nakkararuang, L., Ngamsom, B., and Praserthdam, P. Synthesis, characterization, and catalytic properties of Pd and Pd–Ag catalysts supported on nanocrystalline TiO_2 prepared by the solvothermal method. Catalysis letters 103(1-2) (2005): 53-58.

[18] Hong, J., Chu, W., Chen, M., Wang, X., and Zhang, T. Preparation of novel titania supported palladium catalysts for selective hydrogenation of acetylene to ethylene. Catalysis Communications 8(3) (2007): 593-597.

[19] Chen, M.-h., Qin, X.-j., Chu, W., and Hong, J.-p. Effect of Support on the Performance of Palladium Catalysts for Selective Hydrogenation. Acta Petrolei Sinica Petroleum Processing Section 22(2) (2006): 20.

[20] Panpranot, J., Kontapakdee, K., and Praserthdam, P. Selective hydrogenation of acetylene in excess ethylene on micron-sized and nanocrystalline TiO_2 supported Pd catalysts. Applied Catalysis A: General 314(1) (2006): 128-133.

[21] Kang, J.H., Shin, E.W., Kim, W.J., Park, J.D., and Moon, S.H. Selective hydrogenation of acetylene on TiO_2-added Pd catalysts. Journal of Catalysis 208(2) (2002): 310-320.

[22] Nian, J.-N., Chen, S.-A., Tsai, C.-C., and Teng, H. Structural feature and catalytic performance of Cu species distributed over TiO_2 nanotubes. The Journal of Physical Chemistry B 110(51) (2006): 25817-25824.

[23] Kasuga, T., Hiramatsu, M., Hoson, A., Sekino, T., and Niihara, K. Formation of titanium oxide nanotube. Langmuir 14(12) (1998): 3160-3163.

[24] Bavykin, D.V., Parmon, V.N., Lapkin, A.A., and Walsh, F.C. The effect of hydrothermal conditions on the mesoporous structure of TiO_2 nanotubes. Journal of Materials Chemistry 14(22) (2004): 3370-3377.

[25] Liu, X., et al. Synthesis of Au nanoclusters supported upon a TiO_2 nanotube array. Journal of materials research 20(05) (2005): 1093-1096.

[26] Li, S., Zhang, G., Guo, D., Yu, L., and Zhang, W. Anodization fabrication of highly ordered TiO_2 nanotubes. The Journal of Physical Chemistry C 113(29) (2009): 12759-12765.

[27] Chatterjee, S., Bhattacharyya, S., Khushalani, D., and Ayyub, P. Hydrothermally synthesized aligned arrays of self-assembled multiwalled hydrogen titanate nanotubes. Crystal Growth & Design 10(3) (2010): 1215-1220.

[28] Lin, C.-H., et al. Photocatalytic generation of H_2 gas from neat ethanol over Pt/TiO_2 nanotube catalysts. Catalysis letters 98(1) (2004): 61-66.

[29] Idakiev, V., Yuan, Z.-Y., Tabakova, T., and Su, B.-L. Titanium oxide nanotubes as supports of nano-sized gold catalysts for low temperature water-gas shift reaction. Applied Catalysis A: General 281(1) (2005): 149-155.

[30] Bavykin, D.V., Lapkin, A.A., Plucinski, P.K., Friedrich, J.M., and Walsh, F.C. TiO_2 nanotube-supported ruthenium (III) hydrated oxide: A highly active catalyst for selective oxidation of alcohols by oxygen. Journal of Catalysis 235(1) (2005): 10-17.

[31] Bavykin, D.V., Lapkin, A.A., Plucinski, P.K., Friedrich, J.M., and Walsh, F.C. Reversible storage of molecular hydrogen by sorption into multilayered TiO_2 nanotubes. The Journal of Physical Chemistry B 109(41) (2005): 19422-19427.

[32] Hussain, S. and Siddiqa, A. Iron and chromium doped titanium dioxide nanotubes for the degradation of environmental and industrial pollutants. International Journal of Environmental Science & Technology 8(2) (2011): 351-362.

[33] Putdee, S., Mekasuwandumrong, O., Soottitantawat, A., and Panpranot, J. Characteristics and Catalytic Behavior of Pd Catalysts Supported on Nanostructure Titanate in Liquid-Phase Hydrogenation. Journal of nanoscience and nanotechnology 13(4) (2013): 3062-3067.

[34] Periyat, P., Baiju, K., Mukundan, P., Pillai, P., and Warrier, K. High temperature stable mesoporous anatase TiO_2 photocatalyst achieved by silica addition. Applied Catalysis A: General 349(1) (2008): 13-19.

[35] Boccuzzi, F., Coluccia, S., Martra, G., and Ravasio, N. Cu/SiO_2 and Cu/SiO_2–TiO_2 Catalysts: I. TEM, DR UV-Vis-NIR, and FTIR Characterisation. Journal of Catalysis 184(2) (1999): 316-326.

[36] Boccuzzi, F., Martra, G., Papalia, C.P., and Ravasio, N. Cu/SiO_2 and Cu/SiO_2–TiO_2 Catalysts: II. Identification of the Active Sites during Polymerisation of 2, 6-dimethylphenol in the Presence of Molecular O_2. Journal of Catalysis 184(2) (1999): 327-334.

[37] Chmielarz, L., Kowalczyk, A., Wojciechowska, M., Boroń, P., Dudek, B., and Michalik, M. Montmorillonite intercalated with SiO_2, SiO_2-Al_2O_3 or SiO_2-TiO_2 pillars by surfactant-directed method as catalytic supports for $DeNO_x$ process. Chemical Papers (2013): 1-10.

[38] Nowacka, M., Siwińska-Stefańska, K., and Jesionowski, T. Structural characterisation of titania or silane-grafted TiO_2-SiO_2 oxide composite and influence of ionic strength or electrolyte type on their electrokinetic properties. Colloid and Polymer Science 291(3) (2013): 603-612.

[39] Kang, C., Jing, L., Guo, T., Cui, H., Zhou, J., and Fu, H. Mesoporous SiO_2-modified nanocrystalline TiO_2 with high anatase thermal stability and large surface area as efficient photocatalyst. The Journal of Physical Chemistry C 113(3) (2008): 1006-1013.

[40] Yao, Y., Zhao, N., Feng, J.-j., Yao, M.-m., and Li, F. Photocatalytic activities of Ce or Co doped nanocrystalline TiO_2–SiO_2 composite films. Ceramics International 39(4) (2013): 4735-4738.

[41] Zhang, X., Yang, H., Zhang, F., and Chan, K.-Y. Preparation and characterization of Pt–TiO_2–SiO_2 mesoporous materials and visible-light photocatalytic performance. Materials Letters 61(11) (2007): 2231-2234.

[42] Ren, J., Li, Z., Liu, S., Xing, Y., and Xie, K. Silica–titania mixed oxides: Si–O–Ti connectivity, coordination of titanium, and surface acidic properties. Catalysis letters 124(3-4) (2008): 185-194.

[43] Shin, E.W., Choi, C.H., Chang, K.S., Na, Y.H., and Moon, S.H. Properties of Si-modified Pd catalyst for selective hydrogenation of acetylene. Catalysis Today 44(1) (1998): 137-143.

[44] Shin, E.W., Kang, J.H., Kim, W.J., Park, J.D., and Moon, S.H. Performance of Si-modified Pd catalyst in acetylene hydrogenation: the origin of the ethylene selectivity improvement. Applied Catalysis A: General 223(1) (2002): 161-172.

[45] Kim, W.J., Shin, E.W., Kang, J.H., and Moon, S.H. Performance of Si-modified Pd catalyst in acetylene hydrogenation: catalyst deactivation behavior. Applied Catalysis A: General 251(2) (2003): 305-313.

[46] Seo, H.-K., et al. A study on the structure/phase transformation of titanate nanotubes synthesized at various hydrothermal temperatures. Solar Energy Materials and Solar Cells 92(11) (2008): 1533-1539.

[47] Sreekantan, S. and Wei, L.C. Study on the formation and photocatalytic activity of titanate nanotubes synthesized via hydrothermal method. Journal of Alloys and Compounds 490(1) (2010): 436-442.

[48] Nakahira, A., Kato, W., Tamai, M., Isshiki, T., Nishio, K., and Aritani, H. Synthesis of nanotube from a layered $H_2Ti_4O_9{\cdot}H_2O$ in a hydrothermal treatment using various titania sources. Journal of materials science 39(13) (2004): 4239-4245.

[49] Morgan, D.L., Triani, G., Blackford, M.G., Raftery, N., Frost, R.L., and Waclawik, E.R. Alkaline hydrothermal kinetics in titanate nanostructure formation. Journal of materials science 46(2) (2011): 548-557.

[50] Kim, G.-S., Kim, Y.-S., Seo, H.-K., and Shin, H.-S. Hydrothermal synthesis of titanate nanotubes followed by electrodeposition process. Korean Journal of Chemical Engineering 23(6) (2006): 1037-1045.

[51] Tsai, C.-C. and Teng, H. Structural features of nanotubes synthesized from NaOH treatment on TiO_2 with different post-treatments. Chemistry of materials 18(2) (2006): 367-373.

[52] Yuan, Z.-Y. and Su, B.-L. Titanium oxide nanotubes, nanofibers and nanowires. Colloids and Surfaces A: Physicochemical and Engineering Aspects 241(1) (2004): 173-183.

[53] Chang, Z., Liu, J., Liu, J., and Sun, X. Titanate nanosheets and nanotubes: alkalinity manipulated synthesis and catalyst support application. Journal of Materials Chemistry 21(1) (2011): 277-282.

[54] Tsai, C.-C. and Teng, H. Regulation of the physical characteristics of titania nanotube aggregates synthesized from hydrothermal treatment. Chemistry of materials 16(22) (2004): 4352-4358.

[55] Sheridan, J. 122. The metal-catalysed reaction between acetylene and hydrogen. Part V. Reaction over palladium, iron, and some other catalysts. Journal of the Chemical Society (Resumed) (1945): 470-476.

[56] Tamaru, K. Selective Catalysis. The Catalytic Reaction between Acetylene and Hydrogen. Bulletin of the Chemical Society of Japan 23(2) (1950): 64-66.

[57] Bond, G. and Wells, P. The hydrogenation of acetylene: II. The reaction of acetylene with hydrogen catalyzed by alumina-supported palladium. Journal of Catalysis 5(1) (1966): 65-73.

[58] Bond, G., Webb, G., Wells, P., and Winterbottom, J. Patterns of behavior in catalysis by metals. Journal of Catalysis 1(1) (1962): 74-84.

[59] Bond, G., Dowden, D., and Mackenzie, N. The selective hydrogenation of acetylene. Transactions of the Faraday Society 54 (1958): 1537-1546.

[60] Bond, G., Newham, J., and Wells, P. The selective hydrogenation of unsaturated hydrocarbons. in Proceedings of 2nd International Congress on Catalysis, Technip, Paris, pp. 1177-1180, 1960.

[61] Borodziński, A. and Cybulski, A. The kinetic model of hydrogenation of acetylene–ethylene mixtures over palladium surface covered by carbonaceous deposits. Applied Catalysis A: General 198(1) (2000): 51-66.

[62] McGown, W.T., Kemball, C., and Whan, D.A. Hydrogenation of acetylene in excess ethylene on an alumina-supported palladium catalyst at atmospheric pressure in a spinning basket reactor. Journal of Catalysis 51(2) (1978): 173-184.

[63] Margitfalvi, J., Guczi, L., and Weiss, A.H. Reactions of acetylene during hydrogenation on Pd black catalyst. Journal of Catalysis 72(2) (1981): 185-198.

[64] Asplund, S. Coke formation and its effect on internal mass transfer and selectivity in Pd-catalysed acetylene hydrogenation. Journal of Catalysis 158(1) (1996): 267-278.

[65] Battiston, G., Dalloro, L., and Tauszik, G. Performance and aging of catalysts for the selective hydrogenation of acetylene: a micropilot-plant study. Applied Catalysis 2(1) (1982): 1-17.

[66] Cutmann, H. and Lindlar, H. Partial catalytic hydrogenation of acetylenes. Chemistry of Acetylenes. New York: Marcel Dekker (1969): 355-362.

[67] Davis, S., Zaera, F., and Somorjai, G. The reactivity and composition of strongly adsorbed carbonaceous deposits on platinum. Model of the working hydrocarbon conversion catalyst. Journal of Catalysis 77(2) (1982): 439-459.

[68] Zaera, F. On the mechanism for the hydrogenation of olefins on transition-metal surfaces: The chemistry of ethylene on Pt (111). Langmuir 12(1) (1996): 88-94.

[69] Cremer, P.S., Su, X., Shen, Y.R., and Somorjai, G.A. Ethylene hydrogenation on Pt (111) monitored in situ at high pressures using sum frequency generation. Journal of the American Chemical Society 118(12) (1996): 2942-2949.

[70] Kim, W.J., Kang, J.H., Ahn, I.Y., and Moon, S.H. Deactivation behavior of a TiO_2-added Pd catalyst in acetylene hydrogenation. Journal of Catalysis 226(1) (2004): 226-229.

[71] Sandell, A., et al. Adsorption of acetylene and hydrogen on Pd (111): formation of a well-ordered ethylidyne overlayer. Surface science 415(3) (1998): 411-422.

[72] Palczewska, W. Catalytic reactivity of hydrogen on palladium and nickel hydride phases. Advances Catalysis 24 (1975): 248.

[73] Borodziński, A. The effect of carburization of palladium catalysts on the hydrogenation of acetylene-ethylene mixtures. Polish Journal of Chemistry 72(11) (1998): 2455-2462.

[74] Siller, R.H., Oates, W.A., and McLellan, R.B. The solubility of carbon in palladium and platinum. Journal of the Less Common Metals 16(1) (1968): 71-73.

[75] Liu, R.-J., Crozier, P., Smith, C., Hucul, D., Blackson, J., and Salaita, G. Metal sintering mechanisms and regeneration of palladium/alumina hydrogenation catalysts. Applied Catalysis A: General 282(1) (2005): 111-121.

[76] Weiss, A., Leviness, S., Nair, V., Guczi, L., Sarkany, A., and Schay, Z. The effect of Pd dispersion in acetylene selective hydrogenation. Proc. Int. Congr. Catal. Dechema (1984).

[77] Borodzinski, A. The effect of carbonacious deposits on aluminar on hydrogenation of acetylene-ethlene mixture on Pd-AL_2O_3 catalyst. Polish Journal of Chemistry 69(1) (1995): 111-117.

[78] Bond, G.C. The role of carbon deposits in metal-catalysed reactions of hydrocarbons. Applied Catalysis A: General 149(1) (1997): 3-25.

[79] Bond, G. and Sheridan, J. Studies in heterogeneous catalysis. Part 1.—The hydrogenation of methylacetylene. Transactions of the Faraday Society 48 (1952): 651-658.

[80] Borodzinski, A. and Golębiowski, A. Surface heterogeneity of supported palladium catalyst for the hydrogenation of acetylene-ethylene mixtures. Langmuir 13(5) (1997): 883-887.

[81] Wicke, E., Brodowsky, H., and Züchner, H. Hydrogen in palladium and palladium alloys. in Alefeld, G. and Völkl, J. (eds.),Hydrogen in Metals II, pp. 73-155: Springer Berlin Heidelberg, 1978.

[82] Schwarz, R., Bach, H., Harms, U., and Tuggle, D. Elastic properties of Pd–hydrogen, Pd–deuterium, and Pd–tritium single crystals. Acta materialia 53(3) (2005): 569-580.

[83] Boudart, M. and Hwang, H. Solubility of hydrogen in small particles of palladium. Journal of Catalysis 39(1) (1975): 44-52.

[84] Sarkany, A., Guczi, L., and Weiss, A.H. On the aging phenomenon in palladium catalysed acetylene hydrogenation. Applied Catalysis 10(3) (1984): 369-388.

[85] Kang, J.H., Shin, E.W., Kim, W.J., Park, J.D., and Moon, S.H. Selective hydrogenation of acetylene on Pd/SiO_2 catalysts promoted with Ti, Nb and Ce oxides. Catalysis Today 63(2) (2000): 183-188.

[86] Zhang, Y., Diao, W., Williams, C.T., and Monnier, J.R. Selective hydrogenation of acetylene in excess ethylene using Ag-and Au–Pd/SiO_2 bimetallic catalysts prepared by electroless deposition. Applied Catalysis A: General 469 (2014): 419-426.

[87] Sikhwivhilu, L.M., Coville, N.J., Pulimaddi, B.M., Venkatreddy, J., and Vishwanathan, V. Selective hydrogenation of *o*-chloronitrobenzene over palladium supported nanotubular titanium dioxide derived catalysts. Catalysis Communications 8(12) (2007): 1999-2006.

[88] Sikhwivhilu, L.M., Coville, N.J., Naresh, D., Chary, K.V., and Vishwanathan, V. Nanotubular titanate supported palladium catalysts: The influence of structure and morphology on phenol hydrogenation activity. Applied Catalysis A: General 324 (2007): 52-61.

[89] Torrente-Murciano, L., Lapkin, A.A., Bavykin, D.V., Walsh, F.C., and Wilson, K. Highly selective Pd/titanate nanotube catalysts for the double-bond migration reaction. Journal of Catalysis 245(2) (2007): 272-278.

[90] Landmann, M., Rauls, E., and Schmidt, W. The electronic structure and optical response of rutile, anatase and brookite TiO2. Journal of Physics: Condensed Matter 24(19) (2012): 195503.

[91] Zhou, W., et al. One-dimensional single-crystalline Ti–O based nanostructures: properties, synthesis, modifications and applications. Journal of Materials Chemistry 20(29) (2010): 5993-6008.

[92] Bavykin, D.V., Friedrich, J.M., and Walsh, F.C. Protonated titanates and TiO_2 nanostructured materials: synthesis, properties, and applications. Advanced Materials 18(21) (2006): 2807-2824.

[93] Ou, H.-H. and Lo, S.-L. Review of titania nanotubes synthesized via the hydrothermal treatment: Fabrication, modification, and application. Separation and Purification Technology 58(1) (2007): 179-191.

[94] Bavykin, D.V. and Walsh, F.C. Elongated titanate nanostructures and their applications. European Journal of Inorganic Chemistry 2009(8) (2009): 977-997.

[95] Mozia, S., et al. Physico-chemical properties and possible photocatalytic applications of titanate nanotubes synthesized via hydrothermal method. Journal of Physics and Chemistry of Solids 71(3) (2010): 263-272.

[96] Du, G., Chen, Q., Che, R., Yuan, Z., and Peng, L.-M. Preparation and structure analysis of titanium oxide nanotubes. Applied physics letters 79(22) (2001): 3702-3704.

[97] Chen, Q., Du, G., Zhang, S., and Peng, L.-M. The structure of trititanate nanotubes. Acta Crystallographica Section B: Structural Science 58(4) (2002): 587-593.

[98] Wu, D., Liu, J., Zhao, X., Li, A., Chen, Y., and Ming, N. Sequence of events for the formation of titanate nanotubes, nanofibers, nanowires, and nanobelts. Chemistry of materials 18(2) (2006): 547-553.

[99] Wang, Y., Hu, G., Duan, X., Sun, H., and Xue, Q. Microstructure and formation mechanism of titanium dioxide nanotubes. Chemical Physics Letters 365(5) (2002): 427-431.

[100] Wei, M., Konishi, Y., Zhou, H., Sugihara, H., and Arakawa, H. Formation of nanotubes TiO_2 from layered titanate particles by a soft chemical process. Solid State Communications 133(8) (2005): 493-497.

[101] Derrien, M.L. Selective hydrogenation applied to the refining of petrochemical raw materials produced by steam cracking. Studies in surface science and catalysis 27 (1986): 613-666.

[102] Molnár, Á., Sárkány, A., and Varga, M. Hydrogenation of carbon–carbon multiple bonds: chemo-, regio-and stereo-selectivity. Journal of Molecular Catalysis A: Chemical 173(1) (2001): 185-221.

[103] Peng, G.-W. and Liu, H.-S. FT-IR and XRD characterization of phase transformation of heat-treated synthetic natisite ($Na_2TiOSiO_4$) powder. Materials chemistry and physics 42(4) (1995): 264-275.

[104] Kumar, D.A., Xavier, J.A., Shyla, J.M., and Xavier, F.P. Synthesis and structural, optical and electrical properties of TiO_2/SiO_2 nanocomposites. Journal of materials science 48(10) (2013): 3700-3707.

[105] Bavykin, D.V. and Walsh, F.C. Titanate and titania nanotubes: synthesis, properties and applications. Royal Society of Chemistry, 2010.

[106] Zhang, M., Shi, L., Yuan, S., Zhao, Y., and Fang, J. Synthesis and photocatalytic properties of highly stable and neutral TiO_2/SiO_2 hydrosol. Journal of colloid and interface science 330(1) (2009): 113-118.

[107] Venezia, A., Di Carlo, G., Pantaleo, G., Liotta, L., Melaet, G., and Kruse, N. Oxidation of CH_4 over Pd supported on TiO_2-doped SiO_2: Effect of Ti (IV) loading and influence of SO_2 Applied Catalysis B: Environmental 88(3) (2009): 430-437.

[108] Fang, Q., et al. FTIR and XPS investigation of Er-doped SiO_2–TiO_2 films. Materials Science and Engineering: B 105(1) (2003): 209-213.

[109] Nakatsuji, H., Hada, M., and Yonezawa, T. Theoretical study on the chemisorption of a hydrogen molecule on palladium. Journal of the American Chemical Society 109(7) (1987): 1902-1912.

[110] Binder, A., Seipenbusch, M., Muhler, M., and Kasper, G. Kinetics and particle size effects in ethene hydrogenation over supported palladium catalysts at atmospheric pressure. Journal of Catalysis 268(1) (2009): 150-155.

[111] Borodziński, A. The effect of palladium particle size on the kinetics of hydrogenation of acetylene–ethylene mixtures over Pd/SiO_2 catalysts. Catalysis letters 71(3-4) (2001): 169-175.

[112] Panpranot, J., Kontapakdee, K., and Praserthdam, P. Effect of TiO_2 crystalline phase composition on the physicochemical and catalytic properties of Pd/TiO_2 in selective acetylene hydrogenation. The Journal of Physical Chemistry B 110(15) (2006): 8019-8024.

[113] Weerachawanasak, P., Mekasuwandumrong, O., Arai, M., Fujita, S.-I., Praserthdam, P., and Panpranot, J. Effect of strong metal–support interaction on the catalytic performance of Pd/TiO_2 in the liquid-phase semihydrogenation of phenylacetylene. Journal of Catalysis 262(2) (2009): 199-205.

APPENDICES

APPENDIX A

CALCULATION FOR CATALYST PREPARATION

The calculation shown below is for 1 wt% Pd supported on silica-modified titanate nanotubes catalysts. The support weight used for all preparation is 1 g.

Calculation of various Ti/Si molar rations of silica-modified titanate nanotubes supports.

Based on 1.5 g of titanai powder used, the composition of the silica-modified titanate nanotubes supports will be as follows:

Reagent:

- Titanium(IV) oxide, anatase ≥ 99% (TiO_2)
- Molecular weight = 79.87 g/mol
- Tetraethyl orthosilicate, 98% ($SiC_8H_{20}O_4$)
- Molecular weight = 208.33 g/mol
- Density = 0.933 g/ml

For molar ratio of Ti/Si = 95/5 mol% is shown as follow:

95 mol% of TiO_2 = 1.5 g

= 1.5/79.87 = 0.01878 mol

5 mol% of SiO_2 = (0.01878 × 5)/95 = 0.00099 mol

For SiO_2 = 0.00099 mol was prepared from $SiC_8H_{20}O_4$, 98% purity.

$$SiC_8H_{20}O_4 \text{ required} = \frac{\text{mol of } SiO_2 \text{ required} \times \text{MW of } SiC_8H_{20}O_4}{98\% \text{ purity} \times \text{Density of } SiC_8H_{20}O_4}$$

$$= \frac{0.00099 \times 208.33}{98\% \times 0.933}$$

$$= 0.2256 \text{ mL}$$

Calculation for the preparation of Pd catalysts

Based on 100 g of catalyst used, the composition of the catalyst will be as follows:

Precursors:

- Palladium(II) acetate, 98% ($Pd(CH_3CO_2)_2$)
- Molecular weight = 224.51 g/mol

Palladium = 1 g

Titanate nanotube = 100-1 = 99 g

For 1 g of Titanate nanotube

Palladium required = (1 × 1)/99 = 0.0101 g

Palladium 0.0101 g was prepared from $Pd(CH_3CO_2)_2$ and molecular weight of Pd is 106.42 g/mol.

$$Pd(CH_3CO_2)_2 \text{ required} = \frac{\text{MW of } Pd(CH_3CO_2)_2 \times \text{Palladium required}}{98\% \text{ purity} \times \text{MW of Pd}}$$

$$= \frac{224.51 \times 0.0101}{98\% \times 106.42}$$

$$= 0.0217 \text{ g}$$

APPENDIX B

CALCULATION FOR H_2 CHEMISORPTION

Calculation of the metal active sites, metal dispersion, active metal surface area, and particle size of metal by H_2 chemisorption is as follows:

Volume of active gas dosed from a loop (V_{inj})

$$V_{inj} = V_{loop} \times \frac{T_{std}}{T_{amb}} \times \frac{P_{amb}}{P_{std}} \times \frac{\%A}{100\%}$$

V_{loop}	=	loop volume injected	100 μL
T_{amb}	=	ambient temperature	295 K
T_{std}	=	standard temperature	273 K
P_{amb}	=	ambient pressure	743 mmHg
P_{std}	=	standard pressure	760 mmHg
%A	=	%active gas	100 %

$$V_{inj} = 100\mu L \times \frac{273K}{295K} \times \frac{743mmHg}{760mmHg} \times \frac{100\%}{100\%} = 90.4723\mu L$$

Volume chemisorbed (V_{ads})

$$V_{ads} = \frac{V_{inj}}{m} \times \sum_{i=1}^{n} \left[1 - \frac{A_i}{A_f}\right]$$

Example: for H_2 chemisorption on 1 wt% Pd/Titanate nanotubes is shown as follow:

V_{inj}	=	volume injected	90.4723 µL
m	=	mass of sample	0.1023 g
A_f	=	area of last peak	0.0410625

Peak	A_i	A_i/A_f	$1-A_i/A_f$	V_{ads}
1	0.0339541	0.82688828	0.17311172	153.0970034
2	0.0404679	0.98551963	0.014480365	12.80618398
3	0.0404513	0.98511537	0.014884627	13.1637061
4	0.0405641	0.9878624	0.012137595	10.73427867
5	0.0407289	0.9918758	0.008124201	7.184902414
6	0.0410625	1	0	0
sum				196.9860745

$$V_{ads} = 196.9861 \ \mu L/g = 0.1970 \ cm^3/g$$

% Metal dispersion

$$\%D = S_f \times \frac{V_{ads}}{V_g} \times \frac{M.W.}{\%M} \times 100\% \times 100\%$$

S_f	=	stoichiometry factor, H_2 on Pd	2
V_{ads}	=	volume adsorbed	0.1970 cm^3/g
V_g	=	molar volume of gas at STP	22414 cm^3/mol
M.W.	=	molecular weight of the metal	106.4 g/mol
%M	=	weight percent of active metal	1 %

$$\%D = 2 \times \frac{0.1970 cm^3/g}{22414 cm^3/g} \times \frac{106.4 g/mol}{1\%} \times 100\% \times 100\% \quad = 18.7\%$$

Palladium active sites

$$\textbf{Pd active sites} = S_f \times \frac{V_{ads}}{V_g} \times N_A$$

S_f	=	stoichiometry factor, H_2 on Pd	2
V_{ads}	=	volume adsorbed	0.1970 cm^3/g
V_g	=	molar volume of gas at STP	22414 cm^3/mol
N_A	=	Avogadro's number	6.023×10^{23} molecues/mol

$$\text{Pd active sites} = 1 \times \frac{0.1970 cm^3/g}{22414 cm^3/g} \times \frac{6.023 \times 10^{23} molecules}{mol}$$

$$= \frac{1.06 \times 10^{19} H_2 \text{ molecules}}{g}$$

Active metal surface area (per gram of metal)

$$\textbf{MSA}_s = S_f \times \frac{V_{ads}}{V_g} \times \frac{100\%}{\%M} \times N_A \times \sigma_m \times \frac{m^2}{10^{18}\ nm^2}$$

S_f	=	stoichiometry factor, H_2 on Pd	2
V_{ads}	=	volume adsorbed	0.1970 cm^3/g
Vg	=	molar volume of gas at STP	22414 cm^3/mol
%M	=	weight percent of the active metal	1 %

N_A = Avogadro's number 6.023×10^{23} molecues/mol

σ_m = cross-sectional area of active metal atom $0.0787\ nm^2$

$$MSA_s = 1 \times \frac{0.1970 cm^3/g}{22414 cm^3/g} \times \frac{100\%}{1\%} \times \frac{6.023 \times 10^{23} molecules}{mol}$$

$$\times 0.0787\ nm^2 \times \frac{m^2}{10^{18}\ nm^2} = 83.32\ {}^{m^2}/_{g_{metal}}$$

Average crystallite size

$$d = \frac{F_g}{\rho \times MSA_m} \times \frac{m^3}{10^6\ cm^3} \times \frac{10^9\ nm}{m}$$

F_g = crystallite geometry factor (hemisphere = 6) 6

ρ = specific gravity of the active metal 12.0 g/cm3

MSA_s = active metal surface area per gram of metal $83.32\ m^2/g_{metal}$

$$d = \frac{6}{12 g/cm^3 \times 83.32 m^2/g} \times \frac{m^3}{10^6\ cm^3} \times \frac{10^9\ nm}{m} = 6.0\ nm$$

APPENDIX C

CALIBRATION CURVES

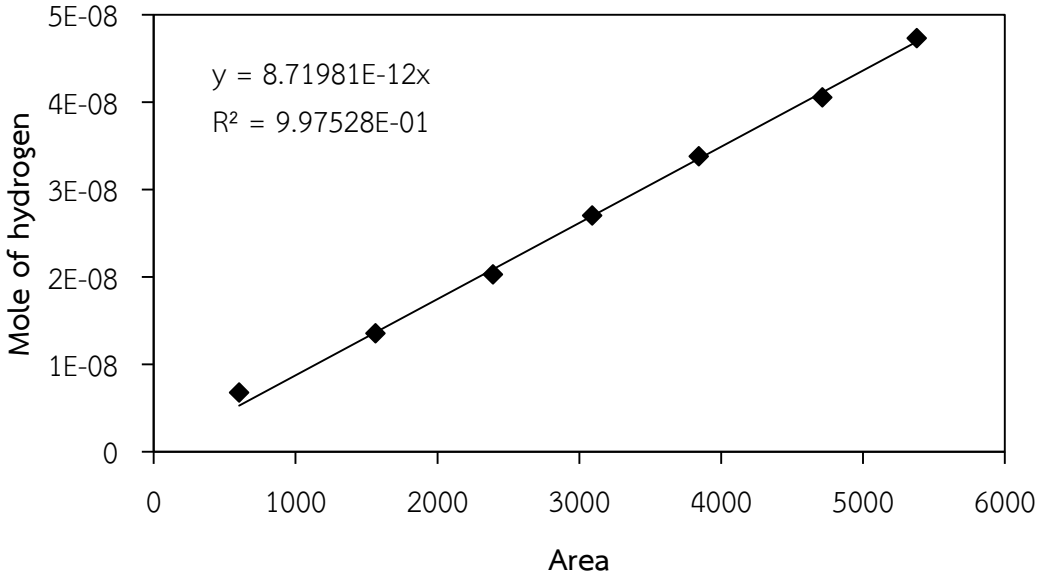

Figure D.1 Calibration curve of hydrogen.

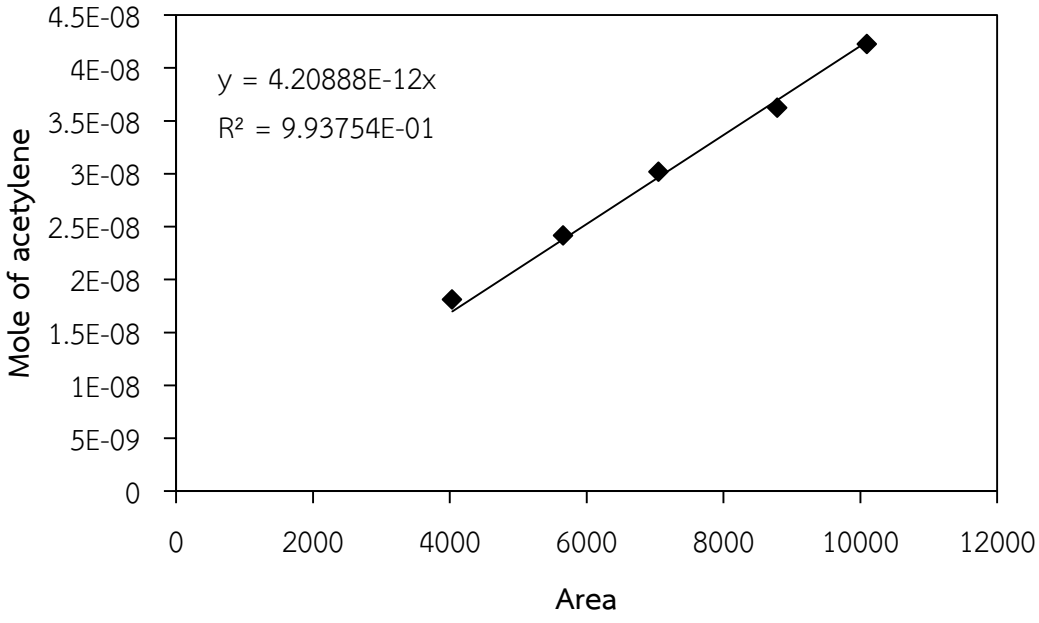

Figure D.2 Calibration curve of acetylene.

APPENDIX D

CALCULATION OF ACETYLENE CONVERSION AND ETHYLENE SELECTIVITY

The catalytic performance for selective hydrogenation of acetylene was evaluated in terms of activity for acetylene conversion and ethylene gain based on following reaction pathway:

$$C_2H_2 + H_2 \xrightarrow{k_1} C_2H_4 \qquad \Delta H = -42{,}000 \text{ kcal/kmol} \qquad (1)$$

$$C_2H_4 + H_2 \xrightarrow{k_2} C_2H_6 \qquad \Delta H = -32{,}900 \text{ kcal/kmol} \qquad (2)$$

Activity of the catalyst for acetylene conversion is defined as mole of acetylene converted with respect to acetylene in the feed:

$$C_2H_2 \text{ conversion } (\%) = \frac{100 \times [\text{mole of } C_2H_2 \text{ in feed-mole of } C_2H_2 \text{ in product}]}{\text{mole of } C_2H_2 \text{ in feed}}$$

Ethylene gain was calculated from moles of hydrogen and acetylene:

$$C_2H_4 \text{ gain } (\%) = \frac{100 \times [dC_2H_2 - (dH_2 - dC_2H_2)]}{dC_2H_2}$$

Where:

dC_2H_2 = mole of acetylene in feed – mole of acetylene in product

dH_2 = mole of hydrogen in feed – mole of hydrogen in product

VITA

Mr. Jittrakorn Jeasadakom was born in April 7th, 1990 in Sa Kaeo, Thailand. He finished high school from Maryvithayakabinburi School, Prajinburi in 2008. After that, he received the Bachelor's Degree in Chemical Engineering from Department of Chemical Engineering, Kasetsart University, Bangkok, Thailand in April 2012. Thereafter, he continued to study in Master's Degree of Chemical Engineering at Department of Chemical Engineering, Chulalongkorn University, Bangkok, Thailand since 2012 and joined center of excellence on catalysis and catalytic reaction engineering research group.